6-2000

Quantitative Investigation of Surface and Subsurface Fatigue Cracks Near Rivets in Riveted Joints Using Acoustic, Electron and Optical Microscopy

Zayna Connor
Northwestern University

NORTHWESTERN UNIVERSITY

Quantitative Investigation of Surface and Subsurface Fatigue Cracks Near Rivets in Riveted Joints Using Acoustic, Electron and Optical Microscopy

A DISSERTATION

SUBMITTED TO THE GRADUATE SCHOOL
IN PARTIAL FULFILLMENT OF THE REQUIREMENTS

for the degree

DOCTOR OF PHILOSOPHY

Field of Materials Science and Engineering

By

Zayna Connor

EVANSTON, ILLINOIS

June 2000

ABSTRACT

QUANTITATIVE INVESTIGATION OF SURFACE AND SUBSURFACE FATIGUE CRACKS NEAR RIVETS IN RIVETED JOINTS USING ACOUSTIC, ELECTRON AND OPTICAL MICROSCOPY

By

ZAYNA CONNOR

Using scanning acoustic microscopy, optical microscopy and scanning electron microscopy, in conjunction with fractography of fractured surfaces, the crack formation and growth kinetics of subsurface fatigue cracks and surface breaking fatigue cracks near rivets have been characterized in detail in this research. The scanning acoustic microscope was used to quantitatively investigate subsurface fatigue cracks (even when they were very small) at and near countersunk rivets in riveted lap joint specimens that are similar to the riveted lap joints found in the fuselages of many aircraft.

It was found that the maximum nominal applied stress influences the fatigue crack initiation and propagation behavior. Eyebrow type cracks develop at lower stresses and centerline cracks develop at higher stresses. At low stress ranges, the fatigue cracks initiate a short distance from the rivet at or near the hidden surface of the chamfered panel. At higher stress amplitudes, the cracks initiate at the blunt knife

edge. Residual compressive stresses and fretting are suggested to play more important roles at lower stress ranges. Both types of cracks initiate in a shear mode but transform to tensile, mode I, cracks as they grow. This transition occurs much more rapidly at the higher stress amplitude. At both high and low stresses, the cracks are longer on the fayed surface of the panel than elsewhere.

In a comparison of Alclad 2024-T3 and Alclad 2524-T3, it was found that the high purity aluminum alloy 2524 nucleates cracks at a greater number of cycles than the less pure aluminum alloy 2024. At high stress, crack initiation plays less of a roll and the 2024 alloy has a longer life.

The scanning acoustic microscope enabled us to study subsurface fatigue cracks. The understanding gained from the characterization of the subsurface fatigue cracks will help in the modeling of crack initiation and growth in the riveted lap joint and will also aid in the improvement of NDE techniques for the detection of these cracks. This novel technique for examining subsurface cracks will be useful in the study of subsurface cracks in other alloys.

Acknowledgments

I would like to give my heartfelt thanks to my advisor and Chair of my committee, Professor Morris E. Fine, who made all of this possible. His unwavering support and kind guidance have helped me to continue at times when I questioned if it were possible. His extensive knowledge never fails to amaze me.

I also extend my thanks to my committee members: Professor Jan D. Achenbach; Professor Julia Weertman and Professor Johannes Weertman for their many suggestions and for their time. Professor Achenbach helped me with the NDE aspects of the research and carefully edited my publications and made many excellent suggestions. In addition, Professor Leon Keer has been very helpful in our discussions with Professor Fine regarding the mechanics of fretting fatigue.

Dr. James Newman gave me guidance on the operation of FASTRAN II - A Fatigue Crack Growth Structural Analysis Program, which he has developed. Dr. Wei Li instructed me on the operation of the scanning acoustic microscope.

Thanks to Professor Mike Meshii for his valuable mentoring in Toastmasters International. Dr. Joe Santner and Mr. John Graebel, who have a great deal of experience in industry, have assisted me with advice regarding the manufacturing world.

I would like to acknowledge the Federal Aviation Administration, the National Science Foundation and Zonta International for support for my research and members

of Zonta International have supported me with their friendship. The material for the test specimens was provided by Dr. Robert Bucci of Alcoa.

I have made many wonderful friends during my stay at Northwestern: Barbara Nichols who is trustworthy, loyal and always helpful; Linda Kearfott who encouraged me and also helped me with complications regarding FAA reporting, computer problems, and phone calls to mention a few; Dr. Chih-Ming Ke who is always cheerful and a real team player; Dr. Hareesh Mavoori who is compassionate and understanding; Michael Gagliano and Robert Gagliano who held many discussions with me about their research and mine and also bolstered me; Dr. Mike Loomans who is steadfast and wise and Rodney McCabe who accompanied me to Toastmasters meetings and gave me beneficial evaluations.

Richard Dojutrek machined numerous specimens, an extremely tedious task of drilling and chamfering rivet holes with great precision. Mark Seniw trained me on the equipment in the Mechanical Behavior Facility. Joanna Gwinn granted me her time and guidance.

My dear family encouraged me throughout, put their own lives on hold to help me when I needed them and always lifted my self-esteem.

Table of Contents

List of Tables

List of Figures

1. Introduction

Riveted joints have been investigated in a wide variety of structures ranging from bridges to airplane bodies to ships. Extensive research has been performed on these riveted joints to determine the modes and causes of failure. Recently, a team of forensic specialists has examined pieces of the Titanic to determine the cause of the hull failing. ["For Want", 1998] Steel bridges are monitored for fatigue cracking using various NDE methods such as acoustic emission, eddy current, and magnetic perturbation. [Chase, 1994; Yaney, 1995; Ghorbanpoor, et al., 1993] At the present time, the fatigue cracks in many of our current structures are sometimes large enough to cause concern but not so large as to be hazardous.

As the costs for replacing structures steadily increases, it becomes more and more attractive to use the existing structures as long as possible. This is the case with commercial and military aircraft that are being flown long past the design life of the aircraft. The design life of aircraft is typically 20 years. [Hoggard, 1991] As time goes on, the percentage of aircraft in operation that is older than the design life increases. Planes are now being flown in excess of four times the design life. The trend is for aircraft to be in operation more than one, and sometimes more than two, economic

lifetimes. [Carlyle, 1993] In 1993, the design retirement age for aircraft was 21 years. [Samsonov, 1995] By the year 2005, the design retirement age for aircraft will be 29 years. This necessitates better inspection methods to insure the safety of the planes.

The first aircraft accidents, which were known to be fatigue, related occurred in 1954 when the fuselages of two Comet I commercial aircraft broke up while in flight. [Burnside, 1993; Müller, 1995; Jones, 1993] Reconstruction of the fuselage of one of these aircraft revealed that a fatigue crack had started at one of the windows probably at a countersunk hole. A full-scale test of a Comet fuselage showed that the fuselage failed when a fatigue crack developed at the corner of an escape hatch. Military aircraft also experienced fatigue failures during this time. [Burnside, 1993; Jones, 1993]

In the early 1950's, the safe life philosophy was used for evaluating aircraft. With this, a safety factor of three or four was used to set limits on the safe life of the aircraft. [Burnside, 1993, Oster et al., 1992] Later the fail safe design approach was added. With this concept, the aircraft should be able to complete its flight and land safely after the failure of any main structural element. In the early 1970's, the U. S. Airforce began to follow the damage tolerance philosophy. [Lincoln, 1997] In the 1970's,the FAA began to subscribe to the damage tolerance approach. With this, the theories of fracture mechanics are utilized to determine the extent and the intervals for inspections of aircraft. The premise of this philosophy is that a crack would be detected and repaired before it grew to a catastrophic length. Using the damage

tolerance approach, an aircraft could theoretically fly indefinitely provided the inspection intervals were such that the aircraft could continue to fly safely between inspections. [Burnside, 1993; Oster et al., 1992] Presently, some aircraft are "retired for cause"; i.e. when the safety factor for continued operation is low enough that it is deemed too risky to continue operation. [Jappe et al., 1995] The U. S. Navy still uses the safe life concept and determines the safe life of the aircraft by full-scale fatigue tests. [Hocson and White, 1999]

Between 1981 and 1995, metal fatigue has contributed to more than 80 aircraft accidents. [Samsonov, 1995] In 1988, part of the fuselage of a Boeing B-737-200 was lost during flight due to the linking up of a number of fatigue cracks. [Oster et al., 1992; "Safety", 1988; Carlyle, 1993; Fitzpatrick et al., 1993; DeMeis, 1989] The Aloha Airlines accident in 1988 drew attention to the need for improving the detection of fatigue cracks in aircraft, especially aging aircraft. Shortly after this, other occurrences involving the airframe include a twelve-inch crack discovered by workers when stripping the paint from a B-737, a fourteen-inch crack in a B-727 found by maintenance workers after the plane made an emergency landing because it lost pressure, a failure in the cargo door of a B-747 and the subsequent loss of a section of the fuselage resulting in nine passengers being sucked out of the plane, and a twenty-inch long fatigue crack in a B-727-100 detected by preflight inspection.[Oster et al., 1992]

These incidents resulted in many studies involving the ability to predict the life of the lap joint in the fuselage of an aircraft and the ability to detect fatigue cracks before they grew to an unsafe length. Airframe sections, which are susceptible to fatigue cracks, include the wings and the fuselage. The fatigue cracks usually initiate at the riveted joints in these components. The cracks grow until they link up causing a great deal of expense and time in repairs and can lead to catastrophic failure. Small cracks may form in many adjacent rivets resulting in what is called multiple site damage (MSD). As a rule, a crack may grow to several inches before the structure is dangerously weakened, but with MSD, the many small cracks at adjacent rivets can weaken the structure rapidly. [Weber, 1995; Cordell, 1995] From results of experiments performed on lap joint specimens like a section of the lap joint in a fuselage and containing machined cracks to simulate MSD, it was concluded that in the presence of MSD, catastrophic failure would occur after the first link up of cracks. [Singh et al., 1994]

Fatigue cracks in the fuselage continue to be a problem as indicated by the Airworthiness Directive issued by the FAA on February 18, 1999, ordering the inspections of lower skin panel lap joints for fatigue cracking on older Boeing 727's, because fatigue cracks had been found in four of the operational 727's in the commercial fleet.* A greater understanding of crack initiation and propagation in

* Associated Press Release on February 18, 1999

riveted joints will aid in developing better inspection techniques and in validating and improving crack growth models. With better crack growth models, crack prediction techniques and inspection techniques, inspections can be scheduled more economically. This thesis is a contribution to this area. The cracks start at or near surfaces that cannot be examined optically making difficult nondestructive evaluation (NDE) of such cracks before they reach outside surfaces. Much of this thesis is devoted to studying hidden cracks.

2. Background

2.1. Introduction

While there have been many extensive studies of fatigue crack initiation and micro-crack growth in bulk aluminum alloy specimens and specimens with stress risers, there have been very few such studies in specimens with rivets. Fatigue cracks have been studied using a variety of methods including optical microscopy, scanning electron microscopy (SEM) and in-situ microscopy but there has been little use of the scanning acoustic microscope to investigate subsurface cracking. This chapter starts with review of selected papers on fatigue at stress risers, followed by riveted specimens. A discussion of acoustic microscopy will complete this chapter.

2.2. Research on Holes, Notches and Saw Cuts 2000 Type Aluminum Alloys

Replicas of surfaces near stress risers have frequently been taken to provide a history of the crack growth. [Connor et al. 1997; Connor et al. 1998; Swain et al. 1984; Newman et al. 1992; Newman et al. 1988; McMillan et al. 1967; Kaynak et al. 1992] These replicas were later viewed in the SEM to gather information about the crack

growth. Initially, studies were done on simple specimens with holes, notches or saw cuts before trying to understand more complex specimens.

One such study on a simple specimen containing a single countersunk hole was performed by Fadragas (1993). In this study, in-situ microscopy was used to measure crack growth in specimens of Alclad 2024-T3. A significant variation of about 300 percent was observed in the cycles to initiation of a detectable 500 μm long crack under closely controlled conditions that were intended to be identical. The holes were made with a computer controlled machine tool and the maximum and minimum loads in the fatigue cycle were constant. The fatigue cracks initiated as microcracks in the "blunt knife edges" of the countersunk rivet holes and then extended as Mode I cracks.

McMillan and Pellox (1967) completed a study of fatigue crack propagation in center-notched panels of 2024-T3 aluminum under variable amplitude loading. In this case, a traveling microscope was used for in-situ crack measurements. Replicas were taken for examination under the scanning electron microscope. The replicas were shadowed in the direction parallel to the crack propagation so that the dark side of each striation always faced the crack front. From examination of the replicas, it was concluded that fatigue crack growth only occurs during the loading portion of the fatigue cycle.

Many studies have been performed in an effort to understand crack initiation and crack growth mechanisms. It is generally agreed that cracks initiate at inclusion

particles, slip bands or voids. [Kung and Fine, 1979; Swain and Newman, 1984; Newman et al., 1988; Kaynak and Ankara, 1992; Newman et al., 1992] Some of the investigations on crack initiation and crack growth mechanisms are discussed in the subsequent paragraphs.

Replicas were used by Swain and Newman (1984) to study initiation and growth of small cracks from edge notches in 2024-T3 aluminum alloy sheets under constant amplitude loading. In this work, they defined small cracks as 5-500 μm. Accurate surface crack lengths for all crack lengths were obtained from the replicas, but marker bands did not give dependable cracks lengths for cracks smaller than 2 mm. The cracks looked as though they had initiated at inclusion clusters. Also, they reported that the orientation of the fatigue striations changes at the grain boundary.

In another study undertaken by Newman et al (1988) on short crack growth behavior in semi-circular notched specimens revealed that cracks nucleated at inclusion particle clusters or voids on the notch surface. Plastic replication was utilized to record the crack growth. The "short-crack" effect was observed i.e. the short cracks grew faster than long cracks.

Kaynak and Ankara (1992) investigated short crack growth behavior on 2024-T3 Al edge-notched sheet specimens. Again, plastic replicas were taken of the cracks to record the growth of the short cracks. Crack initiation sites were usually at inclusion particle clusters. As expected, the cracks generally grew as semi-elliptical

cracks from near the middle of the notch thickness. The large amount of scatter that was seen in the low range of the stress intensity factor was attributed to microstructural effects of the short crack. Increasing the stress level resulted in a corresponding increase in the number of cracks at the notch. An important conclusion was that short crack growth rates increased as R went from 0 to -1.

In a cooperative program between the National Aeronautics and Space Administration (NASA) and the Chinese Aeronautics and Astronautical Establishment (CAE), small crack growth was studied in single-edge-notch-tension (SENT) fatigue specimens of aluminum alloys. [Newman et al., 1992; Newman et al., 1994] Results of these tests showed that small cracks grow below the stress intensity factor threshold of large cracks. Slip band formation in the cladding was one of the mechanisms for crack initiation in the clad material. Cracks also propagated from inclusion particles or voids. Crack growth rates for these small cracks were predicted using a crack-closure model.

A study was carried out by Kung and Fine (1979) on edge notched specimens of 2024-T4 and 2124-T4 aluminum found that at high stresses, the initiation sites for fatigue cracks were on coarse slip lines whereas at low stresses, the initiation sites were often near constituent particles.

Tests conducted on stiffened panels with saw cuts to simulate MSD showed that the residual strength was greatly reduced with MSD. The amount of reduction in

the residual strength increased as the number of crack sites increased. [Newman, 1995] Experiments were run by Bray et al. (1999) to compare 2024-T3 and 2524-T3 panels containing MSD. The lead crack was made by sawing between five central holes and then notching the ends of the crack by electrodischarge machining (EDM). EDM notches at the other holes simulated multisite damage (MSD). Fatigue tests were also run on specimens containing four rows of drilled and deburred holes with no artificially induced cracks. Results from these experiments suggest that the 2524-T3 material offers an improvement over the 2024-T3 material in both residual strength and in fatigue life. Additional studies have been made on riveted joints to determine if the 2524-T3 still has more residual strength and a longer fatigue life than the 2024-T3 in riveted specimens. The results of this study are reported in Chapter 5.

In summary, replicas are often taken when doing studies of crack initiation and crack as a means of observing crack initiation and crack growth. Even in the presence of stress risers, inclusions and constituent particles play important roles in initiation of fatigue cracks. Reducing their number increases the number of cycles to fatigue crack initiation. This is discussed further in Chapter 4. Microcracks and short cracks propagate at stresses much below those for long cracks. Crack closure effects are at least partially responsible for this behavior. Typical of fatigue tests, there is scatter among fatigue lifetime data values for tests intended to be identical.

Many studies have been made on panels with a single drilled or chamfered hole and on riveted joints that have saw cuts or EDM notches machined into the joints prior to fatigue testing. [Samavedan and Hoadley, 1994; McBride, 1999; Gruber et al., 1996; Gruber et al., 1997] However, these do not accurately represent a naturally occurring fatigue crack.

2.3. Riveted Aluminum Alloy Joints

The load transfer conditions for riveted lap joint specimens fatigued in tension are very different from unriveted specimens with a rivet hole. The load is concentrated at the rivets with load by-pass occurring in the panels that are riveted together so that the outer rows of rivets carry the largest load. Moreover, even if the load axis is along the centerline of the riveted panels, there is a bending moment exerted on the outer rivets, and these are the rivets where failure is expected. Other factors, such as the amount of clearance or interference in the fit of the rivet in the hole and friction between the two sheets, also affect the load transfer conditions for a riveted lap joint specimen. [Schijve, 1992; Jones et al., 1992; Newman et al., 1997; Müller,1995] In the case of riveted joints containing chamfered panels, such as the ones used in this research, the chamfered panel will have less cross sectional area at the rivet hole than

the straight drilled panel resulting in cracks occurring in the outer rivet of the chamfered panel. [Connor et al., 1996]

Additionally, residual stresses are present in riveted joints. Using X-ray diffraction, Fitzgerald and Cohen (1994) found these stresses to be compressive in the rivet and tensile in the sheet at low riveting forces, but at higher riveting forces, the stress in the sheet became compressive. Such compressive stresses are expected to increase the initiation time and reduce the crack propagation rate. With finite element analysis, Müller (1995) also found residual compressive stress around the rivet hole and residual tensile stress a short distance away from the hole at higher riveting forces. The fuselage of an aircraft is loaded biaxially and so other Mode I stresses come into play. The curvature of the fuselage results in stresses in the skin of the fuselage. There are also shear stresses resulting from bending and twisting and this produces curving cracks. [Scott, 1997]

2.3.1. Previous Results on Cracks Occurring In Riveted Joints

Mayville and Sigelmann (1993) undertook a study of riveted lap joints. Statistical experimental design was used to reduce the number of tests required. The different parameters studied were stress level, rivet spacing, rivet type, rivet orientation, number of rivet rows and skin thickness. The only ones that were shown to have a significant effect on fatigue life were stress level, rivet type and skin

thickness. It was found that higher stresses made the occurrence of uniform multi-site damage (MSD) more likely. MSD almost always occurs in the critical row (Rivet 3 as shown in Figure 3.4) of rivets with cracks sometimes occurring in the second row of rivets. In Mayville and Sigelmann's investigation, the crack growth rate was found to be fairly constant for cracks up to 0.25 inches. This was determined by analysis of striation spacings on an actual aircraft. Fawaz (1997) also performed scanning electron microscope (SEM) fractographic examination for the purpose of obtaining crack growth data in riveted lap joints. This was accomplished by applying marker loads at intervals during the fatigue cycling. It was found that after about 80 percent of the life, cracks would break the surface of open hole specimens, while after about 70 percent of the life, cracks would break the surface of bonded (no rivets) lap joints. For an asymmetric riveted lap joint loaded to 75 MPa, small MSD cracks grew at about $2x10^{-3}$ μm/cycle. Crack fronts were oblique elliptical until final fast fracture when they became slanted.

Mayville and Sigelmann (1993) found that the benefit of increasing the skin thickness is counteracted by an increase in the measured bending stress just above the critical row of rivets. One possible explanation for MSD given by them is that there exists a small amount of scatter in the fatigue lives of rivet holes. Short cracks can catch up with longer cracks because of an initially decreasing stress intensity factor

with crack length due to the falling off of the stress concentration factor. The compressive residual stresses at the rivet shank vanish with distance from the rivet.

In many of the cases involving fatigue cracks in the fuselage, the cracks occur in the upper row of rivets which has been designated the critical row of rivets. Due to the joint geometry and the loading of the joint, fatigue cracks will develop near the rivets in the outer layer of skin that has the countersunk rivet holes. Furthermore, these cracks will develop at multiple sites at nearly the same time. The solution to this problem is to remove the critical row of rivets, drill out the rivet holes and replace the rivets with a buttonhead type rivet. [Boeing Service Bulletins for Model 747, 737, 727] Mayville and Sigelmann (1993) conducted tests to determine the effectiveness of this repair. Panels were fatigued for a number of cycles varying from zero cycles to the number of cycles until at least one crack of length 0.1 inch was observed. Then the repair was made and the panels were fatigued until failure. After the repair, failure never occurred in the top (critical) row of rivets. Although the lower row of rivets will experience higher stresses than the middle row of rivets, cracks never initiated in the lower row of rivets in the lower skin.

Using strain gages, Scott (1997) detected load shedding to 100,000 cycles before the cracks became visible. Fatigue tests were completed with a maximum load of 32.1 kN and an R of 0.02. With the use of acoustic emission techniques, crack growth was detected as early as 140,000 cycles before the crack became visible.

Neither of these techniques enables the study of crack development prior to the crack becoming visible, because they are only able to detect a defect. It was found that fretting was heaviest in the critical row of rivets at crack initiation sites. Multiple cracking was observed at some rivets. Fatigue life scatter was largely attributed to variation in the number of cycles until crack initiation. Schijve (1994) explained the scatter in crack initiation to be very dependent on the surface conditions, as initiation is a surface phenomenon. Since crack growth is dependent on the bulk material, the scatter in the number of cycles until crack initiation will be greater than the scatter for crack growth.

Piascik et al. (1994) characterized widespread fatigue damage in a full size fuselage test article. By visual in-situ nondestructive examination, cracks were found to initiate first in the outer row of rivets in a specimen containing four rows of rivets. After cracks had linked up at all outer row rivet locations, the pressure testing was stopped. The rivets used in this research were "button" head rivets.

By nondestructive examination (visual at 10x and eddy current), through cracks were usually found in the outer row of rivets in the outer skin. These cracks were noted in the panel either at the horizontal centerline of the rivet hole or in the upper half of the hole. Crack propagation was nearly normal to the fuselage hoop stress. No evidence of cracking was found on the inner surfaces. By in-situ visual examination, MSD was not detected until approximately 83% of the life. [Piascik et al., 1994]

After wide spread damage by destructive examinations, cracks were found in the second row of four rows of rivets in the panel with countersunk holes and were found in the third row of rivets in the panel with straight drilled holes. Cracks initiated at or near rivet hole corners, rivet hole surfaces and both panel surfaces. In some cracks, fretting was found near where the cracks initiated. Defects at the surface cladding, at the rivet hole surface and at the inner skin corner were found to be crack initiators. The initiation sites were along the lap splice joint interface in the area of fretting for the cracks that linked up to form a long crack extending through several rivets. Their results show that these cracks propagated in the subsurface. A correlation was found between the severity of fretting and cracking. While some of the cracks initiated at the centerline of the rivet, many of the cracks depicted in the photographs initiated above the centerline of the rivet. Most of the cracks found in the critical row of rivets nucleated along the faying surface as a result of fretting. Fretting was found to be the main mode for crack nucleation in the critical rivet row. [Piascik et al., 1997] This is in agreement with the results presented herein. As the rivet holes were very carefully drilled, no defects were at the rivet holes and so no cracks initiated there unless a stress much greater than that normally experienced by the fuselage of an aircraft was applied.

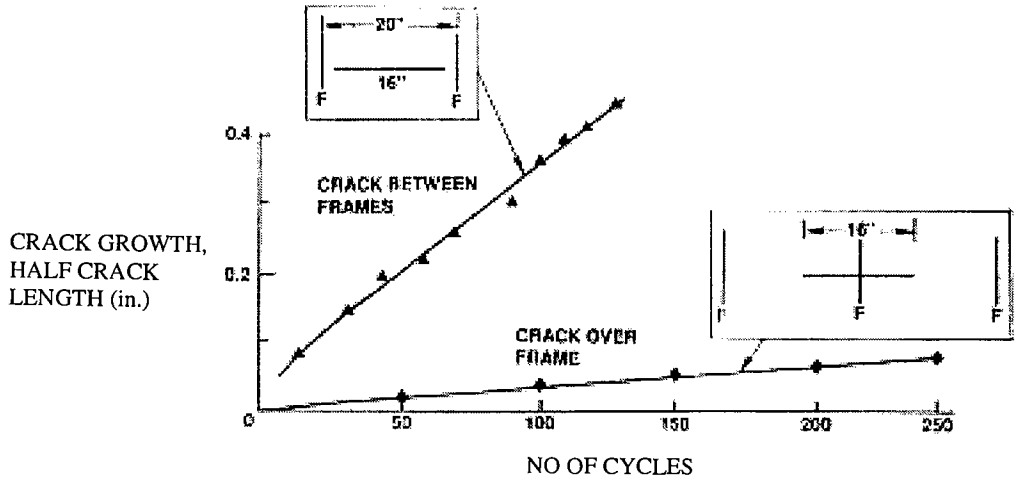

Fig. 2.1. Fatigue test crack growth rate in notched specimens (from Samavedam and Hoadley, 1994, Fracture and Fatigue Strength Evaluation of Multiple Site Damaged Aircraft Fuselages – Curved Panel Testing and Analysis. Final Report, DOT/FAA/CT-94/10, FAA Technical Center, Atlantic City International Airport, NJ, January, 1994, p.57).

Samavedam and Hoadley (1994) designed a test facility for conducting tests on full-sized curved fuselage panels. For these tests, some of the panels had notches machined into the panel before riveting and some of the panels were precracked prior to riveting. The panels were riveted after the notches were machined and after the panels were precracked. Results were given for two of the panels that were notched. Typical crack growth rates for these panels are shown in Figure 2.1. Crack growth rates were given for some of the cracks that grew from the precracked specimens. Results from these are given in Figure 2.2. Flapping occurred when a 24 inch machined-in crack reached the next frames and turned circumferentially; however, tests

with a 12.4 inch initial crack at the critical row of rivets revealed that the crack had no tendency to turn as it grew.

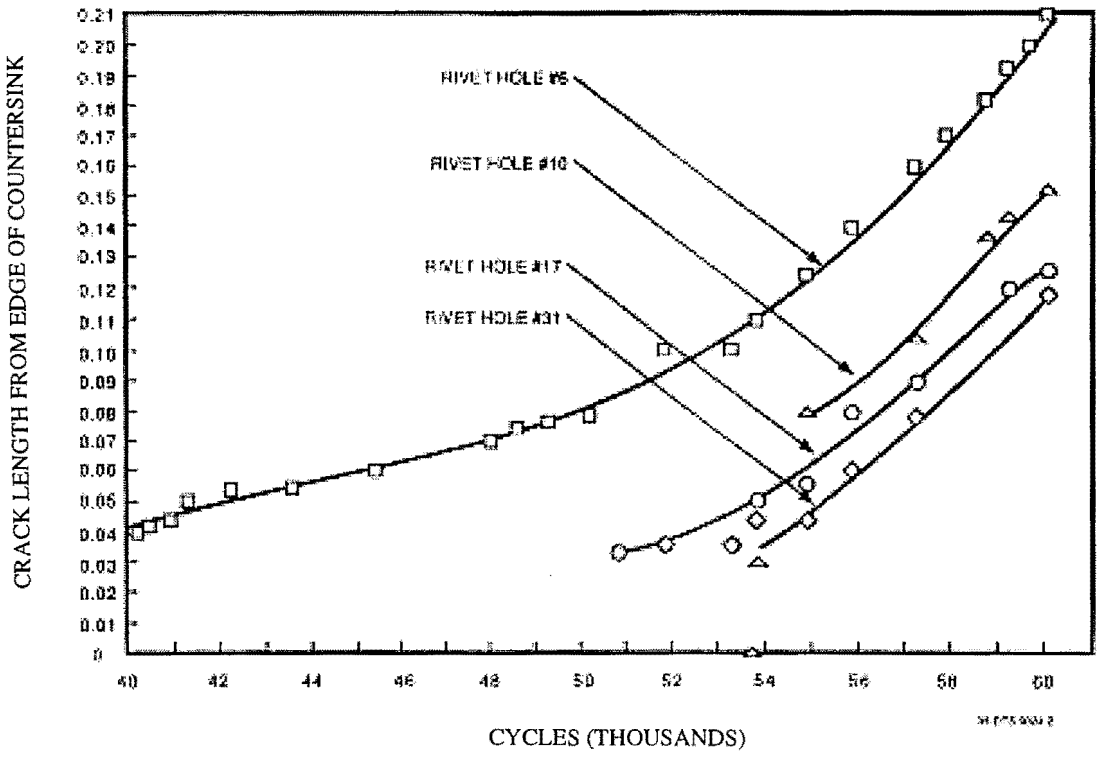

Fig. 2.2. Crack growth data in precracked specimens (from Samavedam and Hoadley, 1994, Fracture and Fatigue Strength Evaluation of Multiple Site Damaged Aircraft Fuselages – Curved Panel Testing and Analysis. Final Report, DOT/FAA/CT-94/10, FAA Technical Center, Atlantic City International Airport, NJ, January, 1994, p. 47).

Studies conducted by Hartman (1971) revealed that the fatigue life for an Alclad 2024-T3 riveted joint is 3 or 4 times that of a 7075-T6 clad-riveted joint, but that the bending factor was about the same for the two alloys. Reducing the load to 75% of the original load resulted in a tripling of the fatigue life.

A holographic nondestructive evaluation (NDE) technique was developed by Baird et al. (1996) to compare the deformation that occurs in riveted lap joints at various loads. The joints consisted of two sheets of 2024 T3 Alclad joined by three rows of 4 mm diameter rivets spaced 25 mm apart. Two exposures were taken at slightly different loads and then superimposed to produce the interferograms. Two different methods of deformation occur, one at low loads and one at high loads. At low loads, the rivet and the surrounding sheet material appeared to move as a single body indicating that friction forces between the two sheets of material in the lap joint was the primary mechanism for load transfer. At high loads, the friction forces seemed to play a much smaller part in the load transfer and a larger portion of the load was transferred through the rivet shank. This is also observed to be the case in the research presented herein.

It was found that by increasing the bucktail diameter, the average number of cycles until crack initiation (0.1 inch crack) was increased by a factor of 2. [Mayville and Sigelmann, 1993]. Cold working the rivet hole has been shown to increase the fatigue life in both new and repaired fuselages. [Reid and Restis, 1997; Leon, 1997] An increase in the residual compressive stress around the rivet hole would result from either increasing the bucktail diameter, by cold working the hole or by increasing the interference fit by carefully machining the rivet hole to be very close to the diameter of the rivet. Carefully machining the rivet hole close to the diameter of the rivet to insure

an equal amount of interference fit was the method used in the research presented herein. In this way, the bucktail diameter was kept within the limits of the Boeing specification being followed.

Müller (1995) discusses the importance of variables such as hole expansion, depth of countersink, and rivet squeeze force. He found that if the amount of squeeze force were great enough that fatigue cracks would initiate outside of the rivet hole whereas at a low squeeze force, the cracks initiate close to the centerline of the rivet and at the rivet hole. The reasons the cracks initiate outside the rivet hole at high squeeze forces is because of the residual compressive stresses near the hole, high bending stresses and fretting. By increasing the rivet head diameter, he found that the fatigue life could be improved by as much as 10 times.

Experiments performed by Sproat (1999) with various amounts of interference fit in rivets showed a potential increase in the fatigue life of the specimens by nearly as much as a factor of ten. The most effective amount of interference is between 0.09 mm and 0.13 mm. An added benefit of this interference is the lessening of production flaws such as roughness.

In summary, initial studies were performed on simple specimens with holes, notches or saw cuts. As expected, cracks formed at the edge of the hole and at the centerline in these simple specimens due to the stress intensity factor being greatest at the edge of the hole. It was found that crack initiation sites were on slip lines, inclusion

particles, or voids. [Kung and Fine, 1979; Swain et al., 1984; Newman et al., 1988; Newman et al., 1992; Kaynak and Ankara, 1992] Loading conditions are more complex on riveted specimens than on simple specimens. When studies were performed on these more complex joints, it was found that the cracks nucleated in the fretted areas, at defects in the surface cladding, at the rivet hole surface, outside the rivet hole and at the inner skin corner. [Heoppner et al., 1996; Piascik et al., 1994; Piascik et al., 1997; Müller, 1995] In the simple specimens, there was a wide variation in the number of cycles until crack initiation. This is due to crack initiation being a surface phenomenon. [Schijve, 1994] In the riveted specimens, there was a wide variation in the number of cycles until failure. This was again contributed to a wide variation in the number of cycles until crack initiation. Factors such as amount of squeeze force, stress level, rivet type, skin thickness, and amount of interference fit have been shown to affect the initiation sites as well as the life of the joint. [Mayville and Sigelmann, 1993; Reid and Restis, 1997; Leon, 1997; Müller, 1995; Sproat, 1999]

A great deal of research has been performed to obtained crack growth data on riveted lap joints. Most of the tests were performed on specimens with EDM notches or on specimens that were cracked prior to riveting. For the research presented herein, tests were performed on specimens without initial cracks so that naturally occurring cracks were studied. In previous research, cracks were examined and crack growth data were gathered after the cracks became surface breaking cracks. However, in the

research performed for this thesis, cracks were examined and crack growth data were gathered for subsurface cracks using the scanning acoustic microscope (SAM).

2.4. Corrosion or Fretting Fatigue as Causes of Fatigue Cracks

McGraw-Hill Dictionary of Science and Engineering (1984) defines fretting corrosion as "surface damage usually in an air environment between two surfaces, one or both of which are metals, in close contact under pressure and subject to a slight relative motion' and defines corrosion fatigue as "damage to or failure of a metal due to corrosion combined with fluctuating fatigue stresses".

From these definitions, it is difficult to determine the difference between the two mechanisms. When fretting corrosion is taking place, the surfaces in contact with each other are damaged by the sliding motion and this results in oxide debris. [Moore, 1990] The debris will weld to the surfaces and then work harden until they break away due to the shear stresses and the corrosive atmosphere. Also, metals with good fatigue strength do not usually have good resistance to fretting fatigue.

A different mechanism is at work with corrosion fatigue. In this case, transgranular cracking with very little branching taking place and usually pitting is observed. No oxide debris would be present during corrosion fatigue except for shear motions of the fracture surfaces against each other. It is important to determine which

of these two mechanisms is taking place, because they are diminished by different means. Increasing surface hardness can reduce fretting fatigue by such means as shot-peening or nitriding; whereas, painting, cladding or plating can decrease corrosion fatigue, but this does not protect fresh crack surfaces from corrosion. [Moore, 1990]

There is often disagreement as to whether a crack developed due to fretting fatigue or corrosion fatigue. In fact, this is the case with the 1988 Aloha incident where both corrosion and fretting fatigue were taking place. Much more attention has been given to fretting fatigue with regards to the fatigue cracks that occur in the riveted lap joints of a fuselage. This may be due to ample evidence of fretting debris in joints containing cracks.

2.4.1. Fretting Fatigue

There is some disagreement as to whether the majority of the life during fretting fatigue involves nucleation or propagation. Using acoustic emission, small cracks have been observed in aluminum after about 0.1 % of the lifetime when the lifetime is 10 million cycles. [Waterhouse, 1981; Hoeppner et al., 1994] On the other hand, Newman's (1992) life prediction code, FASTRAN, predicts that 80% of the lifetime is encompassed in growing a fatigue crack to a length of 0.1 mm. Some of the disagreement as to whether the majority of the life involves nucleation or propagation is due to different definitions of initiation. In a study of riveted lap joints performed

by Mayville and Sigelmann (1993), they defined initiation as the number of cycles until a crack of 0.1 inches in length was detected in the critical row of rivets. This crack length measurement was taken on the surface of the material from the edge of the rivet head. The number of cycles until crack initiation so defined varied from 30,000 to 127,000 cycles. The tests were performed using a fixture capable of applying shear/tension ratios up to 0.2. The crack initiation time, defined by Müller (1995) as the length of time until a crack between 1 and 2 mm had formed, was found to be about 90 per cent of the life. Müller also defined the crack initiation time as the length of time until a crack is visible.

An extensive study on the role of fretting fatigue in riveted Al alloy joints was done by Heoppner et al. (1996). A lap joint panel from a Boeing 707 was examined to determine the crack nucleation sites. It was determined that the cracks nucleated in the fretted areas, but no information was given as to whether the cracks nucleated at the knife edge or elsewhere. Then specimens were fabricated and an antibending system was installed to offset the tendency of the riveted specimens to bend during the tensile loading. In these tests with the fabricated specimens, the locations of the crack nucleation sites were given. For both types of rivets, as determined by post failure examination most of the cracks nucleated at the knife edge.

A study by Nishioka and Hirakawa (1972) found that fretting fatigue strength decreased only slightly as the contact pressure was increased. To them, this implied

that the fatigue stresses arising from the applied forces, rather than the contact pressure, played the major role in reducing the fretting fatigue strength. The wear-based mechanism of crack nucleation entails crack nucleation at the fretted surface. These cracks act as stress raisers and one of these cracks will enter the substrate at some point. [Beard, 1988; Hoeppner et al., 1994]

Waterhouse (1981) found that the initial part of a fretting fatigue crack is open and fills with fretting debris which plays a role in the amount that the crack is held open. Also, the crack grows at an angle to the surface until it gets beyond the influence of the fretting action and then it grows perpendicular to the applied stress.

It has not been determined conclusively what effect the hardness of the materials has on fretting fatigue. The Engineering Science Data Unit [Hoeppner et al., 1994] proposes that harder surfaces are less susceptible to fretting fatigue damage. If the mating surfaces differ in hardness and both surfaces are subjected to bulk stresses, the softer material will often fail first. Other sources claim that less fretting corrosion will occur with two dissimilar surfaces than with similar surfaces. If a metallic coating is applied to a substrate that has a lower yield stress than the substrate, cracks may form in the coating at a substantially lower stress than the yield stress of the substrate. Cracks in the coating will act as stress raisers and will result in crack nucleation in the substrate.

While fretting will expedite the initiation of fatigue because it results in flaws, continued fretting has little effect. The exception to this, of course, is that debris may get into cracks and affect the lifetime. [Reeves et al., 1976; Hoeppner et al., 1994] Nishioka et al. (1969) concluded that the presence of wear, pits and particles caught in the crack can result in a variation in the stress amplitude from cycle to cycle in fretting fatigue.

Fretting has been found to definitely be the cause of cracks in some instances. When cracks nucleate away from rivet holes in aircraft joints, this is an indication that they were caused by fretting. [Hoeppner, 1994] Müller (1995) has shown that the amount of clamp up force used during the riveting process can also change the crack location. The crack will move away from the rivet hole when the riveting force becomes large enough. In analyzing the effect of squeeze force, Fawaz (1997) found that a high squeeze force results in the maximum tensile stress occurring at the edge of the rivet hole and is constant through the thickness, whereas the maximum tensile stress will occur at the faying surface and will decrease through the thickness when moving toward the free surface and when a low squeeze force is used. Figure 2.3 is a sketch of the cross section of the riveted joint and points out the free surfaces and the faying surface. In the research presented in this dissertation, it has been found that the maximum nominal fatigue stress determines whether the crack to nucleate away from

the rivet hole and whether the crack will be at the center line of the rivet and perpendicular to the loading direction. This will be discussed further in Chapter 4.

Results of FE modeling revealed that the least amount of interference between the rivet and the hole is at the fayed surface so that cracks are likely to start on the fayed surface. [Müller, 1995] Also, Müller (1995) showed by FE modeling that the residual stresses are small in the countersink region of the hole and has reasoned that any interference fit will be lost first in this region of the hole. The straight drilled portion of the hole would then bear the load. The smaller area bearing the load in the countersunk sheet as compared with the straight drilled sheet will result in cracking in the countersunk sheet. [Müller, 1995] Fatigue cracks have been seen to initiate near the boundary between the fretted/non-fretted region. [Waterhouse, 1981] Fawaz (1997) obtained centerline cracks when the ratio of the diameter of the bucktail to the diameter of the rivet shank, D/D_0, was less than 1.3.

In riveted joints, three different types of fretting fatigue can occur. These are the flat mated surfaces sliding against one another results in fretting, the rivets sliding in the holes and experiencing changing interface pressures due to the pin loading, and some combination of the aforementioned types. [Forsyth, 1981]

Forsyth (1981) also gives an example of fatigue cracks developing in a wheel to which a square shaft had been keyed. It would be expected that the cracks would develop at the corners of the keyway where the stress is concentrated; however, the

cracks developed some distance up on the side of the slot where fretting was taking place illustrating that fretting has overcome the stress concentration.

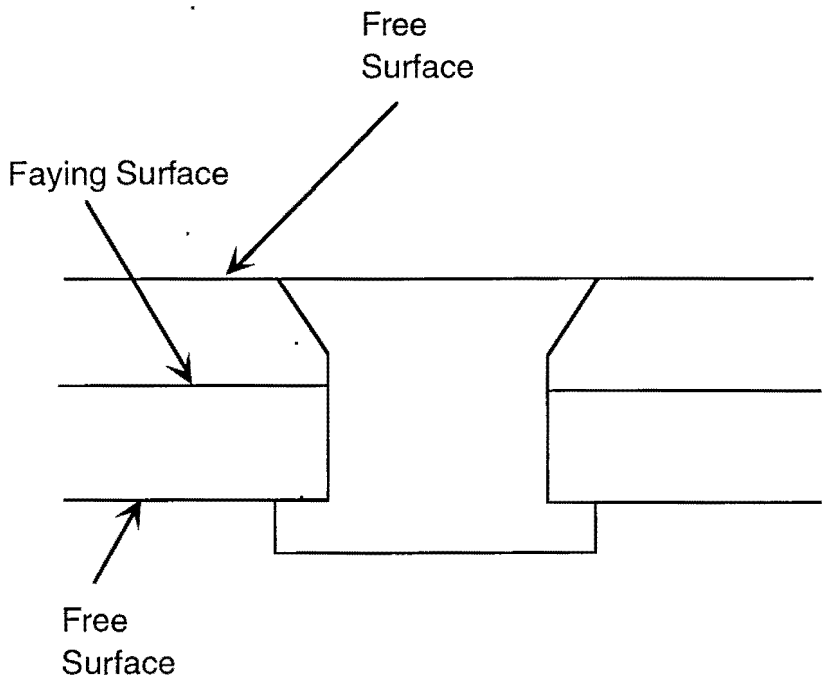

Fig. 2.3. Sketch of cross section of riveted joint

2.4.2. Corrosion Fatigue

It has been shown that the effects of the atmosphere are more pronounced when crack growth is slow. Time plays a factor in corrosion and so the frequency will have an effect on the occurrence of corrosion. As the frequency increases, corrosion will have less influence. [Hoeppner, 1996; Waterhouse, 1981] It is important, therefore, to carefully select the frequency when studying the effects of corrosion.

Endo (1981) found that an Al-4Zn-2Mg alloy was effected by humidity but that the effect of oxygen was negligible. Crack initiation occurred earlier and crack propagation occurred more quickly when a very small amount of humidity was present.

Using 10 mm x 10 mm x 1.6 mm specimens of 2024-T3 aluminum alloy sheet, Wei and Harlow (1996) studied the process of corrosion. Using energy dispersive x-ray (EDX), two types of constituent particles were identified: those containing Al, Cu and Mg and those containing Al, Cu, Fe and Mn. The particles containing Fe and Mn were found to be cathodic with respect to the matrix and so the pits formed adjacent to these particles could grow and link up to form larger pits. In this same study, it was found that a NaCl solution with a pH of 3 resulted in a small amount of pitting, while a solution with a pH of 11 resulted in a great deal of corrosion on the surface. Fatigue crack growth studies were performed using edge-crack specimens.

Circumferential and longitudinal lap joints containing corrosion pillowing and taken from the fuselages of aircraft have been examined by Bellinger et al. (1999) Corrosion pillowing is the deformation that occurs when corrosion products build up between the two sheets of skin material. Using FEA, it was suggested that the corrosion pillowing would result in an increase in stress on the faying surface of the outer skin and a corresponding decrease in stress on the outer surface. Bellinger et al. (1999) give this as an explanation for the crack growing more rapidly along the faying surface than it does through the thickness. Photomicrographs taken of a section

through the rivets and skins of a lap splice joint of a Boeing 707 fuselage revealed very heavy corrosion near the rivets resulting in severe pillowing. The 2024-T3 aluminum sheet in this fuselage was clad only on the outer surface and painted on the inner surface. [Inman et al., 1997] In a corrosion study carried out by Schmidt et al. (1996), it was found that cracks nucleated earlier in clad material than in bare material.

To summarize, while there is a great deal of disagreement as to whether the fatigue cracks in riveted lap joints are caused by fretting fatigue or corrosion, it is believed by this author that the fatigue cracks formed in the research presented herein are due to fretting fatigue as evidenced by a great deal of oxide wear debris found between the two panels. A great deal of fretting debris was also found in the lap joints of the aircraft involved in the 1988 Aloha accident.

2.5. Nondestructive Evaluation (NDE) Methods

Crack detection in commercial and military aircraft has become increasingly important as the lifetimes of aircraft are being extended past the design life. The aging fleet of aircraft requires more frequent inspection and the ability to detect smaller defects. The specification for crack detection of MSD in the top layer of lap joints is a 0.100 inch (2.54 mm) long crack with 90% reliability. [Weber, 1995] If cracks at rivets are detected even prior to this, it is possible to remove the rivet, drill a larger

hole and install a larger rivet thereby greatly reducing the cost of repair and the amount of time in which the aircraft is out of service. To detect these small cracks, NDE methods must be improved.

Currently, the rivets in the fuselages of aircraft are normally inspected using eddy current. [Yu, 2000] This method of inspection is insufficient, because fatigue cracks underneath the rivet head cannot be detected. The cracks are quite large by the time they can be detected using this method. Therefore, another method of NDE needs to be developed for the study and the detection of small fatigue cracks.

2.5.1. NDE Methods Currently Being Considered

McBride et al. (1999) used acoustic emission monitoring (AEM) to detect fatigue cracks at about half the number of cycles necessary to detect the cracks visually. Using acoustic emission and neural networks, Almeida and Hill (1995) have been able to separate crack growth signals from fretting signals in the response signals.

In reverse geometry x-ray (RGX), a raster of point detectors is used to give a two dimensional image. The specimen is placed close to the source (1 inch or less) for a large scan area. Large subsurface cracks have been detected with this method, and NASA Langley Research Center and McClellan Air Force Base are investigating it. [Albert and Froom, 1993] Another possible method for the detection of these subsurface fatigue cracks is computer tomography which uses penetrating radiation (x-

rays or gamma rays). [Azevedo et al., 1993] The imaging is performed using the attenuation of x-rays rather than the penetration of x-rays. This technique is reliable and accurate, but it is slow, expensive and inflexible.

The thermographic technique, thermal-wave imaging, can detect disbond and corrosion even under rivets, but cannot detect cracks under rivets. [Favro et al., 1993] Lesniak et al. (1993) have developed a thermographic technique, forced diffusion thermography, which can find cracks and disbonds by measuring a materials thermal response to a patterned heat flux. The temperature changes associated with the thermoelastic effect are less than 0.01°C. This technique is not practical at the present time because the scan time for a 128x128-pixel image is about one hour.

The Superconducting Quantum Interference Device (SQUID) eddy current technique has the potential for detecting subsurface cracks. [Ma et al., 1993] High-resolution SQUID magnetometers are very sensitive to dc and low frequency magnetic fields. This technique is more expensive than normal eddy current such as that currently being used for the inspection of fasteners in the fuselage, and the data interpretation is complicated. The equipment is more complex and liquid helium is required at the probe. [Wikswo, 1993]

Some promising eddy current techniques are emerging for the detection of cracks beneath rivet heads. The magneto-optic /eddy current imager (MOI) has been developed by Fitzpatrick et al. (1993) and has the advantage of output images that are

easy to interpret. Using MOI, a study was performed at Kelly Air Force Base using trained MOI Air Force NDI inspectors to determine the capability of the MOI inspection technique for the fuselage of the C-5 aircraft. Cracks 2.03 mm in length from the edge of the rivet head and with a probability of detection of 90% and cracks 3.84 mm in length from the edge of the rivet head and with a probability of detection of 90% and a confidence level of 95% were detected. [Fisher et al., 1999] Other methods of eddy current include pulsed eddy current Nortec Eddyscan 30, the Hocking FastScan, the Northrop low-frequency eddy current array and the Rohman Elotest with minirotor and GK Engineering probe. It has been reported that all of these methods can detect a crack 1 mm in length under the rivet head and in the first layer. [Hagemaier and Wilson, 1997] Harlow and Wei (1999) gathered data that had been obtained with the latest eddy current inspection techniques and including 45 inspectors. They found that on a POD scale, a 50 percentile crack 1.51 mm in length and a 90 percentile crack 1.95 mm in length could be detected.

D Sight is an optical process, which was developed by Hageniers (1993, 1995). This technique converts local surface curvature changes into greyscale changes with a sensitivity of 2 μm surface height change. It is fast, easy to use, non-contact, portable, documentable and repeatable, but it can only detect corrosion, not cracks.

It has been suggested that using a potential drop technique could monitor crack initiation and growth in airframes. The principle of this technique is that the current

will be modified when it encounters a defect and this will result in a change in the potential as the defect grows. In fact, crack initiation can be detected because the changes in the microstructure and in the internal stress and strain fields will change the electrical properties and so the potential drop will change. [Wojcik, 1995]

Yan and Nagy ("Laser", 1999) have developed a new method that uses an infrared laser and an ultrasonic system in combination. With this method, small cracks in aircraft details can be detected with much greater accuracy than other techniques. The infrared beam heats the material near the surface causing thermal expansion. The stresses resulting from this thermal expansion close the small fatigue cracks for an instant so that the ultrasonic echo coming from the cracks can be separated from the other parts of the ultrasonic echo. This technique is complicated and expensive and so would only be used for inspections that are extremely significant.

In the development of these new methods, very often notched or pre-cracked specimens are used. The indications from notches or pre-cracked specimens may not necessarily be very similar to the indications from actual fatigue cracks. Further, closed cracks are more difficult to detect than open saw cuts or EDM notches. To develop new NDE methods, it would be helpful to more fully understand the crack initiation and propagation of small naturally occurring fatigue cracks at riveted joints. The scanning acoustic microscope (SAM) may be used to gain this understanding especially in conjunction with fractography. "Rumpling" on the surface is the first

indication of a sub-surface crack; however, with the use of the SAM, sub-surface cracks can be detected long before there is any indication on the surface.

2.5.2. Scanning Acoustic Microscopy (SAM)

The first acoustic microscopes were built in the early 1970's. [Kessler et. al., 1972; Cunningham and Quate, 1973; Lemons and Quate, 1974; Wickramasinghe, 1983] Prior to this time, lenses free of aberrations were not available and piezoelectric thin films were not of a sufficient grade for ultrasonic transducers. It was found that a spherical lens fabricated from sapphire would be free of aberrations when the couplant is water. This is because the sapphire has a high velocity of sound while the water has a low velocity of sound. [Quate et al., 1979; Wickramasinghe, 1983]

Two kinds of acoustic microscopes are generally in use—point focus and line focus. SAMs are of the point focus variety. Lemons and Quate (1974) developed the first SAM in 1974. Here, a focused beam is scanned over and penetrates a specimen immersed in water; the depth of penetration depends on acoustic frequency and material properties. With the SAM, interference fringes are eliminated because the acoustic energy is focused over a diameter of less than one wavelength, and the image is formed by scanning one point at a time so that scattered radiation that causes interference fringes is eliminated. [Quate et al., 1979] Microstructures of specimens

prepared for metallographic examination can also be investigated using a SAM because different phases have different elastic constants.

The Lemons and Quate (1974) microscope employed a through transmission approach and was used to image a 200-mesh copper electron microscope grid. With the through transmission technique, one transducer sends the signal while another transducer receives the signal. The SAM used in the work described here uses the reflection technique where one transducer both sends and receives the signal. This circumvents the problem of aligning the two transducers.

The transducer is made of piezoelectric ZnO sandwiched between layers of gold; the lens is made of single crystal sapphire or silicon both of which have high velocities of sound as compared to the water couplant. [Wickramasinghe, 1983; Quate, 1979] The attenuation of acoustic waves is small in single crystal sapphire and silicon, another reason for selecting these for the lens. [Briggs, 1992] An early SAM for detecting internal flaws in materials was developed by Gilmore et al. (1986) Their system uses broadband acoustic pulses with a center frequency in the range of 10 - 100 MHz and a single crystal silicon acoustic lens.

There have been a great many applications of acoustic microscopy to study material properties and phenomena that occur in materials. Many reviews have been published [Quate, 1979; Hoppe and Beriter-Hahn, 1985; Briggs et al., 1989; Briggs et al., 1991; "Advances", 1995] The series "Advances in Acoustic Microscopy", edited

by Briggs and Arnold, has been published annually beginning with 1995. A particularly good article on detecting and measuring cracks in a variety of materials is that by Knauss et al. ["Advances", 1995]

Much of the work that has been done with the acoustic microscope has been to image the smooth surface of a solid while very little work has been done imaging the subsurface of solids. Some of the advantages of the acoustic microscope include the ability to obtain information in the subsurface, grain structures can be viewed in unetched materials because they are acoustically anisotropic and the mechanical and elastic properties of microstructures can be determined. [Wickramasinghe, 1983; Tsai et al., 1987] When using the acoustic microscope to image the surface, it can provide additional information from that obtained with the light microscope or the electron microscope as already discussed.

2.6. Summary

When imaging the subsurface, the acoustic microscope is in a league of its own. In the work presented herein, the scanning acoustic microscope is used to image the subsurface of riveted lap joint specimens. The fatigue cracks in riveted lap joints form on inner surfaces and is not initially visible on the outside surface. Using the acoustic microscope to examine the subsurface of the specimens in conjunction with the optical

microscope and the scanning electron microscope to examine the surface of the specimens and with fractography of fractured specimens, the formation and growth of subsurface cracks near rivets may be characterized in detail.

A quantitative investigation of fatigue cracks at and near rivet holes in lap joint specimens is reported herein. The effects of varying the maximum applied stress are included. For this study, the scanning acoustic microscope (SAM) was used to characterize subsurface cracks and the subsurface portion of the cracks after they broke the surface. Finally, the optical and scanning electron microscopes (SEM) were also used to characterize surface breaking cracks and to compliment the results of the SAM. For field NDE of aircraft, a subsurface technique is definitely needed, because the cracks in riveted panels are relative long, approximately 8 to 10 mm end-to-end, before they break through to an outer surface that can be view optically.

3. Experimental Procedures

3.1. Introduction

Investigation of the early stages of damage near riveted joints poses difficulties because the initial cracks form on hidden surfaces. When such cracks have grown to be visible on an outside surface, they are already relatively long on the hidden surface. An investigation of the initial stages of fatigue damage in flush head riveted panel specimens of Alclad 2024-T3 Al alloy was carried out using the scanning acoustic microscope (SAM) coupled with analysis of the fracture surfaces. The SAM sees hidden cracks just as they emerge from under the rivet head but before they are visible on the outside surface. This research program began with a study of fatigue damage around chamfered holes in panel specimens where the fatigue cracks are diametral normal to the applied stress. (Fadragas, 1993) With riveted specimens the crack initiation mode was found to be a function of applied nominal stress. At higher loads, the initiation mode was similar to that observed in panel specimens with chamfered rivet holes, that is, a diametral crack normal to the loading direction, but at lower nominal stresses a considerably different mode, an "eyebrow" mode, was observed. (Connor, 1997) At lower nominal stresses the cracks initiate some distance from the

rivet but at higher nominal stresses, they initiate at the rivet hole near the hidden corner.

3.2. Materials

The materials used in this research are commonly used in the fabrication of the riveted lap joints in the fuselages of aircraft. The sheet material used in the specimens is Alclad 2024-T3 aluminum alloy. The clad material is 1050 aluminum alloy and the rivets are 2017-T4 aluminum alloy. Both the fatigue lifetime and the microstructure of Alclad 2524-T3 were compared to Alclad 2024-T3.

3.2.1. Compositions

The compositions for the commercially "pure" aluminum, the 2024-T3 aluminum and the 2017-T4 aluminum are given in Table 3.1. The copper, magnesium and silicon in the 2024 alloy are the main elements aiding in strengthening during precipitation. A small amount of titanium is added as a grain refiner during the casting process. The manganese and chromium control the grain size during the wrought operations. During the preheat prior to the wrought operation, these elements must precipitate in the form of fine dispersoids to effectively control the grain size. [Aluminum, 1993] The 1050 aluminum is used to clad the base metal and galvanically

protect the base metal from corrosion; however, to this author's knowledge, no studies have been performed to determine if the soft aluminum encourages adhesion during fretting fatigue thereby promoting crack initiation.

Elements	*2024 aluminum (weight %)*	*2017 aluminum (weight %)*	*1050 aluminum (weight %)*
Si	0.50	0.20-0.8	0.25
Fe	0.50	0.7	0.40
Cu	3.8-4.9	3.5-4.5	0.05
Mn	0.3-0.9	0.40-1.0	0.05
Mg	1.2-1.8	0.40-0.8	0.05
Cr	0.10	0.10	-----
Zn	0.25	0.25	0.05
V			0.05
Ti	0.15	0.15	0.03
Other	0.15	0.15	
Al	Remainder	Remainder	99.50 (minimum)

✶ Aluminum and Aluminum Alloys. 1993. ASM International. The Materials Information Society. ASM International, Materials Park, OH: p 20.

Table 3.1. Composition of Materials

3.2.2. Properties

The mechanical properties of the Alclad 2024-T3 and the Alclad 2524-T3 alloys are listed in Table 3.2. The ductility of 2024 enables this material to be rolled into thin sheet. It has a very high strength-to-weight ratio of approximately 710 and better corrosion resistance than the 7000 series alloys. [Aluminum, 1993]

3.2.3. Heat Treatments

The temper designation for the 2024 and 2524 aluminum alloys used in the Alclad sheet material is T3 and indicates solution heat treatment followed by cold work i.e. stretching about 3% to give flat plates and then natural aging. [Heat Treating, 1981] The solution heat treatment for 2024 plate material is carried out at 495° C. This solution heat treatment allows the copper, silicon and magnesium to go into solution. GP zones develop from the resultant supersaturated solution at room temperature. The coherency strain fields formed from the interface of the GP zones with the matrix cause a higher stress to be required for deformation of the material. [Heat Treating, 1981] GP-I and GP-II zones are sheared by dislocations and this adds to the strengthening. Dislocations bow around the Ø' giving Orowan strengthening. [Courtney, 1990]

The temper designation for the 2017 aluminum alloy used in the rivets is T4. In this case, the material is solution heat treated and naturally aged with no cold work following the heat treatment.

As given in Table 3.2, the ultimate tensile strength for 2024-T3 Alclad is about 450 MPa (65 ksi). The fatigue strength is about 1/2 UTS for small specimens and about 1/3 UTS for large specimens. [Waterhouse, 1981] This would make the fatigue strength for small specimens about 220 MPa and for large specimens 149 MPa. The nominal applied stresses in these experiments, not greater than 154 MPa in all experiments except one at 206 MPa and one at 180 MPa, are well below the fatigue strength for small specimens. Calculation of the nominal applied stress is given later.

	Test Orientation	*2024-T3 Alclad*	*2524-T3 Alclad*
Ultimate Tensile Strength	L	67 ksi	67 ksi
	LT	66 ksi	66 ksi
Yield Strength	L	50 ksi	50 ksi
	LT	45 ksi	45 ksi
% Elongation	LT	18	18
Fracture Toughness	L-T	126 ksi $(in)^{1/2}$	148 ksi $(in)^{1/2}$
	T-L	128 ksi $(in)^{1/2}$	158 ksi $(in)^{1/2}$

**Private correspondence with Dr. Robert Bucci, Alcoa, 2000.

Table 3.2. Mechanical Properties of Materials

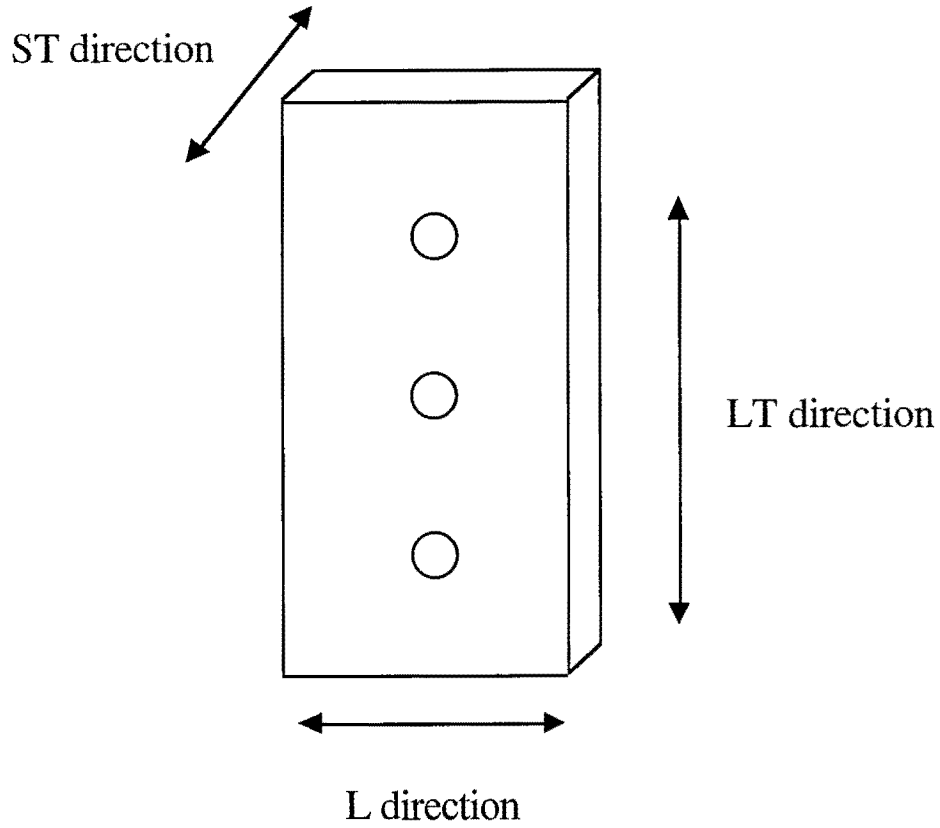

Fig. 3.1. Sketch of the countersunk sheet portion of the test specimen showing the directionality of the grains.

3.2.4. Microstructures

The Alclad 2024 sheet is rolled resulting in elongated grains in the rolling direction, which is called the longitudinal (L) direction. The directionality of the grains in the Alclad 2024-T3 material with respect to the specimens used in the research presented herein is given in Figure 3.1. A representative sample of the microstructure

in the longitudinal direction can be seen in Figure 3.2 and of the microstructure in the short transverse (ST) direction in Figure 3.3. The white phase is $CuAl_2$, the gray phase is either $CuMgAl_2$ or $Cu_2Mg_2Al_5$ and the dark particles are $CuMgAl_2$, Cu_2MnAl_{20} and Cu_2FeAl_7. [Aluminum, 1993] These are constituent particles. The precipitates and dispersoids are not seen at this magnification.

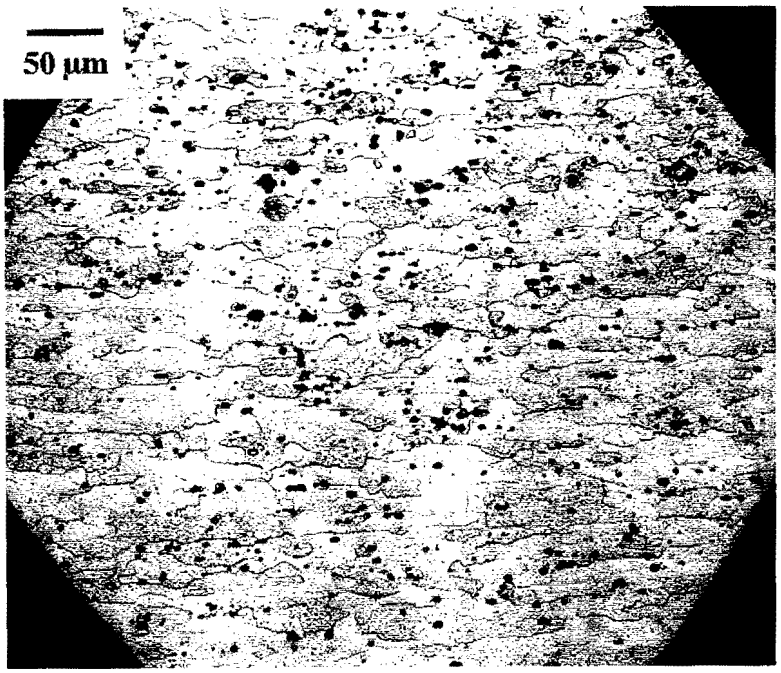

Fig. 3.2. Photomicrograph showing grains in the longitudinal (L) direction

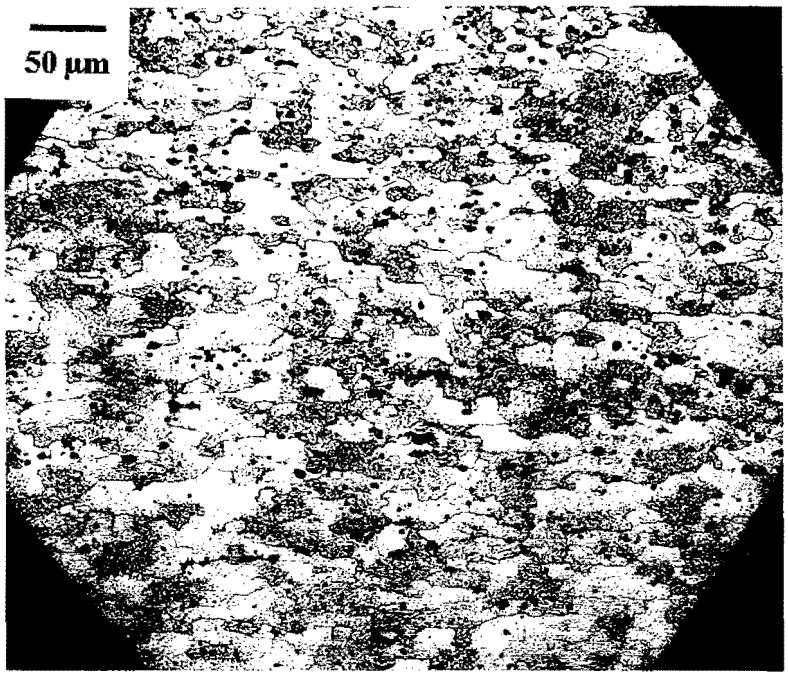

Fig. 3.3. Photomicrograph showing grains in the short transverse (ST) direction

The specimens were mounted in phenolic powder, which was consolidated using a Buehler's Speed Press II mounting press. Then the specimens were ground using 240, 320, 400, and 800 grit silicon carbide grinding papers sequentially with the specimens being carefully cleaned after each step. Then the specimens were polished using first a 0.3 μm alumina suspension and finally a 0.05 μm alumina suspension using a Buehler microcloth polishing cloth. The specimens were etched for about 15 seconds using a standard Keller's reagent consisting of 2 ml HF (48%), 3 ml HCl (concentrated), 5 ml HNO_3 (concentrated) and 190 ml H_2O.

3.3. Lap Joint Specimen Preparation

3.3.1. Three Rivet Specimen

Lap joint specimens were assembled from two pieces of Alclad 2024-T3 aluminum alloy sheets, one piece with countersunk rivet holes and one piece with straight drilled holes, using 2017-T4 aluminum alloy flat head rivets. The specimen geometry and dimensions are given in Figures 3.4a and 3.4b. The specimens for the comparison of Alclad 2024-T3 and Alclad 2524-T3 were fabricated in the same manner as other specimens with sheet material of Alclad 2024-T3. The sheet material for the comparison tests was 1.27 mm thick while that for all of the other tests was 1.02 mm thick.

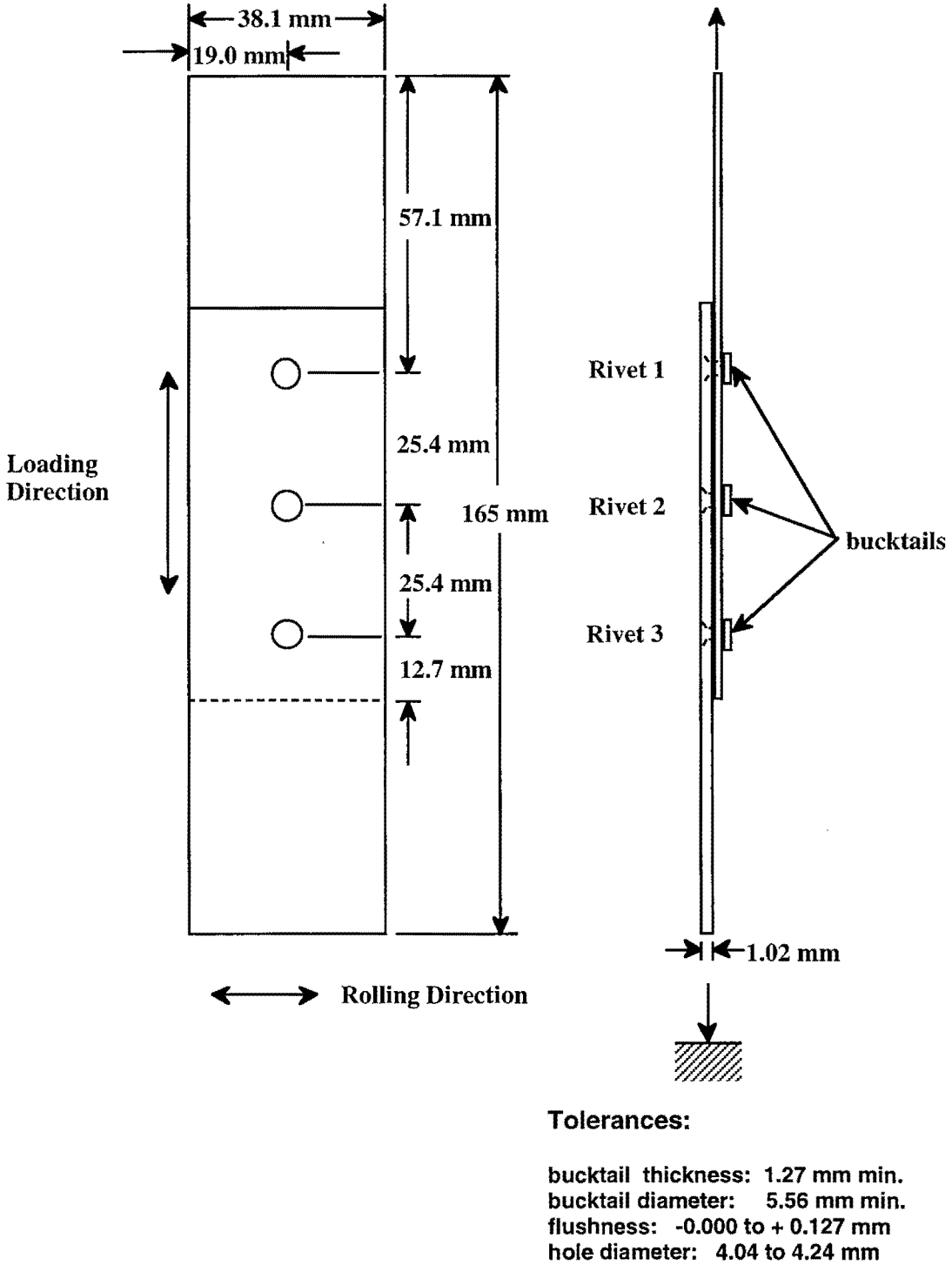

Fig. 3.4. a) Drawing of three rivet assembled specimen

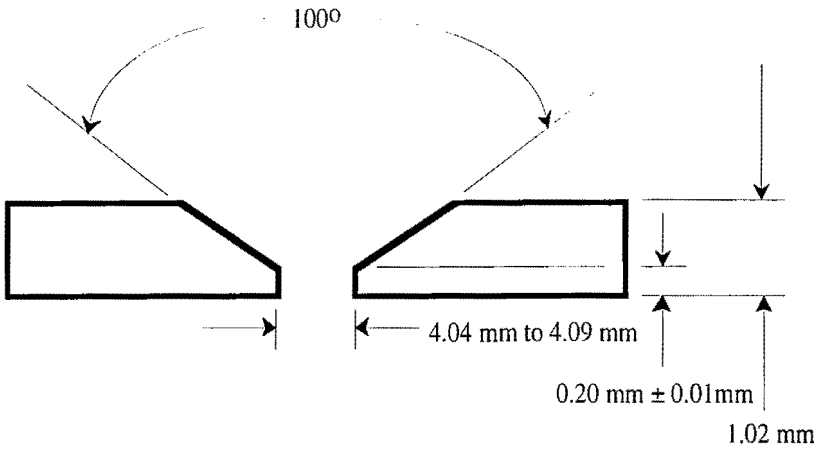

Fig. 3.4. b) Drawing of countersunk rivet hole

Schijve (1992) has shown that S-N curves are approximately the same for lap joints and asymmetric butt joints of 2024-T3 Alclad material. This was the rationale behind the test specimen geometry, and the results of this study are expected to be pertinent to both kinds of joints. The sheet material was 1.02 mm thick including a layer of 1050 aluminum alloy cladding 0.05 mm thick on each side. The chamfered rivets were 3.97 mm in diameter in the shank and 6.35 mm in length.

The rivet holes were drilled and countersunk using a computer controlled machining center. The holes were drilled at a speed of 2.54 mm/min. (0.1 in./min.), and there was a four second dwell time for the chamfer. The drilled hole diameters were between 4.04 mm and 4.09 mm. The limits for the hole diameter given in the Boeing

specification being followed are between 4.04 mm and 4.24 mm, with the smaller diameter being favored. [Boeing, 1970; Boeing, 1987] Due to the hole diameter being very close to the rivet diameter, there was an interference fit at all of the holes after the riveting process. The countersunk rivet holes had a 100^{o} included angle. The depth of the countersink was gradually increased until a knife edge of 0.20 mm ± 0.01 mm was obtained. This gave a knife edge of approximately 20% of the thickness of the panel as shown in Figure 3.4b. Typical flushness requirements for the rivet heads in aircraft panels, +0.102 mm to –0.000 mm, were met by the specimen geometry. ["Installation", 1990]

The panels were riveted together on a manually operated hydraulic press where the rivets were compressed between two flat plates at a constant load of 44.6 kN (5 tons) for the three rivet specimens and 133.8 kN (15 tons) for the seven rivet specimens. This load gave bucktail diameters of 6.12 mm ± 0.05 mm. A study has shown that the fatigue life is not dependent on the installation method i.e. hydraulic, pneumatic or by hand. [Hartman, 1968] Each specimen contained three rivets oriented in line parallel to the loading direction and the rivets were 25.4 mm apart in this direction. All variables were carefully controlled during the manufacture of the riveted joints. This included the hole diameter, the depth of the countersink and the amount of squeeze force that was applied during the riveting process. The amount of squeeze force will determine the amount of interference fit. Close tolerances were held on the

hole diameter so that an interference fit could be achieved each time. The fatigue life of the lap joint will normally increase with an interference fit. [Ekvall, 1986; Hoeppner, 1994] These specimens were not precracked or notched prior to riveting.

3.3.2. Seven Rivet Specimen

Seven rivet specimens were made in the same manner as the three rivet specimens but these specimens contained three columns of rivets with the distance between the columns of 38.1 mm (1.5 inches). By strain gage measurements, Müller (1995) found that the rivets in the outside columns of specimens with multiple columns of rivets carry approximately 10% more load than the other rivets. Using a computer code, Newman et al. (1997) found that the outside rivets carry about 6% higher load. This results in cracking occurring in these rivets first. To force cracking at the middle rivet in the critical row of rivets, the two outside rivets in the middle row were eliminated from the specimens in this research. This resulted in cracking at the middle rivet in the critical row of rivets.

3.4. Fatigue Test Procedure

An MTS servohydraulic uniaxial fatigue testing machine with a rating of 100 kN was used to perform the experiments, which were run in load control. The three-

rivet lap joint specimens were loaded in uniaxial tension with an R ratio of 0.1. A positive R ratio was selected to prevent damage to the crack surface from crack closure. The majority of the tests were performed at a maximum load of either 4 kN or 6 kN. Neglecting the rivet hole (which is filled with the rivet and in a state of compression) and using the cross sectional area of one panel, the maximum nominal stresses during the cycle for 4 kN and 6 kN maximum loads are 103 MPa or 154 MPa respectively. Fuselage stresses range from 90 MPa to 100 MPa (13 ksi to 15 ksi) for a wide range of aircraft types. [Newman, 1996] Different nominal stresses were applied to other specimens to determine the effect of applied stress on the mode of fatigue cracking. Shims of the same thickness as the panels were placed in the grip section to center the load axis with the centerline of the specimen. A saw-tooth wave with a frequency of 5 Hz as shown in Figure 3.5 was applied with a function generator and fine tuned with the use of a digital recording oscilloscope. If the frequency is less than about 200 Hz, the fatigue behavior should not be effected. [Courtney, 1990]

The lap joint specimen gives rise to bending due to the asymmetric loading: the loads being transferred through the upper and lower plates are offset. Because of this bending moment, Rivets 1 and 3 (Figure 3.4a) experience a larger load than Rivet 2. Also, due to load bypass, the plates are more heavily loaded at Rivet 3 in the top plate and Rivet 1 in the bottom plate. Müller (1995) calculated the load transmission to be 37.5% of the applied load while Fawaz (1997) gave a conservative estimate of 35%.

Because of the load bypass and because the countersunk plate has less cross sectional area than the straight drilled plate, crack initiation can be expected at Rivet 3 in the countersunk plate.

In general, two propagating cracks formed one on each side of the rivet. Definitions of individual crack length, a, and end-to-end crack length, 2c, are given in Figure 3.6.

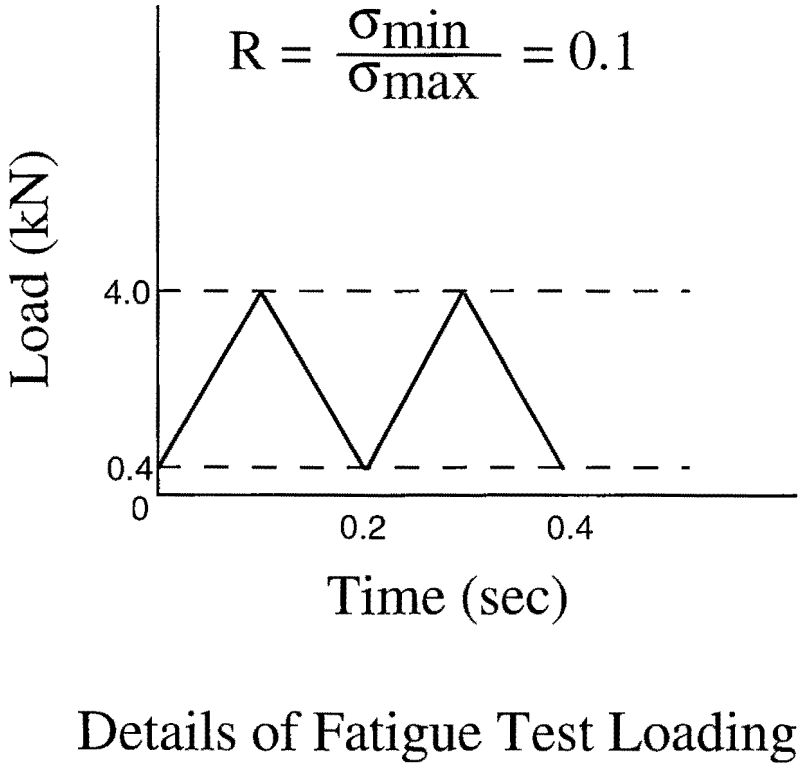

Fig. 3.5. Sketch of saw tooth wave used in fatigue tests

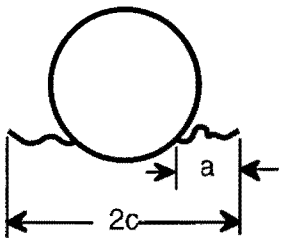

Fig. 3.6. Drawing defining the crack length

3.5. Microscopes

The flush head riveted specimen surface (outside surface) was observed during the tests with an Olympus microscope (Model 225143) at a magnification of 40x. This microscope was mounted with an x-y micrometer base on the MTS machine so that observations of plastic deformation and surface breaking microcracks and strain markings (rumpling) could be made and later propagating crack lengths measured. Many tests were continued until failure, but many tests were stopped much earlier in the fatigue process, and the specimens were examined more carefully with other microscopes including stereomicroscopes in a metallography laboratory. For those tests, which were stopped prior to failure, the rivets were removed from the specimens, the panels were separated and the chamfered panels were pulled in tension

until fracture. Additionally, a scanning electron microscope (SEM) was used to view fracture surfaces and replicas of the specimen's surface. Energy Dispersive X-ray (EDX), a feature of the SEM, was used to analyze wear particles. An important feature of this research was the use of the scanning acoustic microscope to examine subsurface fatigue cracks in the specimens. The maximum obtainable resolutions for various inspection techniques are given in Table 3.3.

Optical Microscope	2000 Å
X-ray Analysis	500-700 Å
Acoustic Microscope	200 Å
Scanning Electron Microscope	35 Å
Tunneling Microscope	2 Å

*As given by [Quate, 1985]

Table 3.3. Resolutions for Various Inspection Techniques

3.6. Replicating Technique

For those specimens that were investigated using the SAM, plastic replicas were generally taken at the commencement of the fatigue test and at intervals during the fatigue test. The replicas were taken of the area on the surface of the specimen

where the plastic deformation would occur. This served as a permanent record of the condition of the surface, and any changes on the surface could readily be seen by comparing replicas. The replicas were made using 127 μm thick cellulose acetate replicating film. Submersing it in acetone for approximately 12 to 15 seconds softened the film. The surface of the specimen was not cleaned prior to making the replica so that any wear particles that were present would be picked up onto the replica. Because of the crevice between the rivet head and the countersink, it was necessary to allow the replicas to dry until they fell from the specimen or for a minimum of 45 minutes to avoid tearing the replicas. The gap also made it more likely to get air bubbles in the replicas so that sometimes 3 or 4 attempts were made before a satisfactory replica was obtained that contained no air bubbles in the area of interest. After the replicas were removed, they were mounted onto SEM stubs, trimmed and then coated in a vacuum chamber using aluminum wire and shadowed using gold wire. The replicas were taken with the specimens loaded at 80 percent of the maximum load, so that the cracks would be open and the replicating material would penetrate into the cracks.

3.7. Scanning Acoustic Microscope

3.7.1. Theory

The focused transducer used with the acoustic microscope has a narrow spot in the center of the spherical lens surface, which generates longitudinal waves at normal incidence. It also has a narrow ring near the edge of the sphere, which generates leaky surface waves at the critical angle as shown in Figure 3.7. Other positions on the spherical lens surface generate rays that are reflected at angles that either miss the transducer or hit it obliquely so that this response does not contribute much to the signal. The responses from both longitudinal and leaky surface waves are obtained by defocusing (i.e., moving the transducer closer to the surface of the object than the focal point--see Figure 3.7). As the transducer is moved closer to the surface of the specimen, the specular reflection from the center of the sphere and the leaky surface acoustic waves from the edge of the sphere interfere with each other destructively and constructively in cycles. [Quate, 1985; Tsai and Lee, 1987; Briggs, 1992] Even if the transducer is extremely defocused, the resolution is not affected much, because the vast majority of the energy is localized at the center. [Briggs, 1992] In the research described herein, the transducer was defocused for maximum constructive interference between the longitudinal and leaky surface waves.

The limit of the frequency of the transducer that can be used is determined by the attenuation of sound in the liquid. The maximum frequency transducer that can be used in water is about 1500 MHz giving a wavelength of 1 μm. This gives a resolution of less than 1 μm. To improve the resolution (by increasing the frequency), another liquid, other than water, is required. [Attal and Quate, 1976]

As the frequency increases, the resolution improves but the depth of penetration decreases; thus, a trade off exists between improved resolution and depth of penetration. [Hoppe and Thaer, 1986] The best obtainable resolution is determined by the depth of penetration desired. The desired depth of penetration coupled with a minimum pulse length enables determination of the highest usable frequency. These factors are thus used to determine the best resolution. The lens of the transducer for the acoustic microscope is made of single crystal sapphire, because the attenuation of the acoustic waves in this material is small. [Briggs, 1992]

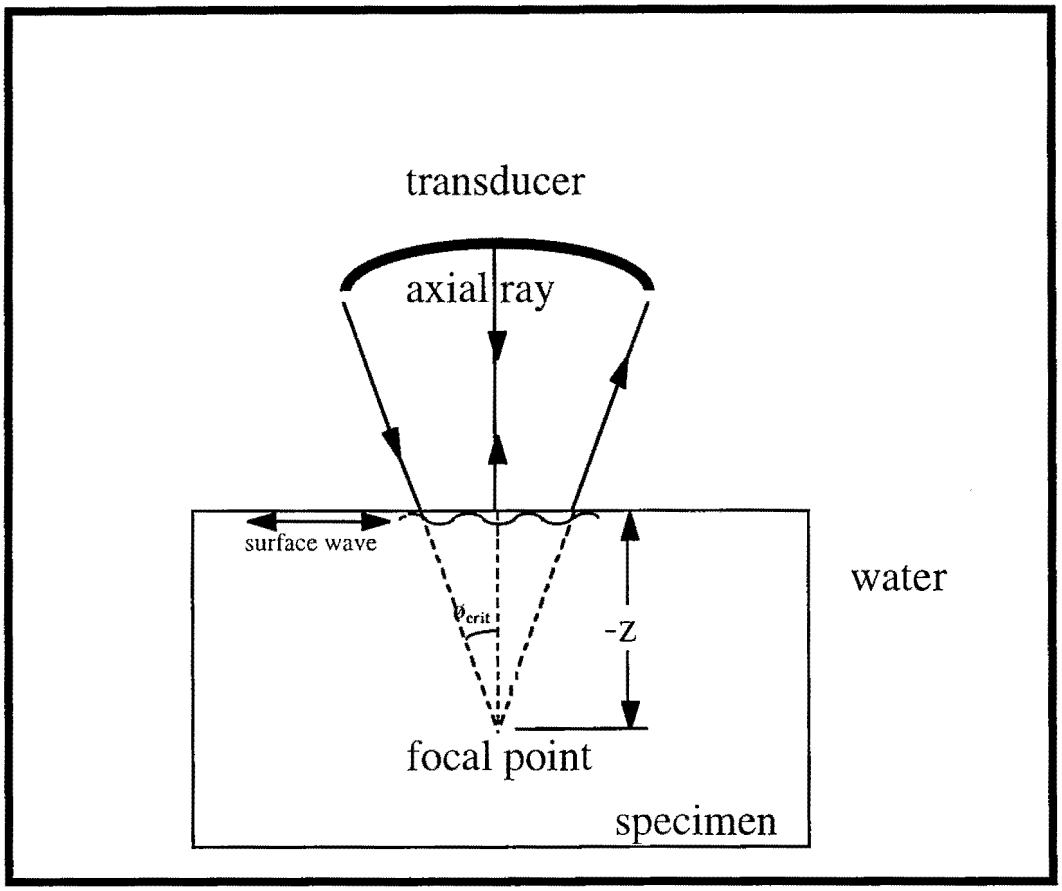

Fig. 3.7. Sketch of acoustic wave generation in a focused transducer

The primary advantage of the scanning acoustic microscope recording one point at a time over standard ultrasonic methods that display the entire field of view at once is the elimination of interference fringes as stated earlier. These are eliminated because energy is focused over a diameter of less than one wavelength, i.e.; the image is scanned

one point at a time so that scattered radiation, which causes interference fringes, is eliminated. [Quate et al., 1979]

The refractive index is the ratio of the velocity in the liquid over the velocity in the solid. As the refractive index gets smaller, the refraction angle (and the difference between its sine and tangent) gets smaller. This results in the aberrations being smaller. The acoustic microscope is basically monochromatic so that chromatic aberrations do not occur. [Briggs, 1992] The velocity of the sound waves in water is about 1500 m/s, the velocity of the longitudinal waves in aluminum is about 6400 m/s, and the velocity of the shear waves in aluminum is about 3000 m/s [CRC, 1978]. This gives a refractive index for these experiments between 0.234 and 0.5.

The minimum focal spot size occurs when [Briggs, 1992]:

$$\frac{h_{opt}}{s_b} = \frac{1.089}{\sqrt{(1-n)}}\left(\frac{\lambda_1}{s_b}\right)^{1/4} \tag{3.1}$$

and θ_{opt} is given by the formula [Briggs, 1992]:

$$\theta_{opt} = \arcsin\left[n \sin\left(\arctan\left(\frac{h_{opt}}{s_b} \right) \right) \right] \tag{3.2}$$

where $n = \frac{v_{water}}{v_{Al}}$ with $v_{water} = 1497 m/s$ and $v_{Al} = 6420 m/s$ [CRC, 1978] so that n is equal to 0.233 in this case; h_{opt} is the optimum distance from the central axis to the point at which a ray passes through the surface of the solid; λ_l is the wavelength in the solid, which is 30 μm for rolled aluminum [CRC, 1978]; and s_b is the depth of paraxial focus and is between 0.5 and 1 mm [Briggs, 1992]

Therefore, θ_{opt} is approximately 6° to 7° for this setup of rolled aluminum and water. The semi-angle of the lens that was used in these experiments is between 5° and 10°, which is very close to θ_{opt}.

The resolution of a microscope can be defined as the minimum size of a feature that can be determined. An expression for the resolution of the reflection acoustic microscope is given by the equation [Briggs, 1992]:

$$\omega = \frac{0.51\lambda_o}{\text{N. A.}} \tag{3.3}$$

where N. A. is the numerical aperture and is equal to sin θ_O, which is the semi-angle, subtended. The wavelength, λ_o, *is* given by v_o / f, where v_o is the velocity of sound in the fluid and f is the frequency.

The center frequency of the transducer used in these experiments is about 50 MHz. The velocity of sound is 1496.7 m/sec in distilled water, giving a wavelength of 2.99×10^{-2} mm. Estimating θ_O to be between 5^0 and 10^0, the same as θ_{opt}, gives a resolution between 88 μm and 175 μm. From this, a conservative estimate of the resolution of the acoustic scans is between 90 μm to 180 μm.

The shear velocity is roughly one half the longitudinal velocity and this results in different arrival times for the returning signals. Interaction of these signals result in either constructive or destructive interference depending on the distance between the lens and the specimen. [Briggs, 1992]

3.7.2. SAM Technique

A focused transducer with a center frequency of ca 50 MHz was used in conjunction with a Panametrics Hyscan system. A block diagram of the scanning acoustic microscope is shown in Figure 3.8. The specimens were submerged in a tap water tank for examination. The focused transducer, made of single-crystal sapphire, was attached to an automated computer-controlled x, y, z stage and was excited by a Panametrics Pulser-Receiver (Model 5601A/ST) to generate ultrasonic waves. The

focused beam was reflected by the specimen and returned to the transducer that also acted as a receiver. When one transducer is used to both transmit and receive the signal, this is commonly called the pitch-catch method. This circumvents the problem of aligning two transducers. The transducer is made of piezoelectric ZnO sandwiched between layers of gold; the lens is made of single-crystal sapphire or silicon, both of which have high velocities of sound as compared to the water couplant. [Wickramasinghe, 1983; Quate et al., 1979] The attenuation of acoustic waves is small in single-crystal sapphire and silicon, another reason for selecting these for the lens. [Briggs, 1992] The transducer output signals, digitized by a Tektronix TDS-540 four channel digitizing oscilloscope and processed by a Panametrics Gated Peak Detector (Model 5608) were finally acquired by a personal computer to produce a C-scan image.

The signal reflected from the back surface of the plate with countersunk rivet holes was maximized, and then the transducer was defocused to give the best image of the crack. The best image of the crack was obtained by focusing so that the longitudinal waves and surface waves interfered constructively. When using the acoustic microscope to investigate the subsurface cracks in the riveted lap joints, the back surface reflection signal was gated, as this is where the crack initiates, and its peak value provided the data for the C-scan image of this plate. The through-thickness of the plate that contained cracks was projected onto a surface.

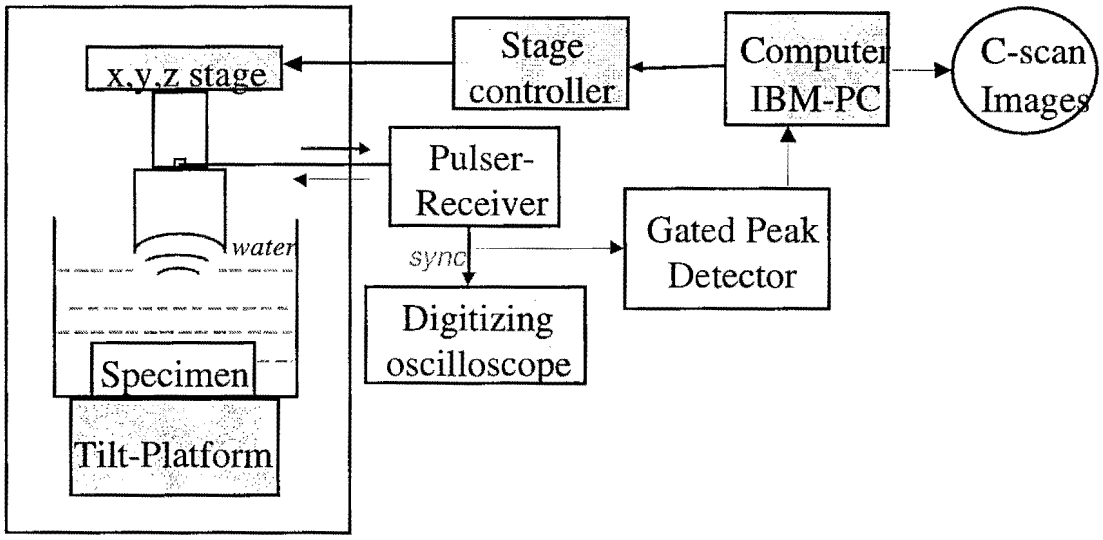

Fig. 3.8. Diagram of setup for scanning acoustic microscope

3.8. Summary

Specimens at various stages in the fatigue process that had already been carefully examined with optical microscopes were investigated using a scanning acoustic microscope (SAM) to obtain C-scan images of the specimens. The subsurface fatigue cracks were examined with the SAM after selected numbers of cycles and then returned to the fatigue apparatus for further cycling. Crack lengths on the acoustic scan images were also measured vs. the number of cycles. Testing was discontinued and specimens were disassembled after various stages of subsurface fatigue cracking were observed with the scanning acoustic microscope. To disassemble the specimens, the rivets were carefully removed and the panels were separated. After disassembly, the countersunk panels, which always contained the fatigue cracks, were pulled in tension until fracture to reveal the fatigue fracture surfaces, which were examined microscopically using a stereomicroscope and a SEM. Some tests were continued until long surface breaking cracks were obtained. Comparisons were then made between the crack lengths as shown with the SAM and with the optical microscope. The testing of some of these specimens was stopped after cracks were observed in the acoustic scans.

4. Microscopic Analysis

4.1. Introduction

Since fatigue cracks have been found in aircraft, many studies have been performed involving prediction of the life of lap joints in the fuselage of an aircraft and the ability to detect fatigue cracks before they grew to an unsafe length. The nondestructive evaluation of these cracks while they are still small has been difficult as the cracks form on a subsurface of the joint and are a number of mm long by the time they reach a surface which is visible with either the optical microscope or the scanning electron microscope. With the use of the scanning acoustic microscope, the study of subsurface cracks is presented herein.

4.2. Cross Section of Riveted Joint

A cross section of an unfatigued riveted joint through the center of the rivet is shown in Figure 4.1. Two observations are pointed out in the photomicrographs taken of this cross section. First, the soft aluminum cladding has been pushed away from the sheet material near the rivet hole during the formation of the bucktail as shown by the arrow in Figure 4.2. The bucktail is at the bottom of the figure. This is probably not a cause of fatigue crack initiation. Secondly, a small lap in the cladding material on the

fayed surface is seen near the rivet shank a short distance from the knife edge as shown in Figure 4.3. A lap is a defect in the material (the material folds over on itself). This occurs when the material is being compressed during the riveting process. This frequently occurs during test trials of new forging dies. This is a possible site of fatigue crack initiation as this location will be very sensitive to stress raisers such as those caused by fretting debris. Cracks or irregularities in the cladding material will act as stress raisers and may result in crack nucleation in the substrate. [Hoeppner et al., 1994]

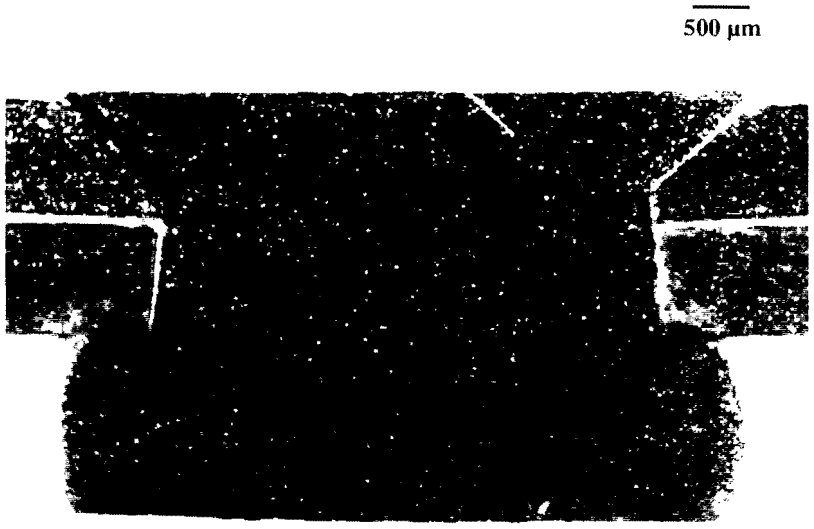

Fig. 4.1. Cross section of unfatigued riveted joint through the middle of the rivet

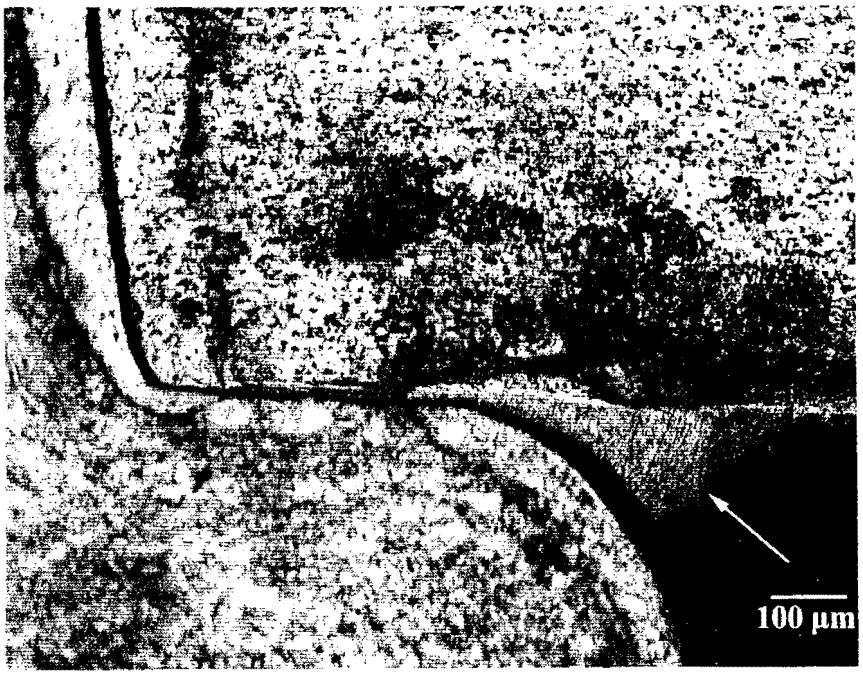

Fig. 4.2. Photomicrograph of riveted specimen showing the aluminum cladding near the rivet hole on the fayed surface that has been pushed away from the sheet material

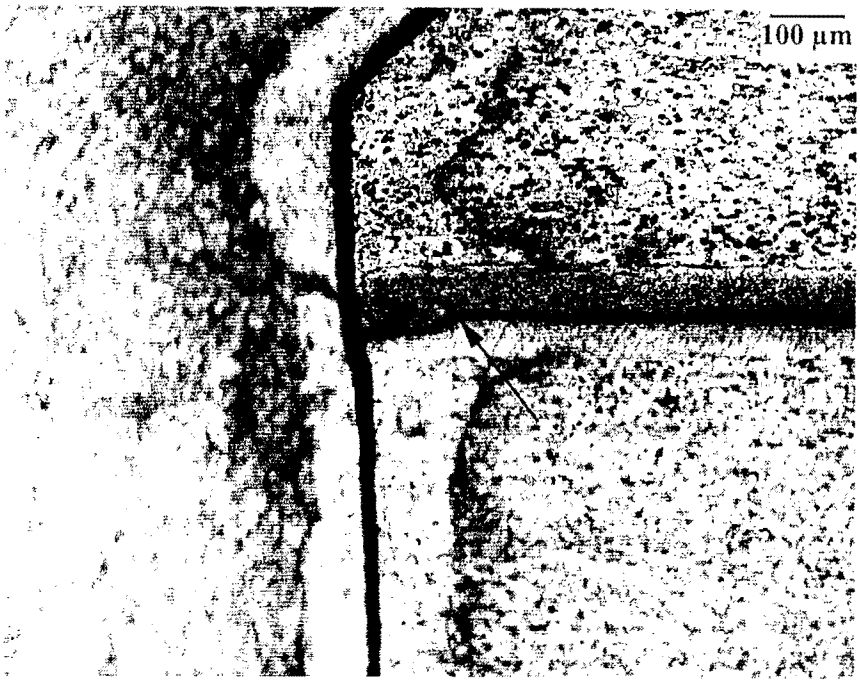

Fig. 4.3. Photomicrograph illustrating defect in cladding material on the fayed surface near the knife edge of the rivet hole

4.3. Comparison of Microstructures of 2024-T3 and 2524-T3

Representative samples of the microstructure of the 2524-T3 material in the longitudinal direction and the short transverse direction are seen in Figures 4.4 and 4.5 respectively. The number of inclusions is less in the 2524-T3 material than in the 2024-T3 material (see Figures 3.2 and 3.3); hence, there are less initiation sites for fatigue cracks in the 2524-T3 material. Inclusions nucleate cracks and the cracks will hop to other inclusions; consequently, it is expected that the 2524-T3 material will nucleate cracks at a greater number of fatigue cycles than the 2024-T3 material.

Dislocations will pile up at hard brittle inclusions hindering the plastic flow of the material. This results in the areas around the inclusions being less ductile; therefore, a more pure alloy with fewer inclusions will be more ductile. The pile up also contributes to crack nucleation because dislocation energy is given up when the crack forms. In commercial alloys, voids or microcracks form at these inclusions. Evidence of voids forming at these inclusions is given in the micrograph in Figure 4.22, showing cuplets containing particles. In a noncoherent inclusion, there will be a difference in the number of atomic planes in the particle as compared with the surrounding matrix, resulting in a strain. [Courtney, 1990] The difference in the number of atomic planes is relieved by the formation of geometrically necessary dislocations. The internal stress of the dislocations is added to the applied tensile stress. As the plastic strain increases, the total stress increases. If the plastic strain is sufficient to cause the particle to break or for decohesion to occur between the inclusion and the matrix, microcracks or voids form at the inclusion. Crack growth evaluation results are given in Chapter 5.

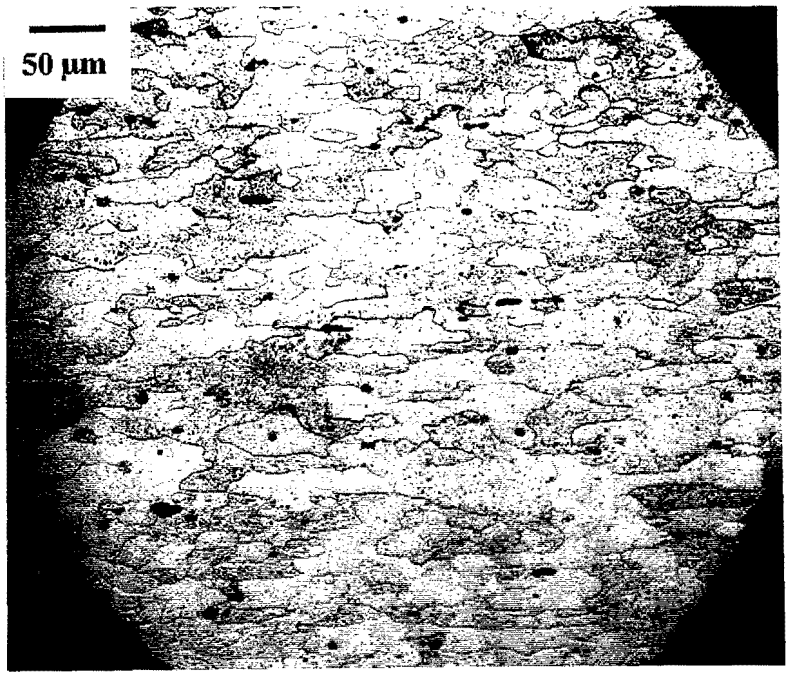

Fig. 4.4. Photomicrograph showing grains in the longitudinal (L) direction in 2524-T3 material

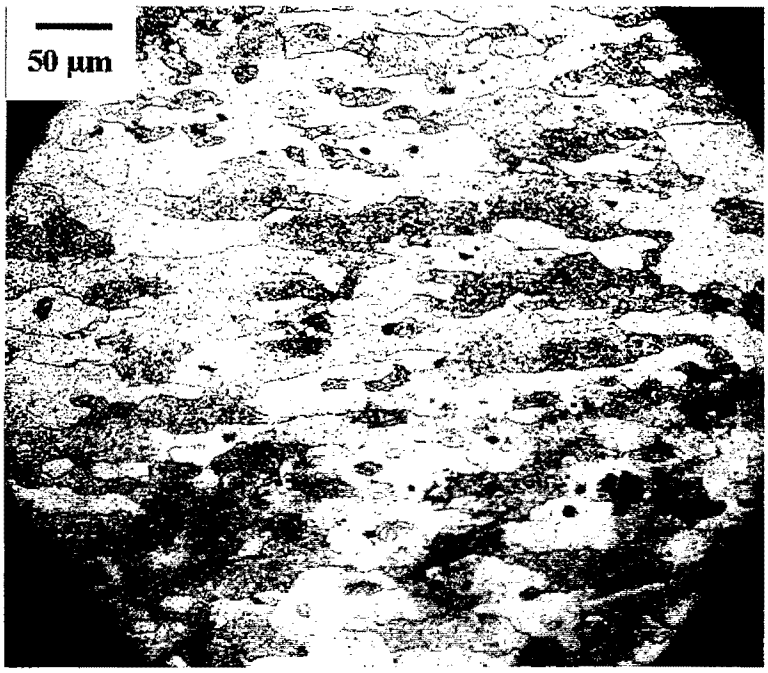

Fig. 4.5. Photomicrograph showing grains in the short transverse (ST) direction in 2524-T3 material

4.4. Fatigue at Low Nominal Applied Stress

Since one way to make cracked riveted specimens for NDE that are more realistic than those with cracks simulated using EDM notches is to rivet together specimens where one panel is already cracked by fatigue cycling, an experiment was performed to determine if riveting will change the crack opening of a pre-existing crack. An unriveted panel containing a countersunk hole was fatigued until a crack appeared that extended beyond the countersunk area of the specimen. Fiducial lines were then

drawn on both sides of the crack. This specimen was then riveted with increasing pressure and micrographs were taken after each increase in pressure. After compressing the rivets under four tons of pressure, there was no apparent change in the fiducial line separation. Compressing the rivets under four tons of pressure gave an average bucktail diameter of 5.89 mm; however, the Boeing specification requires a bucktail diameter of 6.12 mm ± 0.05 mm. [Boeing, 1970] After compressing the rivets under five tons of pressure, an average bucktail diameter of 6.12 mm was obtained and the separation of the fiducial lines was 0.01mm ± 0.005mm greater than initially. Thus, an actual crack produced by fatiguing an already riveted panel may be different than one produced by riveting a panel with a pre-existing crack. For this reason, the specimens tested in this research were not precracked or notched prior to riveting. Furthermore, as shown in the present work, the crack initiation process and the location of the macroscopic crack are much different in a specimen with a countersunk rivet hole than in a specimen containing a rivet. In a chamfered rivet holed specimen the crack forms at the knife edge [Fadragas, 1993], but the initiation is much different in a riveted specimen at maximum nominal stresses comparable to those experienced by aircraft.

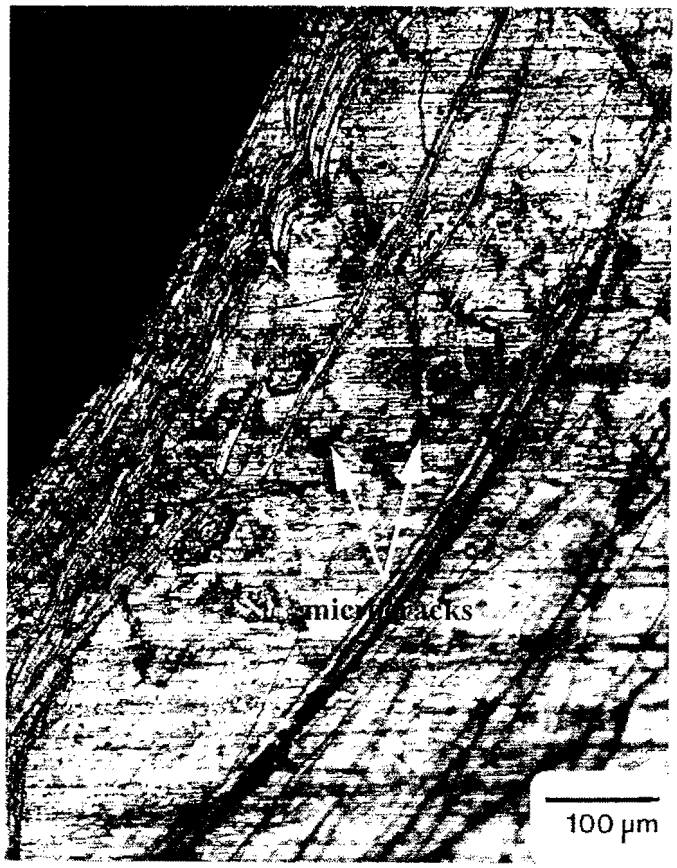

Fig. 4.6. Optical photomicrograph showing the rumpled region near the rivet head prior to the emergence of a propagating radial crack. Two microcracks are pointed out with arrows. (215,000 cycles)

4.4.1. Initial Optical Microscope Study

This investigation of fatigue in riveted lap joints began with optical microscope observations on the "outside" surface i.e. the visible surface of the chamfered panel. Initially, studies were performed at a maximum nominal applied stress of 103 MPa, and crack growth measurements were taken on the outside surface of the chamfered panel in

the riveted specimen with a 40 times magnification optical microscope that was mounted to the MTS machine. On cycling, the first indication of fatigue damage was a rumpled region that consists of slip steps and microcracks. The microcracks were approximately 100 to 200 microns in length when the rumpled region was first observed. These microcracks were near the rivet head and were wiggly and in various directions with respect to the applied stress. The dominant cracks in the plates were at angles that were not normal to the loading direction. The cracks became normal to the loading direction on growth. This indicates combined tensile and shear mode fracture occurred until the crack propagation became normal to the loading direction. Typical microcracks are shown in the photomicrograph in Figure 4.6. Rumpling was first noticed at 175,000 cycles. This photomicrograph was taken at 215,000 cycles. A portion of the rivet head is seen in the upper left corner. The machining marks (large radius) are very superficial. A typical crack with the specimen loaded at a maximum nominal stress of 103 MPa is shown in the photomicrograph in Figure 4.7. These radial cracks form at the lower edge of the rivet head similar to the sketch in Figure 3.6.

Several specimens were disassembled after a number of fatigue cycles by grinding off the bucktail and carefully removing the rivet, and all showed evidence of fretting as seen by black particles that were present. One specimen was disassembled before a radial crack was seen in the region of the plate adjacent to the rivet head. After fatiguing and disassembling, the plate with the countersunk holes showed microcracks near the rivet hole on the fayed (mated) surface. An example of these microcracks is shown in the photomicrograph in Figure 4.8. Both circumferential and radial

microcracks were observed. These microcracks did not originate at the knife edge and had not penetrated to the outer plate surfaces. This was observed in most of the disassembled specimens that were fatigued at a maximum nominal applied stress of 103 MPa and showed only rumpling. The aforementioned region is where fretting occurs in the plates.

Fig. 4.7. Photomicrograph of a radial crack emerging from microcracks. (120,000 cycles)

Fig. 4.8. Photomicrograph of back surface of panel with countersunk rivet holes showing microcracks. (120,000 cycles)

With the optical microscope, the first indication of fatigue damage on the outer surface of the chamfered panel of the specimens, as already noted, was microcracks and strain markings, caused by the plastic deformation associated with the growing subsurface crack. A typical example of the rumpled region is shown in the already referred to photomicrograph in Figure 4.6. Thus a significant crack exists before evidence of damage can be seen optically. This surface rumpling appeared near (but

not always at) the rivet head of Rivet 3 identified in Figure 3.4a. Rivet 3 is in the location that would be called the critical row of rivets in an assembly of rivets in aircraft outer skins.

4.4.2. Scanning Acoustic Microscope Studies

Since direct optical examination of subsurface fatigue cracks and hidden surfaces cannot be made, the scanning acoustic microscope (SAM) in the C-scan mode was used for this purpose. A C-scan image of the same specimen as shown in the photomicrograph in Figure 4.6 is shown in Figure 4.9. The black region in the center of the C-scan is the area of the rivet head and indicates a total loss of the signal that is returned to the transducer after it has traveled through the specimen. The back surface of the reflected signal from the countersunk panel is gated and explains the loss of signal at the rivet head as there is no surface in this area for a reflected signal. Subsurface cracks on both sides of the rivet head are clearly shown. The orientation of the crack shown in Figure 4.9 has been referred to as the "eyebrow" orientation and was characteristic of all fatigue cracks that formed in the specimens studied at this maximum nominal stress (103 MPa) and R-ratio of 0.1. Such cracks start off propagating at an angle of ca 20° to the stress axis normal but turn to normal to the stress axis as they become longer and approach the normal diametral direction of the rivet eventually becoming mode I cracks (Stage II cracks in Forsyth's nomenclature). This is indicated in Figure 4.10 where the left side crack is almost normal to the stress direction.

The length of the rumpled region in the photomicrograph, Figure 4.6, is ca. 0.8 mm whereas; the length of the eyebrow crack on the left in the C-scan image is longer, ca. 1.3 mm, Figure 4.9. While microcracks are seen optically only on the surface on one side of the rivet, cracks are shown on both sides of the rivet in the C-scan image. The shorter subsurface crack on the right side of this rivet in Figure 4.9 is ca 0.2 mm long. In this instance the subsurface radial crack was seen before any rumpling (shear bands and microcracks) was seen on the surface using an optical microscope. This is further evidence that the subsurface radial crack did not arise from the surface rumpling even though the latter indicates fatigue damage, but the surface rumpling results from the crack propagating underneath the surface.

The average number of cycles until a crack was observed at 103 MPa nominal stress in the acoustic C-scans was found to be 192,000 cycles while the average number of cycles until a propagating radial crack on the rivet head panel surface was seen to have emerged was found to be 263,000 cycles. The average number of cycles for an 8 mm crack to form was found to be 302,000 cycles so that approximately 85% of the life to an 8 mm crack is taken in forming a surface breaking crack, while about 60% of the life to an 8 mm crack is in forming a crack which is detectable by the acoustic microscope. Here the crack length is defined as 2c as given in Figure 3.6.

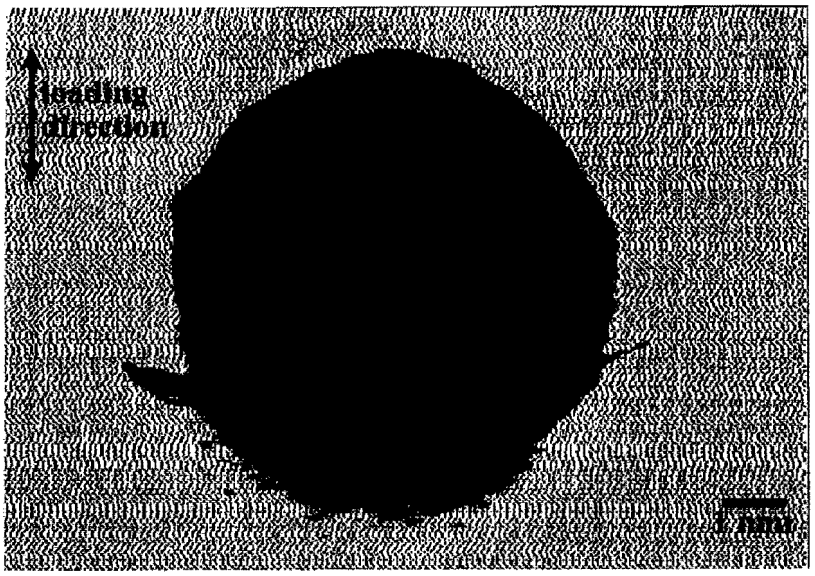

Fig. 4.9. Scanning acoustic microscope C-scan image of the specimen shown in Figure 4.6. (215,000 cycles)

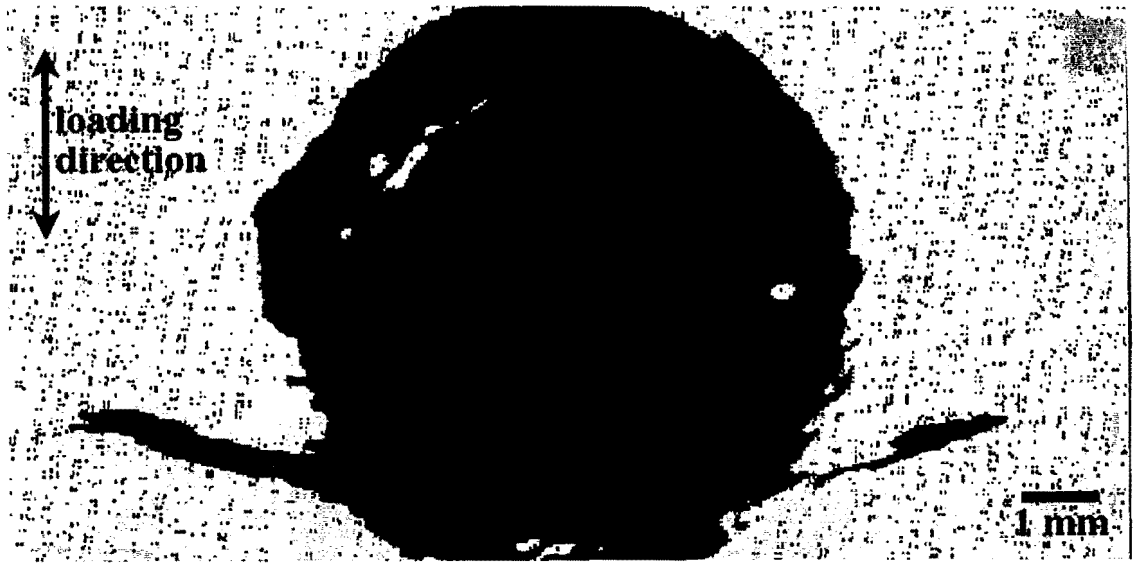

Fig. 4.10. Scanning acoustic microscope C-scan image of a specimen showing a well developed eyebrow crack at an angle of about 20° to the stress axis normal (200,000 cycles).

Figure 4.10 is an example of a C-scan image of a specimen with a fully developed eyebrow crack on each side of the rivet. The end-to-end crack length is ca. 12 mm. Figure 4.11 is an example of a C-scan image of a specimen with the eyebrow crack detected only on one side. Figure 4.12a is another example of cracks on both sides of the rivet. This specimen was cycled for 220,000 times and the cracks are 4.8 mm and 1.5 mm long in the C-scan image giving an end-to-end crack length also of 12 mm. Optically measured, these cracks were smaller, 3.9 mm and 1.1 mm. Figures 4.12b and 4.12c are optical micrographs of the left and right side of the areas of the specimen in which the cracks occurred, respectively. Figure 4.12b clearly shows the

long crack on the left side of the rivet and a rumpled region on both sides of the crack near the rivet head. In Figure 4.12c, a short crack is seen which does not extend to the rivet head. This is due to the crack not having yet reached the surface in the region between the crack and the rivet head. The arrows point out the ends of the crack as seen on the outer surface of the specimen.

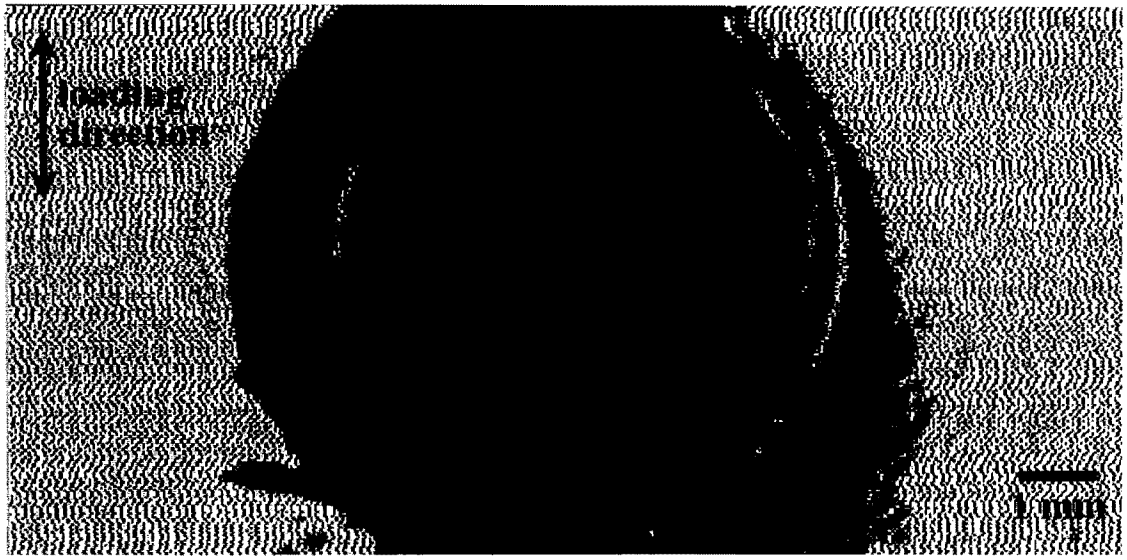

Fig. 4.11. Scanning acoustic microscope C-scan image of a specimen showing a crack on only one side after 160,000 cycles.

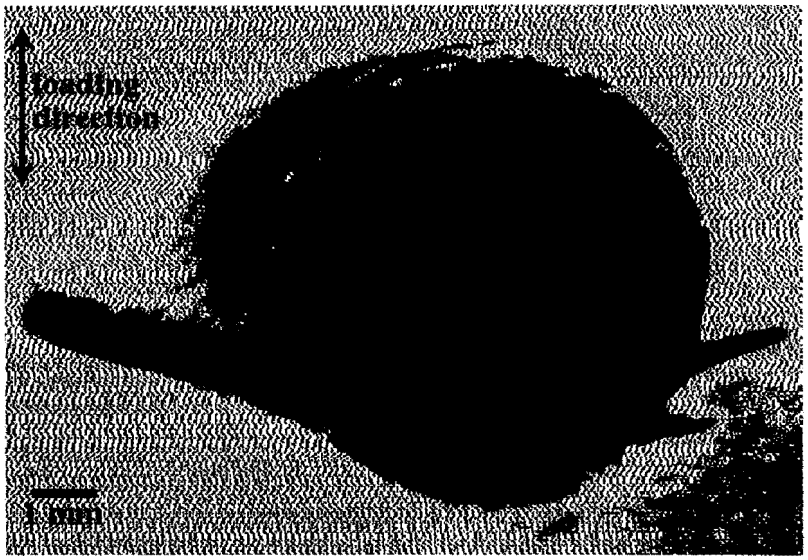

Fig. 4.12a. C-scan image of specimen with eyebrow crack after 220,000 cycles.

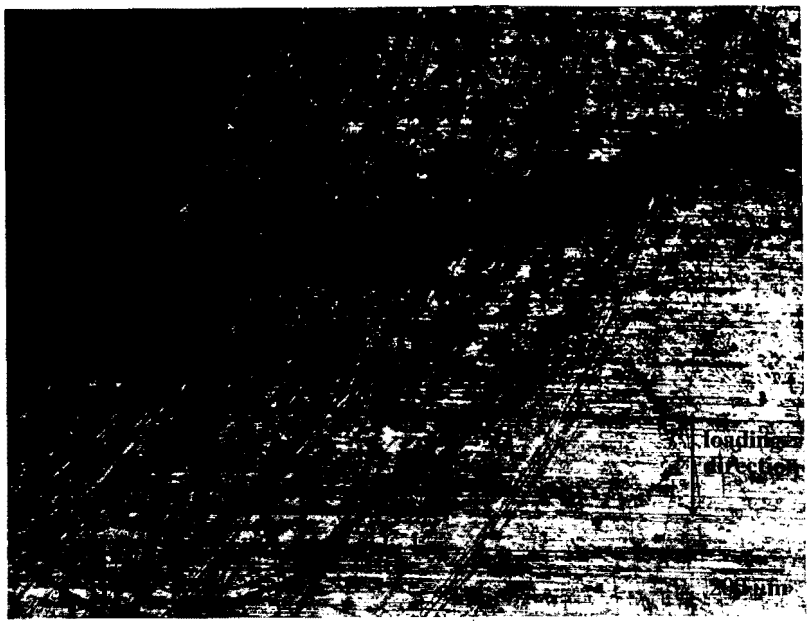

Fig. 4.12b. Optical micrograph of left side in crack region of specimen shown in Figure 4.12a. The optical micrograph is a mirror image of the specimen.

Two cracks appear on the right side of this specimen in the C-scan image (Figure 12a). This has been observed in other specimens. It is not known if this shorter crack has arrested or whether it will grow with additional cycling until it meets the longer crack. Evidence of a shorter crack that has arrested is given in Figure 4.13, an optical micrograph showing a short crack as shown by the arrow in a specimen which was cycled to failure from another crack. Arrested cracks are also observed in other C-scan images in this research and are commonly found in fretting fatigue [Nishioka et al., 1969] as well as in general when a short crack has been bypassed by a longer crack.

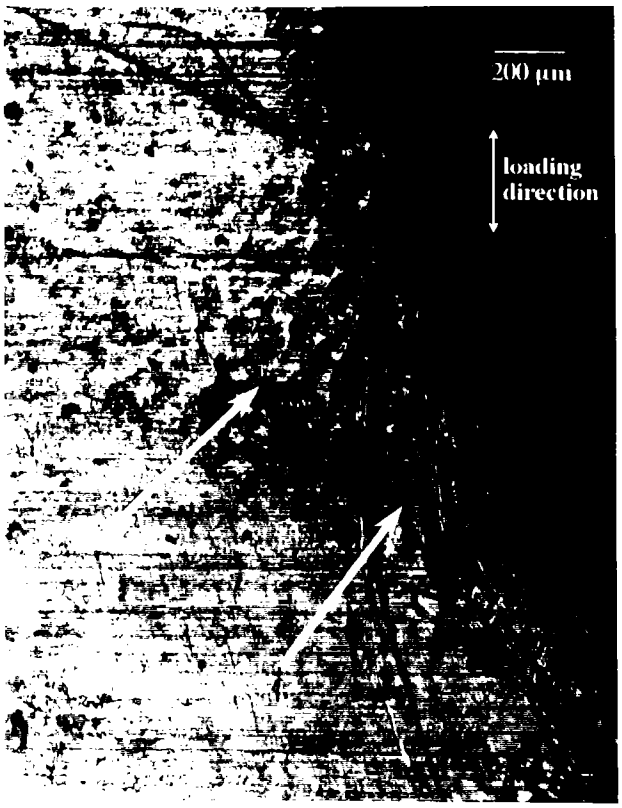

Fig. 4.12c. Optical micrograph of right side in crack region of the specimen shown in Figure 4.12a. The arrows point out the ends of the crack as seen on the outer surface of the specimen. The optical micrograph is a mirror image of the specimen.

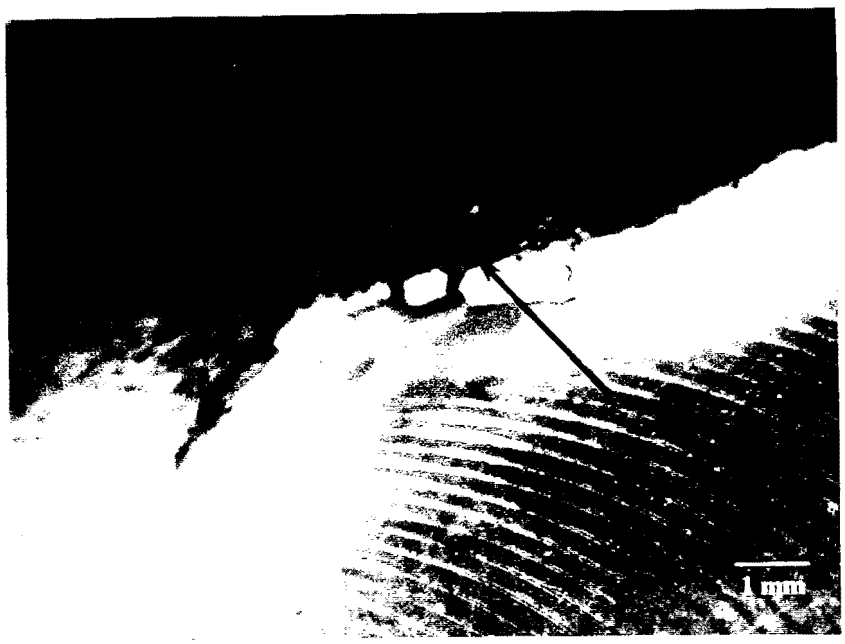

Fig. 4.13. Optical micrograph of a short arrested crack as shown by the arrow in a specimen that was cycled to failure (293,000 cycles). The striations are not a part of the specimen but a part of the surface of the component on which the specimen is resting.

Figure 4.14 is a micrograph of the damaged fayed surface of a specimen that was fatigued for 205,000 cycles at a maximum nominal applied stress of 103 MPa. This damage occurred during the fatigue cycling. Note that the area in the figure around the entire rivet shows damage.

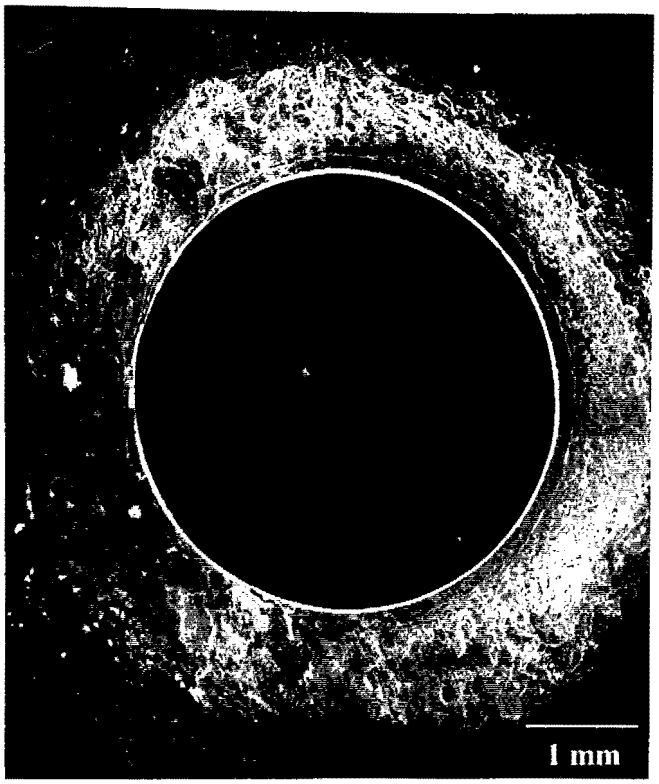

Fig. 4.14. Micrograph of the damaged surface of a specimen fatigued at a maximum nominal applied stress of 103 MPa. (205,000 cycles)

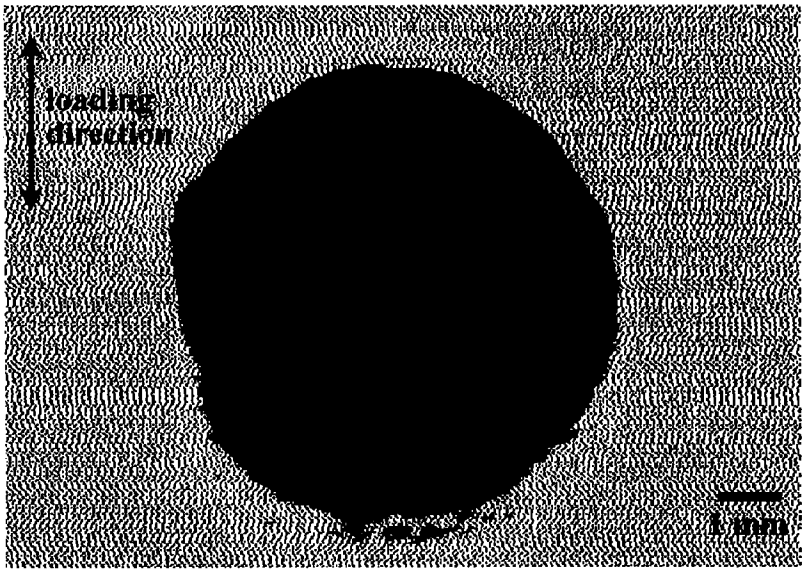

Fig. 4.15. Acoustic C-scan of specimen when crack was first detected at 140,000 cycles.

The number of cycles between the first observance of a crack on the acoustic scans and the observance of surface rumpling as seen when viewing the replica using the SEM was 55,000 cycles in a specimen where the two were compared. A crack on the right side was first observed in the acoustic C-scan at 140,000 cycles shown in Figure 4.15. Faint surface rumpling from this crack was first observed at 195,000 cycles and is shown in the scanning electron micrograph of the replica in Figure 4.16. Figure 4.17 is the C-scan of the specimen at 195,000 cycles. In some of the earlier scans of this specimen, there is possible evidence of two cracks on the left side, which are growing together.

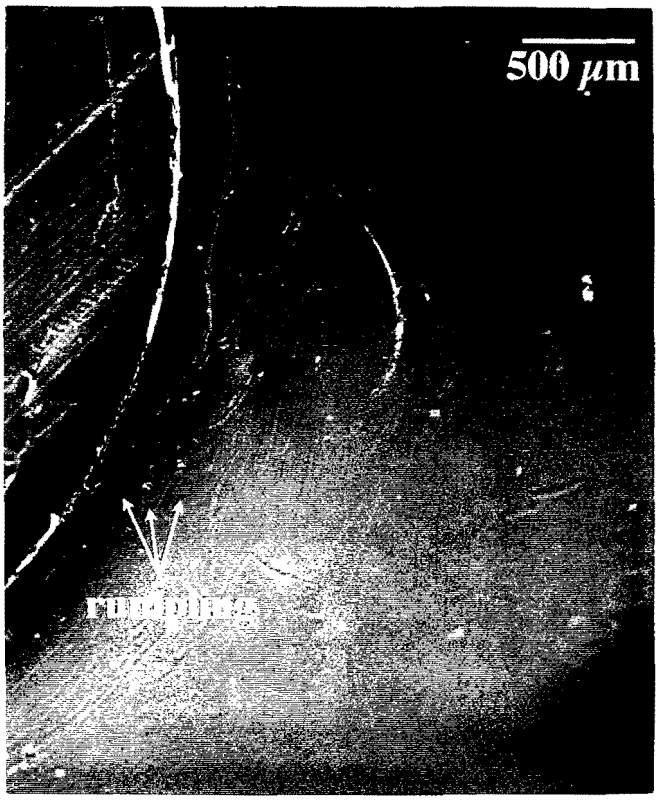

Fig. 4.16. Scanning electron micrograph of replica of the same specimen shown in Figure 4.15 but taken at 195,000 cycles and showing surface rumpling in the area indicated by the arrows.

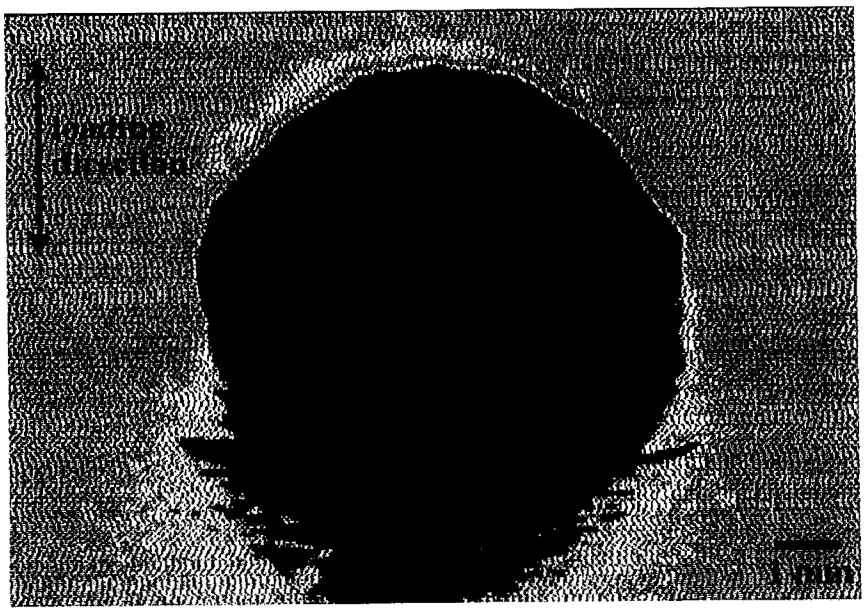

Fig. 4.17. Acoustic C-scan of the same specimen shown in Figure 4.15 but at 195,000 cycles.

4.4.3. Fractography of Specimens Fatigued at 103 MPa Maximum Nominal Stress

To determine the initiation sites of cracks and other crack characteristics, the fracture surfaces of specimens were examined. The test of the previous paragraph was stopped after 205,000 cycles, and the specimen was disassembled by removing the rivets and separating the panels. The countersunk panel, which always contained the fatigue crack, was fractured in tension to reveal the fatigue fracture surfaces. A scanning electron micrograph of the fracture surface is shown in Figure 4.18. The fatigue crack surface is outlined by the dotted white line. Interestingly, when the

specimen was fractured, the fatigue crack was observed to be near the rivet hole but not through it. Cracks initiated on each side of the rivet, and as they grew they eventually linked up bypassing the rivet and hole. The initiation sites for the cracks were located on or very near the hidden surface some distance from the rivet hole. A large particle is observed on the left side and appears to be at or near one of the initiation sites. This will be discussed in more detail later. The crack path linking the cracks on each side of the rivet for this eyebrow crack, as already stated, was located a short distance below the rivet hole. It avoided the region of extensive plastic deformation in the countersunk panel formed by the cyclic load transfer between the rivet and the panel, a region of compressive residual stress. This is a *true* eyebrow crack.

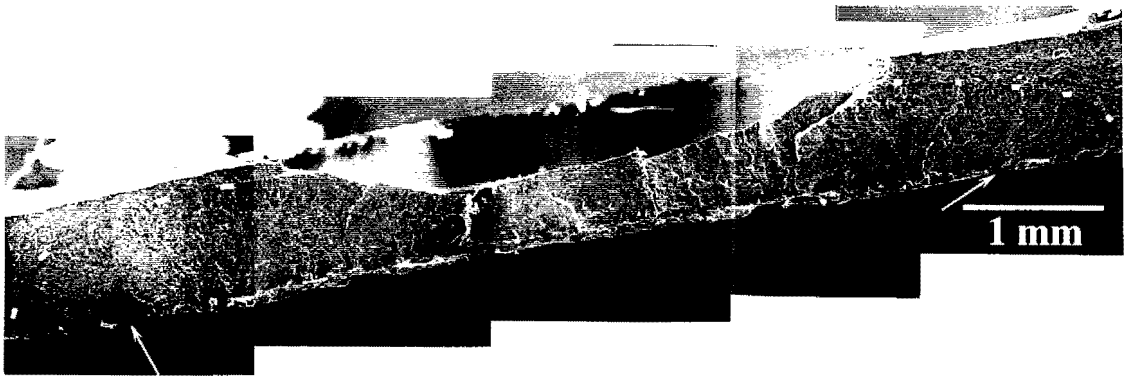

Fig. 4.18. Scanning electron micrograph of the top fracture surface of the specimen shown in Figures 4.16 and 4.17 after 205,000 cycles The end-to-end crack lengths are given by the plot in Figure 4.19.

The crack length vs. cycle number as measured from the acoustic C-scans for this specimen is given in the plot in Figure 4.19. The average crack growth rate, d(2c)/dN, from 6 to 8 mm is approximately 5 x 10^{-5} mm per cycle. The SAM C-scan and the scanning electron micrograph of the fracture surface both showed the crack to be 8.1 mm in length. The crack was still not a surface breaking crack.

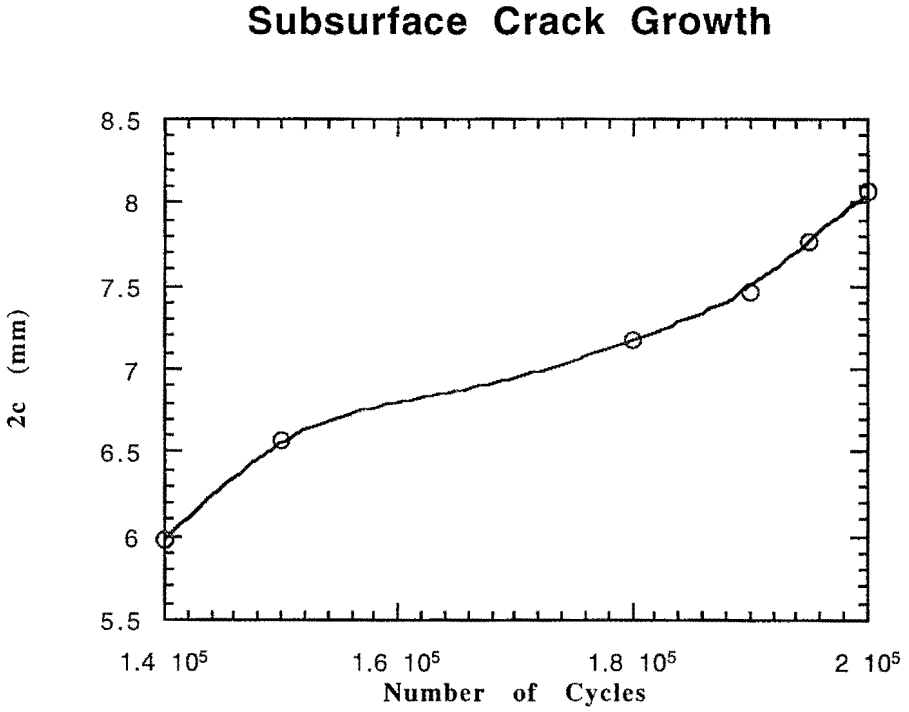

Fig. 4.19. Plot of end-to-end crack length vs. number of cycles for a subsurface crack as viewed in the acoustic C-scans. While a crack on one side was seen before 1.4 x 10^3 cycles, cracks on both sides were not seen before this examination of the specimen.

Figure 4.20 is an acoustic scan taken after 240,000 fatigue cycles for another specimen fatigued at 103 MPa. Cracks are seen on both sides of the rivet. This

specimen was then pulled apart, and scanning electron micrographs of the crack on each side of the rivet hole are shown in Figure 4.21. The arrows in the micrographs point to crack initiation sites, which again are some distance from the rivet hole. From these micrographs, it can again be seen that the crack has not yet reached the surface of the panel and additionally has not yet reached the rivet hole. Figure 4.22 is a micrograph of the fracture surface of this specimen in which the arrows indicate the boundary between the fatigue crack region in which radial markings pointing to the initiation site are seen and the ductile fracture region. The latter fracture occurred when the panel was pulled apart in tension to reveal the fatigue fracture surface. In the ductile part of the fracture, microvoids form at inclusions in commercial alloys such as the 2024 T3 used in this research. The microvoids then grow and coalesce to result in the ductile fracture. The microvoids make the surface look dimpled. Void-initiating particles can be seen at the bottom of some of the microvoids.

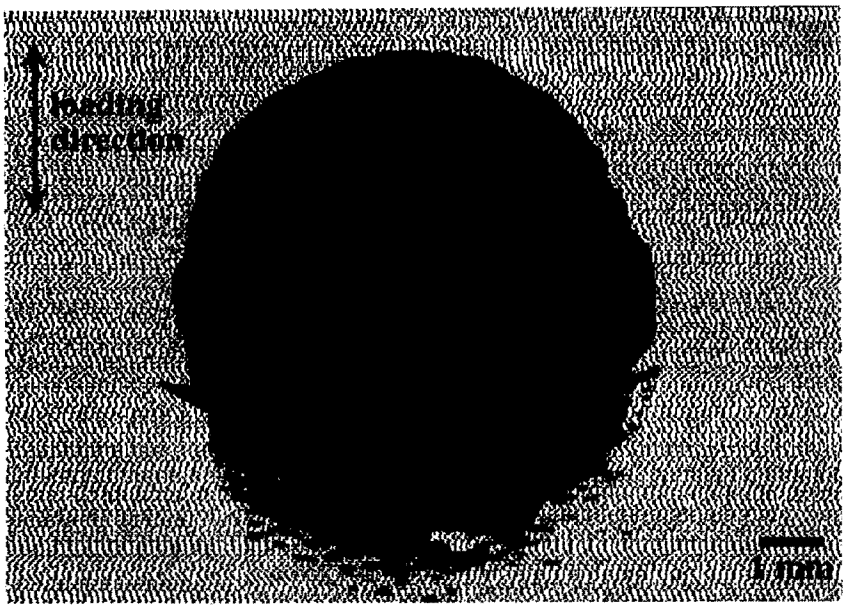

Fig. 4.20. Acoustic C-scan of a specimen after 240,000 fatigue cycles

The subsurface cracks formed when a maximum stress of 103 MPa is applied propagate as asymmetrical semi-elliptical cracks until they reach the countersunk surface. When they appear on the outside surface, they are a short distance from the rivet head. As mentioned previously, prior to emergence of the macrocrack on the observable surface, an array of radial and circumferential microcracks are observed using optical and scanning electron microscopy. These microcracks are a sign of fatigue damage and are the product of the propagating subsurface crack.

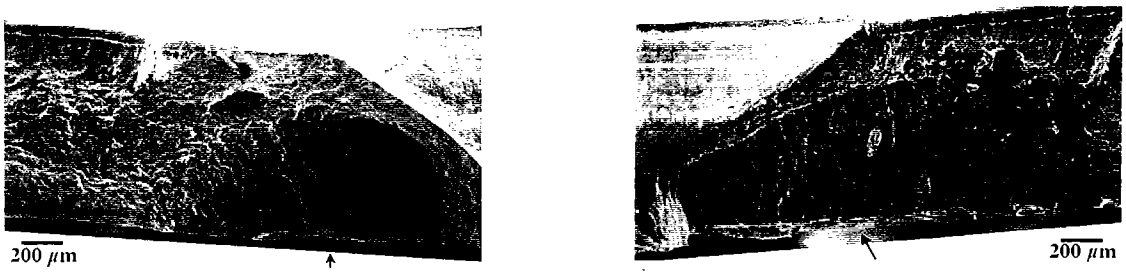

a) b)

Fig. 4.21. **a)** Scanning electron micrograph of the bottom fracture surface showing the crack that corresponds to the crack shown on the right side of the acoustic scan in Figure 4.20.

b) Scanning electron micrograph of the bottom fracture surface showing the crack that corresponds to the crack shown on the left side of the acoustic scan in Figure 4.20.

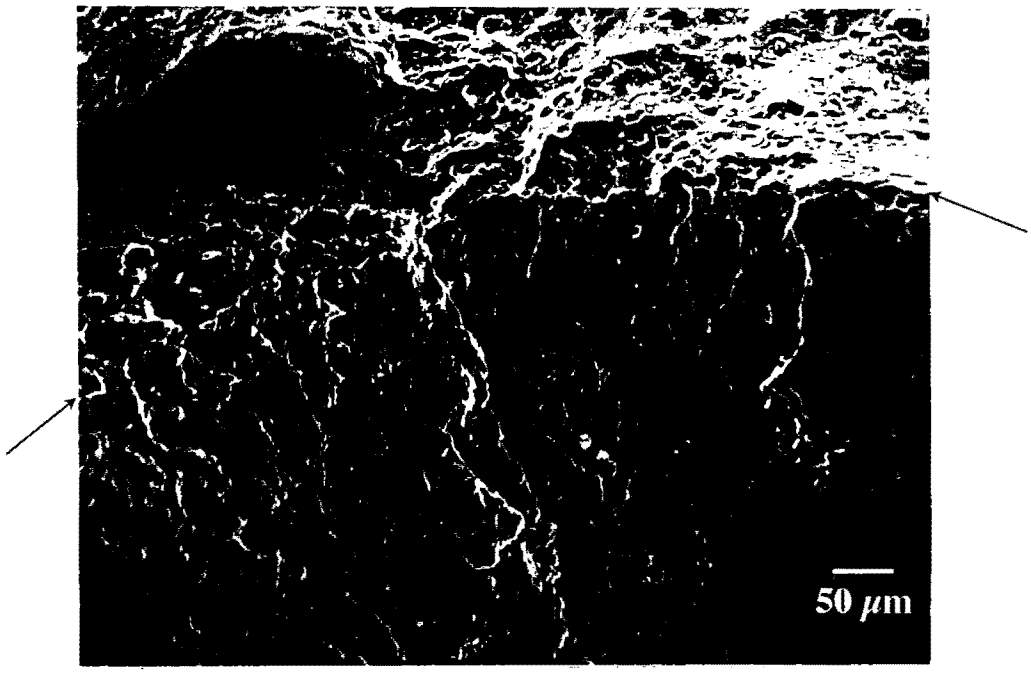

Fig. 4.22. Micrograph of the fracture surface of a specimen with arrows indicating the boundary between the fatigue crack and the dimpled ductile fracture resulting from pulling the specimen apart. (240,000 cycles)

A SAM C-scan showing a barely visible crack formed at a maximum nominal stress of 103 MPa is shown in Figure 4.23. This crack had just emerged from under the rivet head but was below the outside surface. No rumpling was seen on the outside surface. The fatigue fracture surface is shown in Figure 4.24, a scanning electron micrograph of the fracture surface. The fatigue crack on the right is the one imaged in Figure 4.23. It has extended about 500 μm beyond the top of the chamfer and rivet head and has its maximum length on the hidden surface of the chamfered panel. The crack on the left side, clearly visible in the fractograph, has not yet emerged from under

the rivet head and was not seen by the SAM. The fracture surface of this specimen exposes several fatigue crack initiation sites on each side of the rivet head. The initiation sites for all of these cracks are located on or very close to the hidden surface some distance from the rivet. By tilting the specimen and examining it under an optical microscope, these cracks were determined to be shear cracks initially. The initial cracks form along shear bands oriented close to the maximum shear direction.

The multiple cracks that had initiated grew laterally and outward from the initiation sites and eventually would have linked up to form single cracks such as the ones shown in Figure 4.21. Growth normal to the hidden surface of the panel is slower; the crack shape is semi-elliptical. Note that the cracks on each side of the rivet in Figure 4.24 have not linked up in the interior of the panel and the crack front is cusp-shaped. Initial formation of many cracks and emergence of a dominant crack by faster growth and coalescence with other cracks is often observed in fatigue failures.

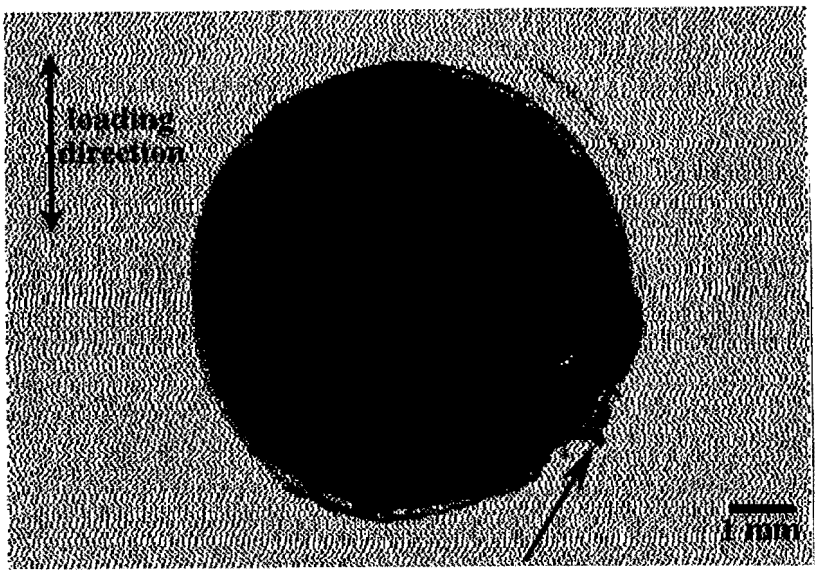

Fig. 4.23. C-scan showing a barely visible crack that formed at a maximum stress of 103 MPa. The arrow points to the indication. (100,000 cycles)

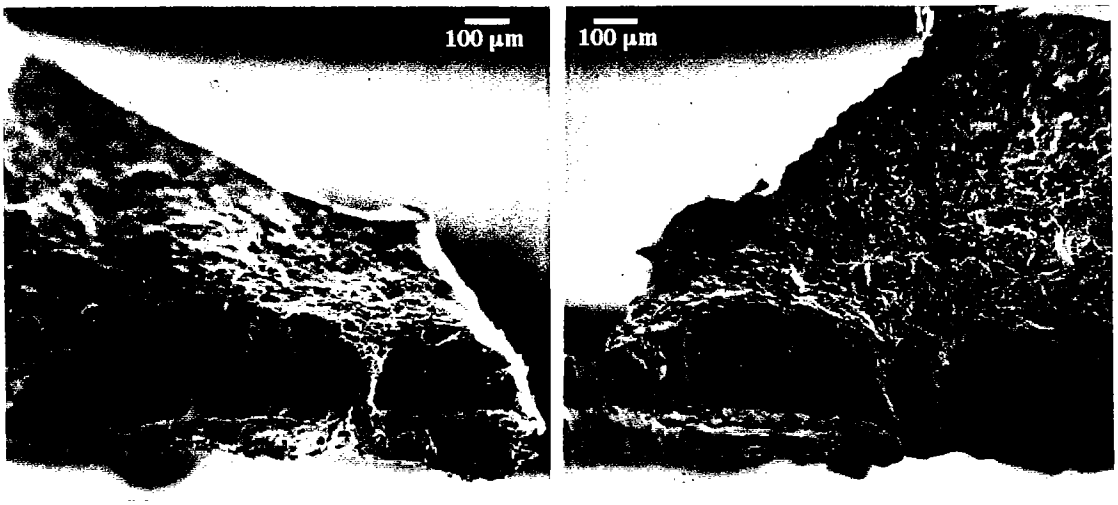

Fig. 4.24. Scanning electron micrograph of the fracture surface of the specimen on which the C-scan was taken in Figure 4.23. Multiple initiation sites are seen on each side of the rivet.

4.4.3.1. Shear Cracking

At a very early stage of the fatigue process, shear cracking was observed as seen in the scanning electron micrographs in Figure 4.25a and 4.25b. This specimen was fatigued for a total of 80,000 cycles, and then the rivets were removed. The two sheets had to be pulled apart, which is evidence of adhesion that occurs at early stages of fretting fatigue and promotes crack initiation. No cracks were seen with the SAM, when the fatigue cycling was stopped.

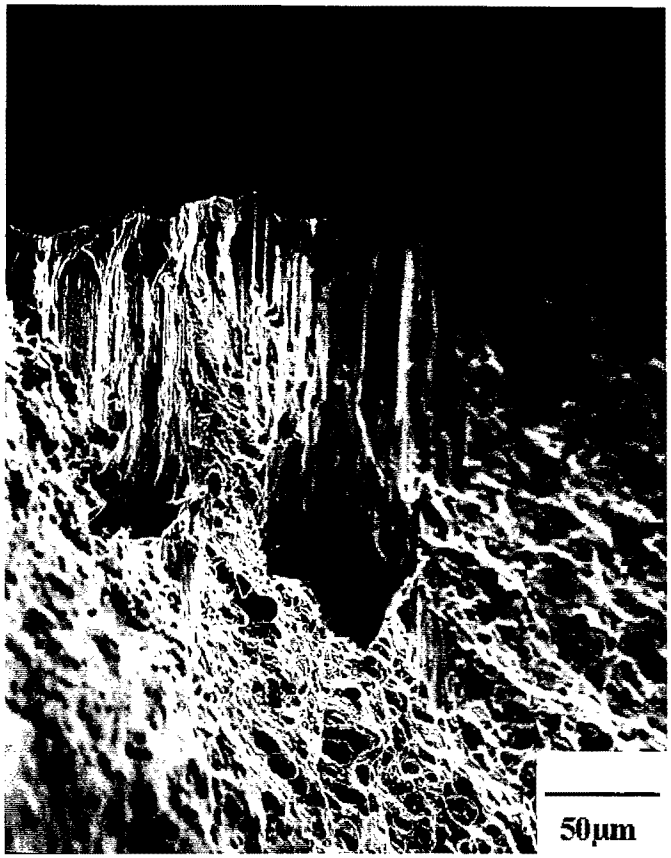

Fig. 4.25a. Shear cracking in a specimen fatigued for a total of 80,000 cycles. The fretted surface is shown at the top of the photomicrograph.

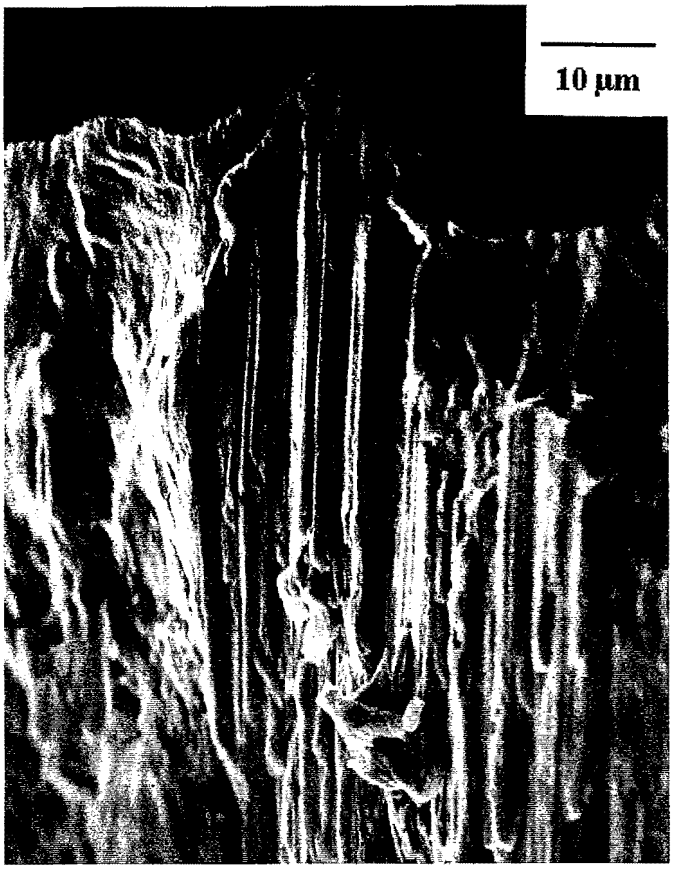

Fig. 4.25b. Shear cracking on same specimen as Fig. 4.25a at a higher magnification. Note planar stepped fracture surfaces.

4.4.3.2. Evidence of Fretting

Sometimes delamination of the Alclad layer from the 2024 alloy was observed. The mechanical deformation from the fretting leads to compressive surface residual stresses and tensile residual stresses away form the surface. This may be the source of

the delamination and may have contributed to the crack formation by fretting pit formation. Electron Dispersive X-ray (EDX) analysis revealed only aluminum in the wear particles. As the particles are quite bright due to charging in the SEM current, this is an indication that the particles are not conductive. Since the SEM cannot detect oxygen, it is concluded that the wear particles are a non-conducting compound, no doubt Al_2O_3. The white embedded particle in Figure 4.26 is an example of this. A crack is seen emanating from the tips of this particle as pointed out by the arrows. In Figure 4.27, a wear particle that is just beginning to break away from the substrate is observed. Another example of this with the wear particle at a later stage in the erosion process is given in Figure 4.28.

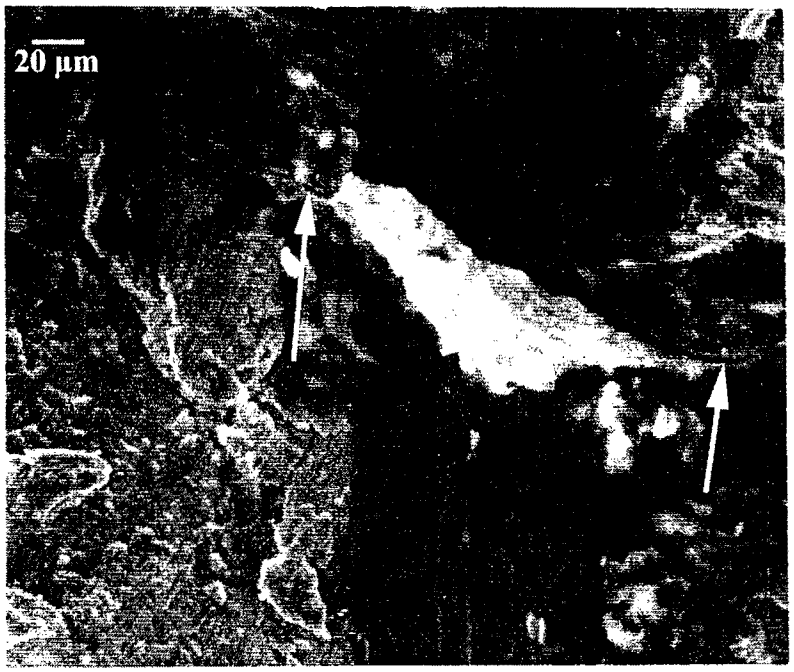

Fig. 4.26. White particle with cracks emanating from the tips and embedded in the fretted surface of a specimen. (80,000 cycles)

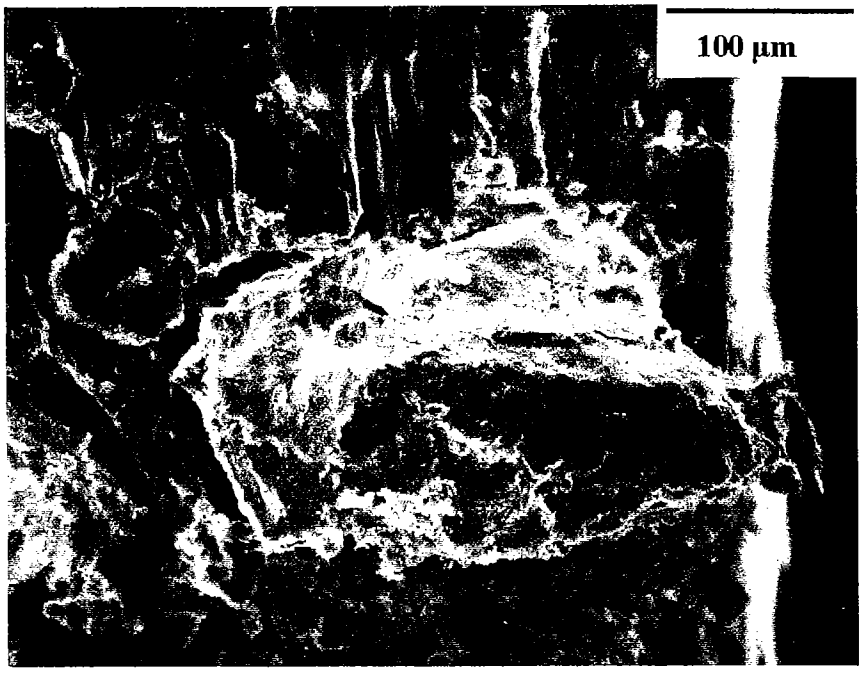

Fig. 4.27. Wear particle beginning to break away from the substrate. (3600 cycles)

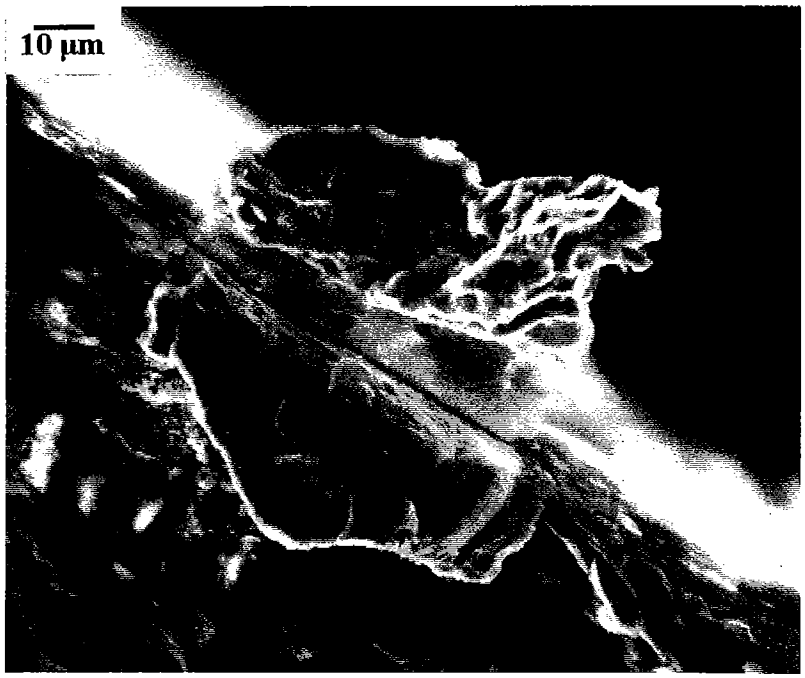

Fig. 4.28. Wear particle at a later stage in the erosion process. (80,000 cycles)

4.4.4. Possible Mechanisms for Crack Initiation and Growth at 103 MPa Maximum Nominal Stress

It was not possible to fully characterize the nucleation of the cracks in these riveted lap joints and decide exactly how they formed. All of them may be active. Recall multiple initiation sites were seen. There are at least three mechanisms by which these cracks may nucleate:

1. Dislocations will pile up at inclusion particles until slip band cracking occurs to relieve the localized plastic strain and reduce the local dislocation density.
2. When wear particles break away from the substrate due to the observed fretting, pits will be left behind in the substrate. These pits act as stress raisers; cracks nucleate at the pits and then grow as microcracks by hopping from inclusion to inclusion. Also, wear debris resulting from the fretting action results in very high stress concentrators.
3. The wear particles will score the surface of the substrate causing stress raisers. Cracks will nucleate at these stress raisers and then grow as microcracks by hopping from inclusion to inclusion.

Any of these scenarios would account for the more pure 2524-T3 Alclad material having a longer fatigue life than the 2024-T3 Alclad material.

4.4.5. The Role Fretting Plays on Crack Initiation Sites

It is the belief of this author that the fatigue cracks initiate by a fretting mechanism and then propagate by a dislocation mechanism. The initiation sites for

fatigue cracks are typically where there is a stress concentration. As mentioned above, both pits and embedded particles are sites of stress concentration. Evidence of this is shown in Figure 4.26 where an embedded particle has cracks emerging from both ends of the particle. Wear particles that are breaking away from the substrate are observed in Figures 4.27 and 4.28. Wear particles are seen at or near initiation sites in Figure 4.18 and Figure 4.29. Black particles are seen on the fayed surfaces at Rivet 3. As already mentioned, analysis of wear particles with EDX analysis indicated that they were Al_2O_3. Also as already mentioned, the delamination of the Alclad layer from the 2024 alloy was observed. This could result in fretting pit formation. Additionally, the soft aluminum cladding is easily scored by hard oxidized wear particles.

The initiation sites for specimens fatigued at a maximum applied stress of 103 MPa, as already noted, are located some distance from the blunt knife portion of the rivet hole. (Figures 4.21 and 4.24) When cracks nucleate away from rivet holes in lap joints, this is an indication that they were likely caused by fretting (Forsyth, 1981; Beard, 1988; Hoeppner, 1994; Müller, 1995; Fawaz, 1997) as opposed to cracks initiating at the centerline of the rivet hole as is expected since this is where the stress intensity factor is the greatest for a countersunk hole. In results reported by Piascik et al. (1997), fretting was the major cause of crack nucleation in tests performed on a full-scale fuselage. There was a correlation between the degree of fretting and cracking.

The cracks do not initiate at the centerline at the stress of 103 MPa as expected and is further evidence that the fatigue cracks initiate by a fretting mechanism. Still more evidence is seen when viewing the mating surface of the specimens fatigued at the

different levels of stress. At 103 MPa, a great deal of fretting damage is seen around the entire rivet hole (Figure 4.14) while little fretting damage is seen around the bottom of the rivet hole at 154 MPa (Figure 4.33b) When fretting occurs around the entire rivet hole, this indicates fretting is the primary cause of fatigue rather than the stress concentration at the hole. [Forsyth, 1981] At the higher stress of 154 MPa, crack nucleation results *primarily* due to the stress intensity factor at the centerline of the rivet hole.

More light on the fretting fatigue is given by the holographic NDE studies of Baird et al. (1996) on the deformation that occurs in riveted lap joints at various loads. In their research, at low loads, the rivet and the surrounding sheet material appeared to move as a single body indicating that friction forces between the two sheets of material in the lap joint was the primary mechanism for load transfer. At high loads, the friction forces seemed to play a much smaller part in the load transfer and a larger portion of the load was transferred through the rivet shank.

Fig. 4.29. Photomicrograph of the fracture surface of a specimen showing an embedded wear particle at or near the initiation site of one of the cracks. Several microcracks have linked up to form one macrocrack. (240,000 cycles)

4.5. Fatigue at High Nominal Applied Stress

When specimens were fatigued at a maximum nominal applied stress of 103 MPa and an R ratio of 0.1, as already discussed, "eyebrow" type cracks formed. When the maximum nominal applied stress was increased to 154 MPa or higher, a diametral radial crack formed. (A similar behavior was noted on stress increase with seven rivet specimens). These are schematically shown in Figure 4.30 and the two kinds of cracks are shown in the C-scans in Figures 4.31 and 4.32. The former was fatigued at 103 MPa nominal stress for 205,000 cycles. The end-to-end crack length is 8.1 mm. The

specimen in Figure 4.32 was fatigued at a maximum nominal applied stress of 154 MPa for 5500 cycles giving end-to-end crack length of 9.7 mm.

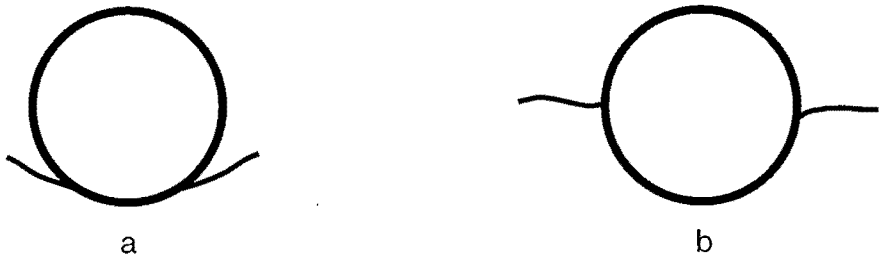

Fig. 4.30. a) Sketch showing an eyebrow type crack **b)** Sketch showing a centerline type crack

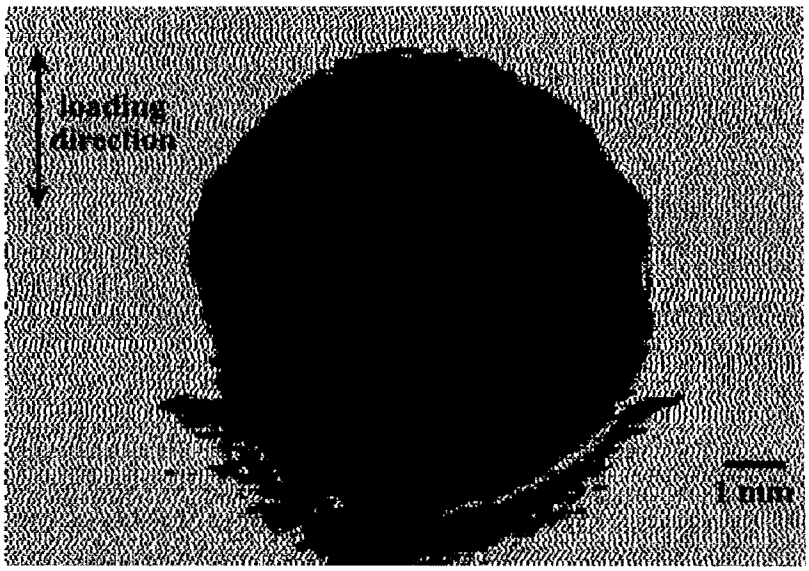

Fig. 4.31. C-scan showing an eyebrow type crack. This specimen was fatigued at a maximum nominal applied stress of 103 MPa for 205,000 cycles and has an end-to-end crack length of 8.1 mm

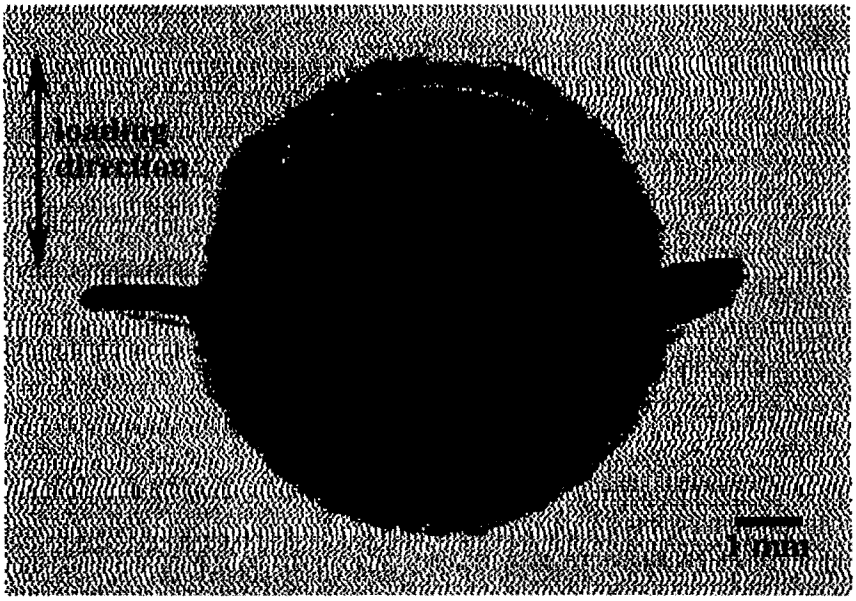

Fig. 4.32. C-scan showing a centerline type crack. This specimen was fatigued at a maximum nominal applied stress of 154 MPa for 5500 cycles and has an end-to-end crack length of 9.7 mm.

Figure 4.33a is an optical micrograph of the front surface of a specimen fatigued at a maximum nominal applied stress of 206 MPa for 900 cycles. The centerline crack is clearly visible. The micrograph shows that at this high load the rivet is beginning to pull out and that there is competition between the specimen fracturing due to the fatigue crack or the specimen failing due to the rivet pulling out. These observations are important, because the fuselage of an aircraft will experience higher stresses as cracks grow resulting in the cross sectional area decreasing so the stress is higher at adjoining rivets. Figure 4.33b is a micrograph of the damaged surface of the same specimen as

shown in 4.33a focused on the panel and reveals that the area surrounding the bottom half of the rivet hole appears to be relatively free from damage. The end-to-end centerline crack length as measured in the acoustic C-scan is about 10.0 mm. When the end-to-end crack length was measured optically, it was about 9.2 mm, so the crack at this length is longer than measured on the outside surface of the chamfered panel. As already discussed, similar behavior is seen for short eyebrow type cracks. The maximum bending stress due to the bending moment in the riveted specimen is on the back surface of the countersunk panel at the rivet head of Rivet 3 resulting in the visible surface being in compression and the fayed surface being in tension as already discussed. This is one source for the cracks being longer on the fayed surface. The centerline crack is initiated on a subsurface at the knife edge as shown later. In a panel with a chamfered hole, the initiation is also at the knife edge. [Fadragas, 1993]

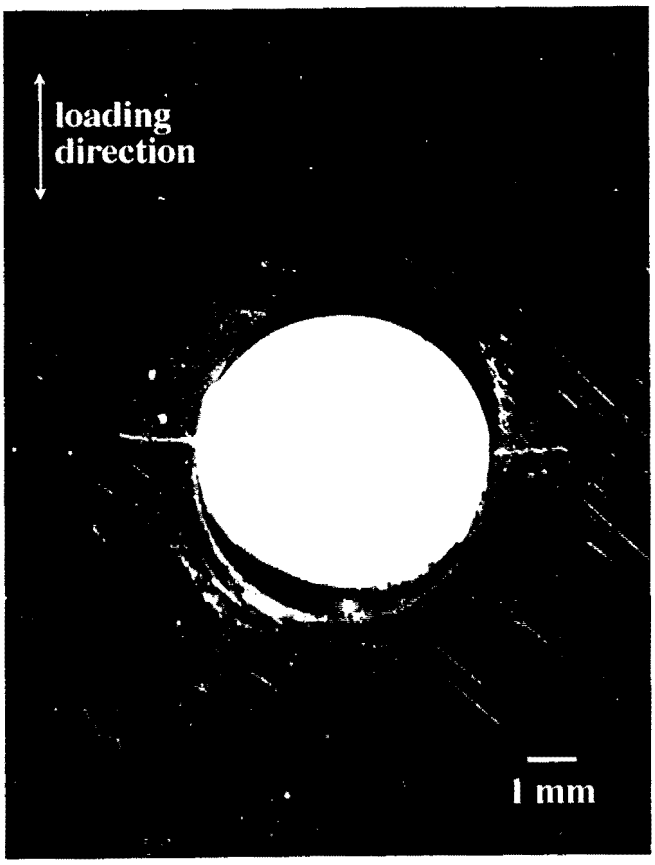

Fig. 4.33a. Optical micrograph of the front surface of a specimen that has a centerline type fatigue crack. This specimen was fatigued at a maximum nominal applied stress of 206 MPa and an R ratio of 0.1. (800 cycles)

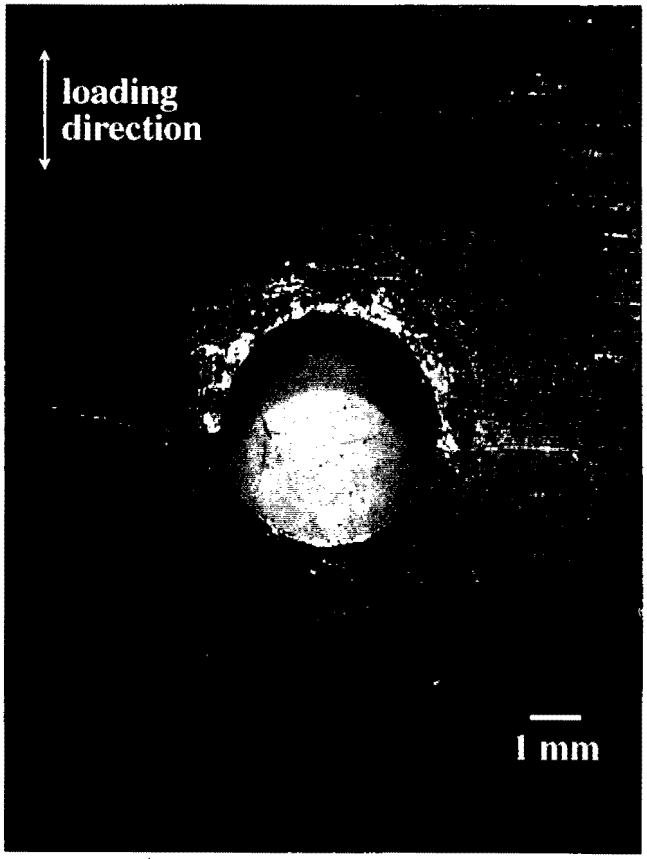

Fig. 4.33b. Optical micrograph of the damaged surface of the specimen shown in Figure 4.33a. Note that the area surrounding the bottom half of the rivet appears to be relatively free from damage. (800 cycles)

Specimens were tested at maximum nominal stresses of 180 MPa, 154 MPa, 129 MPa and 103 MPa to determine the effect of applied stress on the mode of fatigue cracking. At 180 MPa and 154 MPa, the fatigue cracks that formed were located radially at 3 and 9 o'clock around the rivet with respect to the stress direction such as shown in Figure 4.33a and 4.33b, but at 129 MPa, the fatigue cracks that emerged on the surface were somewhere between a centerline type crack and an eyebrow type crack. So, between 103 MPa and 154 MPa, there is a change in the cracking mode. (A similar behavior was noted on stress increase with seven rivet specimens.) As already discussed, the initiation sites of the cracks in specimens fatigued at 103 MPa were at some distance from the rivet hole and on the inner surface of the countersunk panel as shown in Figures 4.21 and 4.24, while as shown later, the initiation sites for the centerline cracks are at or very close to the knife edge.

4.5.1. Fractography of Specimens Fatigued at 154 MPa Maximum Nominal Stress

Figure 4.34 is a scanning electron micrograph of the fracture surface of a specimen fatigued at a maximum nominal stress of 154 MPa. An enlargement of the blunt knife edge region on the left in Figure 4.34 is shown in Figure 4.35. The figure shows the chamfered region, which is lighter in shading than the fracture surface. The crack in the panel starts as a shear crack near the centerline of the rivet hole and on the fayed surface between the rivet and panel somewhere near or at the blunt knife edge - hidden surface corner. After a very small amount of crack growth, it changes to a mode

I crack. The specimen was tilted 20° in the SEM to more clearly show the shear region and the rivet hole illustrating the change in mode from a shear crack to a mode I crack. The boundary on the fracture surface between shear and mode I has been marked by a dotted white line. The just initiated crack is expected to be a shear crack nucleated by a dislocation process. At 154 MPa nominal stress range, the transition from a shear to a mode I fatigue crack occurs at a very much smaller crack length than at 103 MPa. Both Mode I and mixed mode eyebrow cracks are seen in aircraft skins. Note that the fatigue crack shown in Figure 4.34 has not reached the outer surface and would not be seen by optical examination of the outer surface.

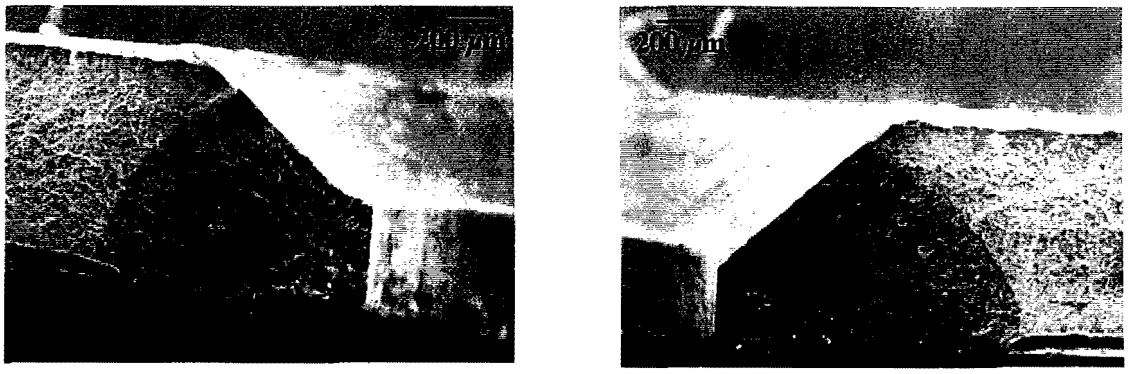

Fig. 4.34. Scanning electron micrograph of the fracture surface of a specimen, which was fatigued at a maximum stress of 154 MPa. (3600 cycles)

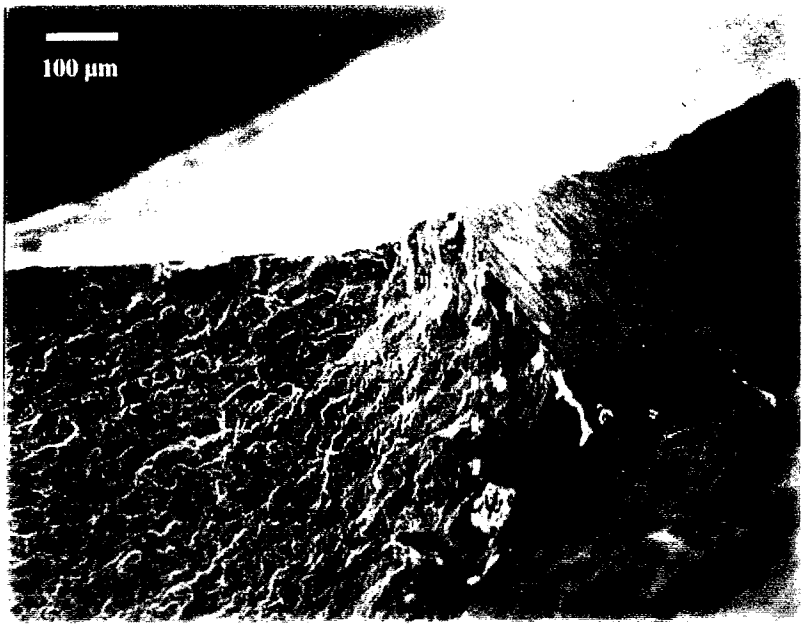

Fig. 4.35. Scanning electron micrograph of the crack on the left side in Figure 4.34. The transition from a shear crack to a crack that is propagating normal to the direction of the applied stress is given by the dotted line. (3600 cycles)

A SAM image of a crack formed at a maximum nominal stress of 154 MPa that has just emerged from under the rivet head is shown in Figure 4.36, and the corresponding fracture surface as viewed with the SEM for this specimen was given in Figure 4.34. While there are cracks on both sides of the rivet, the SAM only indicated the larger of the two.

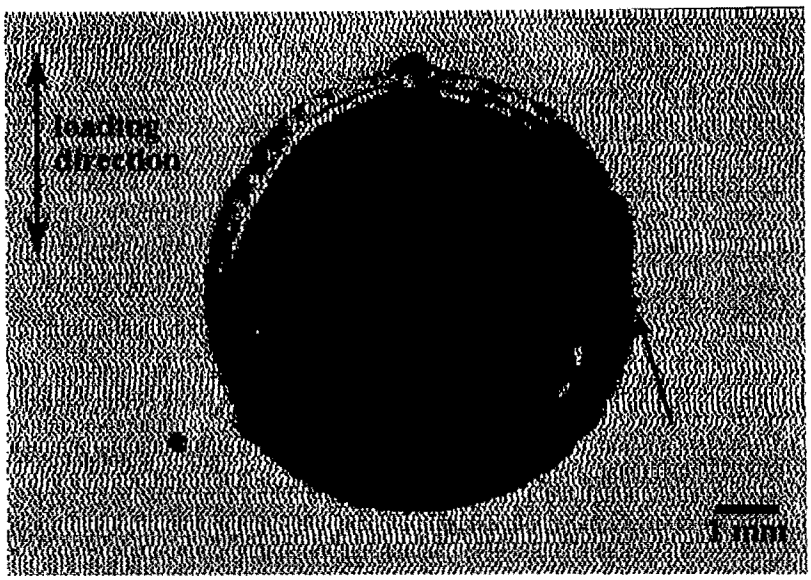

Fig. 4.36. C-scan image of a fatigue crack formed in a specimen at a maximum stress of 154 MPa. The arrow shows the indication. (3600 cycles)

Figure 4.37 is an optical micrograph of the fayed surface of a specimen fatigued at 154 MPa. A propagating crack is seen emanating from the rivet hole at the boundary between the damaged surface and the surface, which is relatively free of damage. When fretting occurs only on one side of the fatigue crack, Forsyth (1981) concluded that the propagating crack occurred before a major amount of fretting damage has occurred. The figure shown is evidence for this.

Fig. 4.37. Optical micrograph of the fayed surface of a specimen fatigued at 154 MPa. (3000 cycles)

4.5.2. Characteristics of Fracture Surface for Specimens Fatigue at High Stress

At the higher nominal stress of 154 MPa, regions of ductile fracture were seen in the fatigue crack area. (Figures 4.38a and 4.38b) This happens when microscopic crack linking occurs as the crack advances. Both photomicrographs in Figures 4.38a and

4.38b are of the same specimen with a higher magnification in Figure 4.38b. Voids, void linking, microcracks as well as fatigue striations are seen.

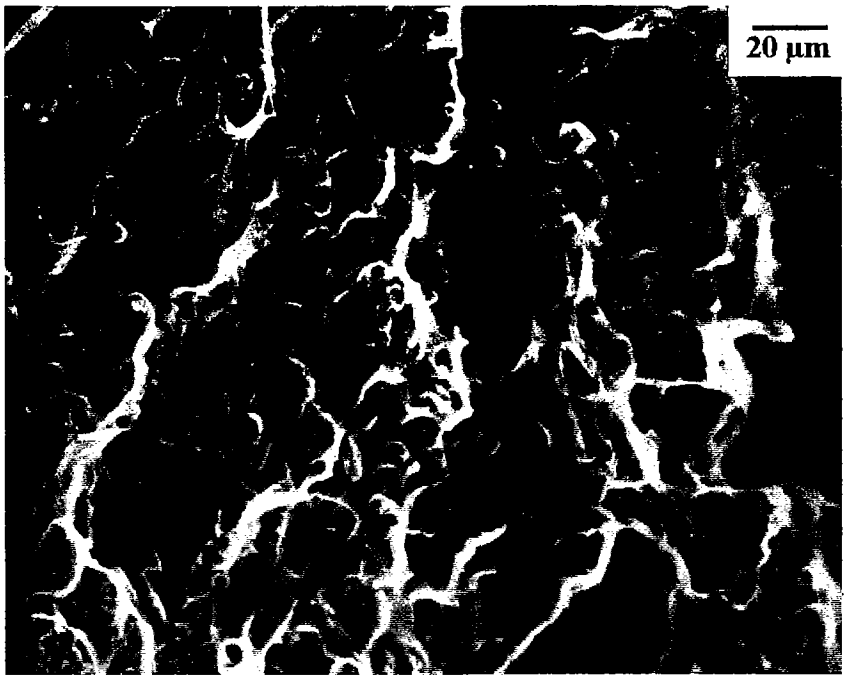

Fig. 4.38a. Optical micrograph showing regions of ductile fracture and fatigue fracture on the fracture surface of a specimen fatigued at a maximum nominal stress of 154 MPa. (3000 cycles)

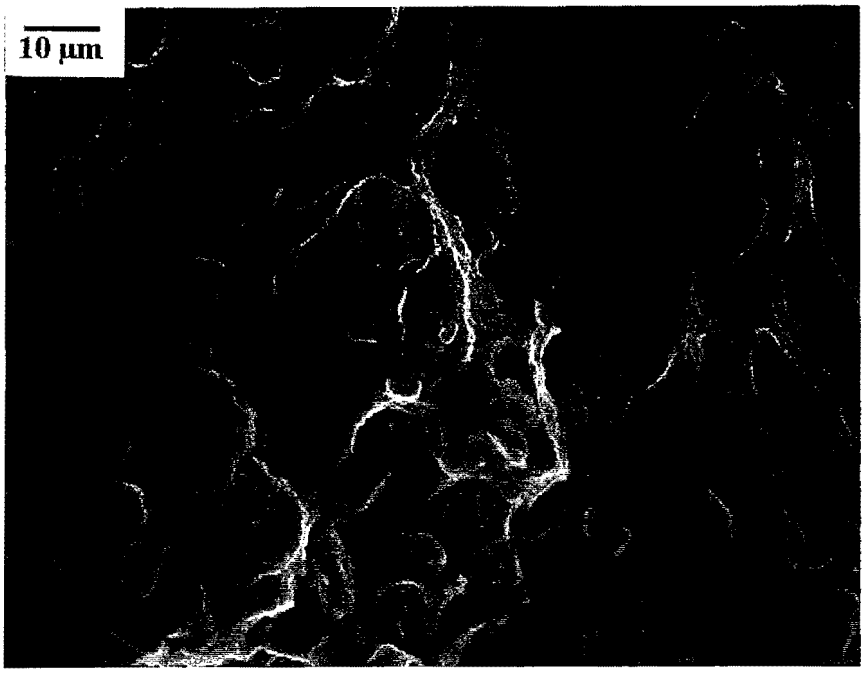

Fig. 4.38b. Optical micrograph at a higher magnification of the same specimen as in Figure 4.38a showing regions of ductile fracture and fatigue fracture.

4.6. Summary

The scanning acoustic microscope has been useful in the characterization of small cracks on or near the faying surface of riveted lap joints. More than one initiation site is observed on each side of the rivet hole in the critical row of rivets at stresses comparable to those experienced by many types of aircraft. The microcracks eventually join to produce one macrocrack on each side of the rivet hole. These macrocracks are

quite long before they break the outer surface. The cracks start as shear cracks at both high and low stresses. This has been observed in a number of specimens that have been studied in this research and is an indication that slip bands are in play.

There is competition between the two observed kinds of fatigue cracks; the eyebrow cracks i.e., cracks that intersect the rivet hole off the centerline observed at lower stresses and the diametral cracks observed at higher stresses. The former initiates at or near the hidden surface of the chamfered panel some distance from the rivet hole. The latter initiates in the portion of the blunt knife edge near the hidden surface. The radial crack becomes a mode I crack soon after initiation. The eyebrow crack also transforms to a mode I crack but at a very much longer crack length. At high stresses the cracks initiated at or near the corner where the faying surface and the rivet hole meet. The cracks at various lengths after they were detected by the acoustic microscope were characterized primarily by fractography. The detection of these cracks long before they break the outer surface with the acoustic microscope enables the study of these cracks when they are very small. Fretting fatigue reduces the cycles to initiation of an eyebrow type crack.

The microstructures of Alclad 2024-T3 and Alclad 2524-T3 were compared. The inclusions in the 2524 alloy are less than the 2024 alloy thereby providing fewer crack initiation sites.

5. Crack Growth Evaluation

5.1. Introduction

The well known Paris equation for macrocrack propagation:

$$dc/dN = C(\Delta K)^m \tag{5.1}$$

where c is the fatigue crack length, N is the number of fatigue cycles, ΔK is the stress intensity factor range and C and m are constants, has been used to analyze fatigue cracks in specimens of Al Alclad 2024-T3 with a single chamfered hole. [Fadragas, 1993] Of course, the formula for calculating ΔK varies with the specimen geometry.

Equation 5.1 may be modified to:

$$dc/dN = A(\sigma c^{(1/2)}))^m \tag{5.2}$$

where c is the half crack length, σ is the peak stress and A includes the unknown geometric connection. The usual value for m in the Paris equation is 4. [Frost et al., 1974]

The length, c, on each side of the rivet cannot be unambiguously obtained either optically or with the scanning acoustic microscope, because the crack is initially hidden beneath the rivet. For this reason, a crack length of 2c, as shown in Figure 3.6, was

used to obtain both surface and subsurface crack lengths. The crack length, a, is defined in Figure 3.6 as the length of the crack that extends beyond the rivet head on the surface of the specimen and was initially used to measure crack lengths with the optical microscope.

5.2. Maximum Nominal Applied Stress of 103 MPa

Originally, surface crack growth curves were obtained on specimens by in situ measurements of surface crack lengths at intervals in the fatigue cycling. This was accomplished using an optical microscope mounted onto the MTS machine. The surface crack growth curves for five specimens fatigued at a maximum nominal stress of 103 MPa are plotted as a vs. N in Figure 5.1. There was a wide variation in the number of cycles until the first propagating radial crack was seen. It occurred on one side of the specimen and then later occurred on the other side of the specimen. Its length when first seen was in the range of 0.5 mm to 1.7 mm. The variation in the number of cycles until a propagating crack was seen is ascribed to variations from specimen to specimen in machining the hole and in riveting. This was controlled more carefully than in industry, so more variation is expected in industry. The number of cycles between the first observation of rumpling and the first propagating radial crack

were between 20,000 to 80,000 cycles. Observations were made every 10,000 cycles initially and more frequently after rumpling was observed. The normal probability plot given in Figure 5.2 shows a normal distribution and a standard deviation of about 120,000 cycles as estimated by taking the difference between the eighty-fourth the fiftieth percentiles.

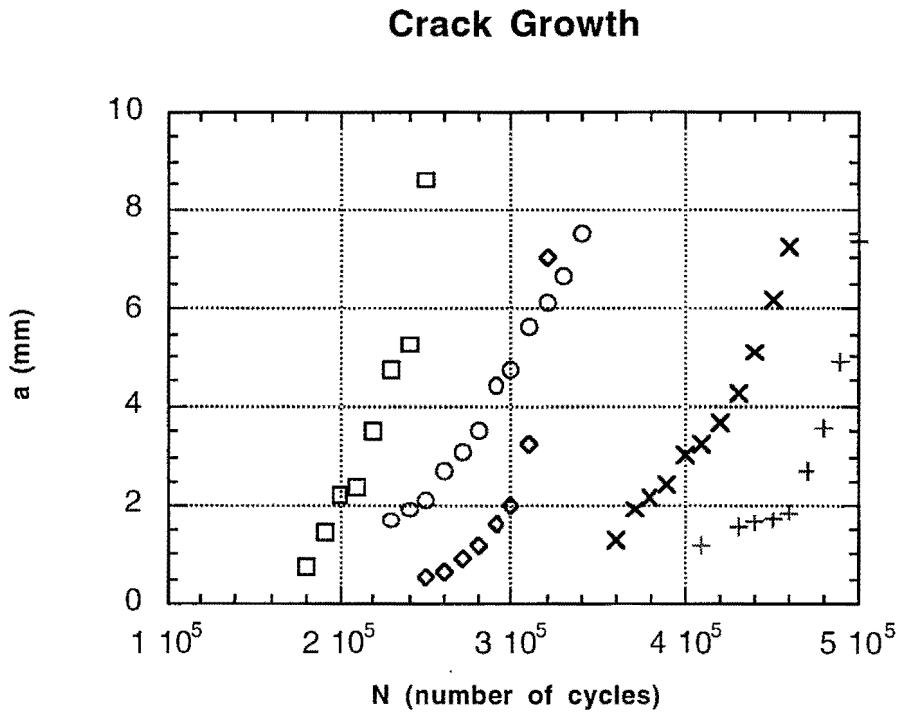

Fig. 5.1. Crack growth data on surface of five specimens fatigued at a maximum nominal stress of 103 MPa. Note the wide variation among specimens in the number of cycles until a growing macrocrack was first observed.

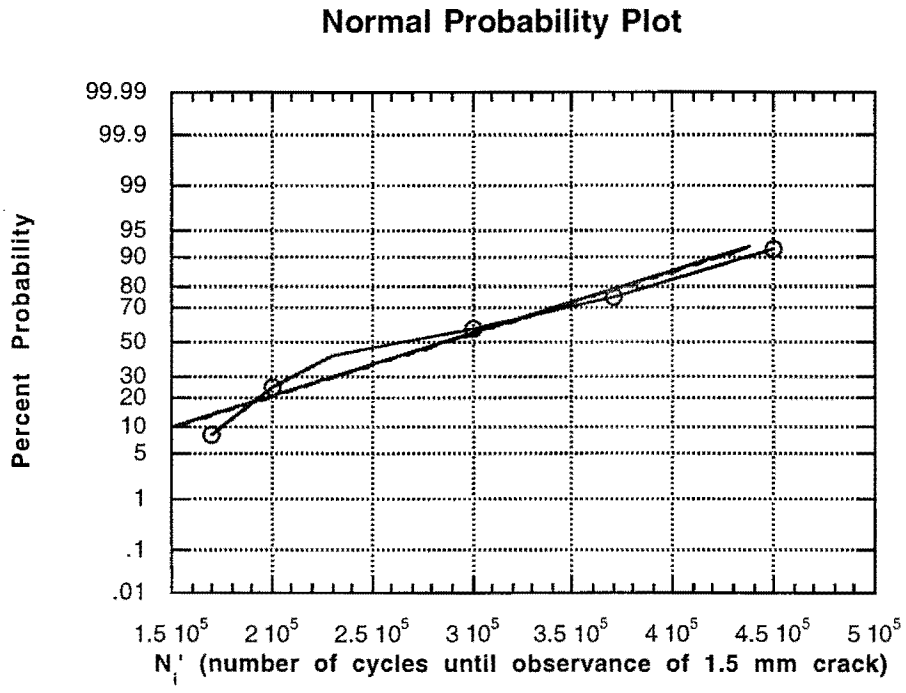

Fig. 5.2. Normal probability plot for the number of cycles until the observance of 1.5 mm crack on the surface. From this, the standard deviation is about 120,000 cycles.

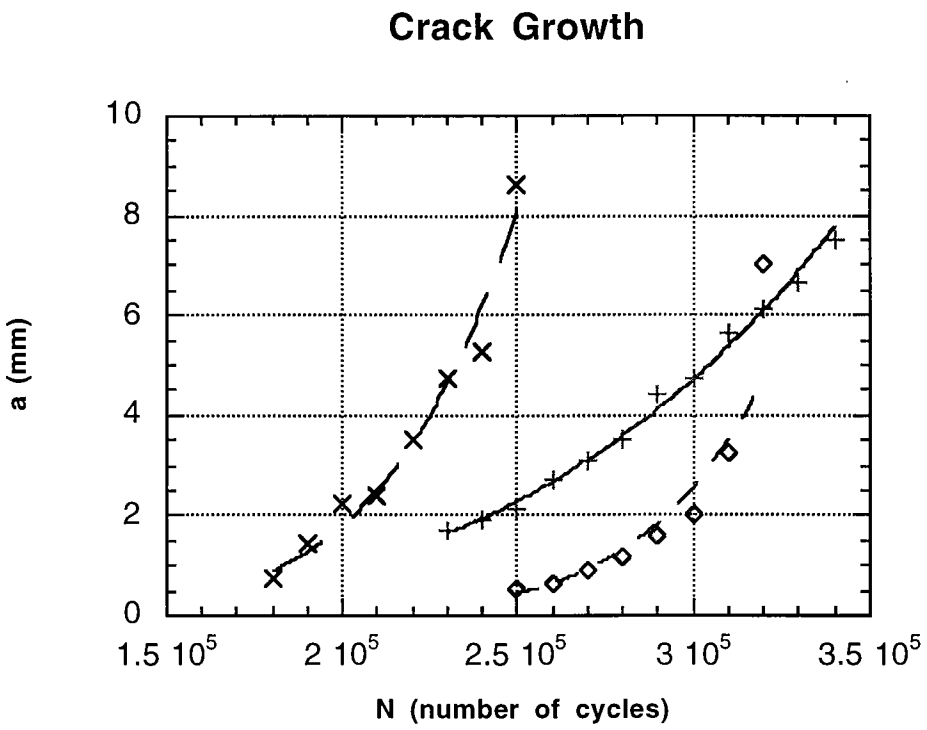

Fig. 5.3. Crack growth data of first three specimens fatigued at a maximum nominal stress of 103 MPa in Figure 5.1 on an expanded scale to better show initial crack growth.

Typical crack growth data for the first radial crack seen is exhibited in Figure 5.3 on an expanded scale for three specimens. The rate of growth increases with length increase as expected. There is an interval of approximately 20,000 to 60,000 cycles during which crack growth is slow and an opportunity exists for early crack detection. This occurs when the length of a, as defined in Figure 3.6, is less than about 3 mm.

When a is equal to 3 mm, the leading crack edge is 12mm from the edge of the specimen and any edge effect should be minimal. Figure 5.4, which is a plot of a vs. N_{total} - $N_{2\ mm}$, shows that the number of cycles between a crack of approximately 2 mm and 7 mm in length is 20,000 to 105,000 cycles, a difference of 85,000 cycles. Thus there is significant difference in growth rate of the crack lengths on the chamfered surface from specimen to specimen as well as initial radial crack formation. Defining N_i as the number of cycles until a 2 mm radial crack had grown past the rivet head, it is observed that most of the lifetime is in this stage. N_i in the five specimens varied from 200,000 cycles to 450,000 cycles, a variation of 250,000 cycles. The average value of N_i was 310,000 cycles. Thus the variation in the number of cycles for crack initiation defined as a 2 mm radial crack is much greater than the variation in the number of cycles for crack growth from 2 to 7 mm as also reported by Schijve (1992). A greater variation is expected in commercial panels because the specimens made in the laboratory were held to much closer tolerances than called for in the Boeing specification that was followed in drilling the chamfered hole and making the rivet bucktail.

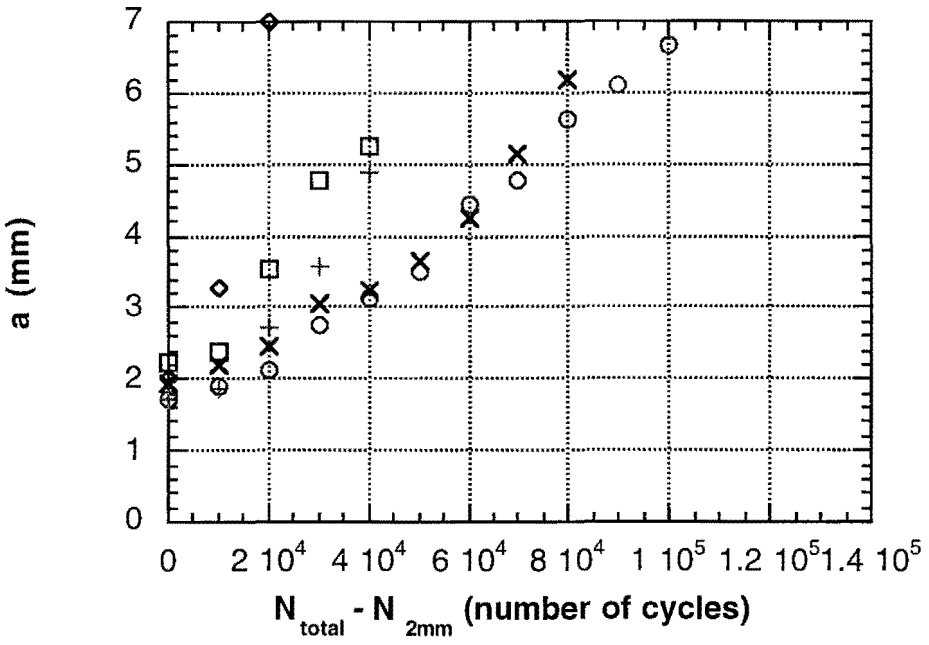

Fig. 5.4. Crack growth after formation of a surface crack 2mm in length, a vs. N_{total}-N_{2mm}. Specimens were fatigued at a maximum nominal stress of 103 MPa. Most of the variation in the total cycles to 7 mm is in the number of cycles for formation of a surface crack 2 mm long.

Since ΔK cannot be calculated, log d(2c)/dN was plotted vs. log σ_{eff} $(2c)^{1/2}$ for these experiments rather than vs. ΔK as for the Paris equation. The effective stress, σ_{eff}, is defined as the maximum applied load divided by the total cross-sectional area, including the rivets. Such a plot for the 5 specimens is shown in Figure 5.5. d(2c)/dN was determined from 2c vs. N crack growth curves after radial cracks on

both sides of the rivet were seen. The range of 2c plotted is 6 mm to 20 mm. Macrocrack growth is divided into three regions: Region I is near threshold initial slow crack growth; Region II is power law growth; and Region III is unstable growth to final failure. In several specimens, the near threshold region of slow crack growth (Region I) was observed. Later a power law (Paris type) behavior indicative of Region II is suggested. Region III (unstable crack growth) occurs much later in the life of the specimen than plotted in the figure.

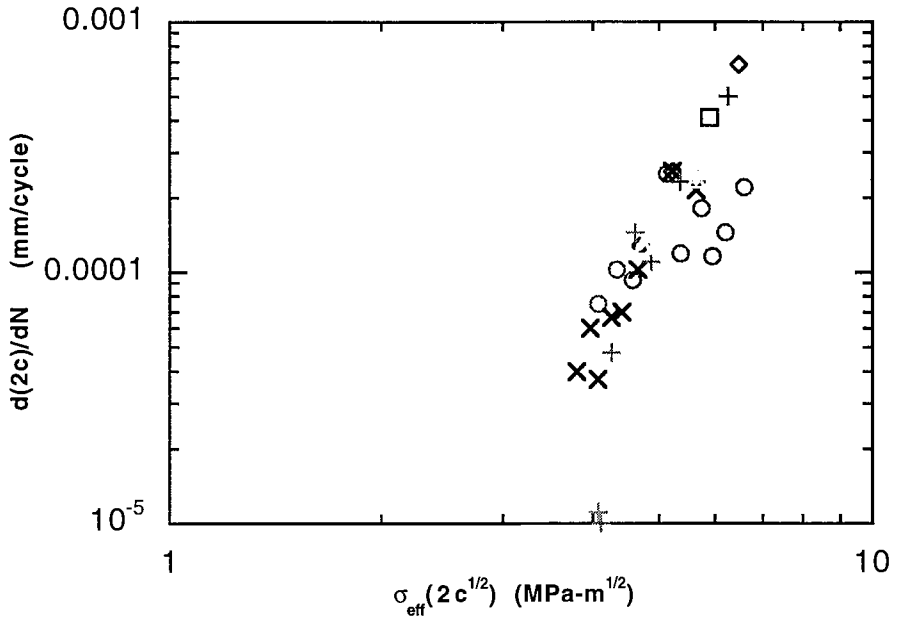

Fig. 5.5. Plot showing crack growth rate of end-to-end crack on both sides of the rivet as a function of the effective stress times square root of end-to-end crack length, 2c. Specimens were fatigued at a maximum nominal stress of 103 MPa.

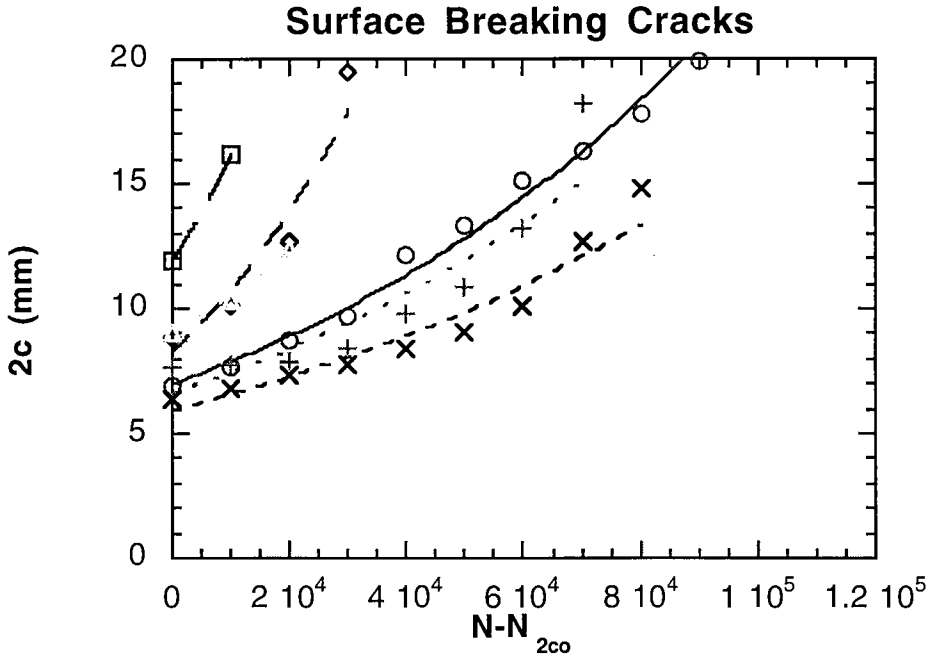

Fig. 5.6. Plot showing end to end surface crack growth vs. cycles in 6 specimens. N_{2co} is defined as the number of cycles until a crack of length 2c was first observed on the outer surface. 2c is defined in Figure 3.6. Specimens were fatigued at a maximum nominal stress of 103 MPa.

A series of experiments were done with different sets of specimens to better compare crack growth on the surface and in the interior. Defining N_{2co} as the number of cycles until a crack of length 2c was first observed on the outer surface, and N as the total number of cycles, a plot of the end-to-end crack length, 2c, vs. N - N_{2co}, is given in Figure 5.6. Crack length, 2c, is defined in Figure 3.6. While the rivet head is 6 mm in diameter for these eyebrow cracks, the chord is smaller than 6 mm. The variation in

length for $2c_o$ is partially due to the crack not always emerging next to the rivet head but some distance away and partially due to measurements being taken every 10,000 cycles so that the crack was not always detected as soon as it broke the surface. Using the acoustic microscope, the approximate number of cycles until a crack of length 2c was first seen in three specimens different from those in Figure 5.6 on which subsurface crack growth measurements were taken was defined as N_{2cs}. Using the same scale for the x and y axes as that in Figure 5.6, a plot of the subsurface crack length, 2c, vs. N- N_{2cs} is given in Figure 5.7. N_{2co} represents a more developed crack than N_{2cs}, because the crack is detected later on the surface than in the subsurface. At N_{2cs} no crack would be seen on the outer surface; however, at any give surface length the crack is longer on the subsurface. Comparing these two figures, it is obvious that the subsurface crack growth is much slower than the crack growth observed on the surface after the crack has broken the surface. Again, the measurements taken on these specimens were for *subsurface* crack lengths. $2c_s$ were between 6 and 8 mm when first detected. The fatigue tests were stopped prior to the cracks breaking the surface. Figure 5.8 is a plot of crack growth taken on three specimens *until failure* using the acoustic microscope. Data until about 17 mm is shown.

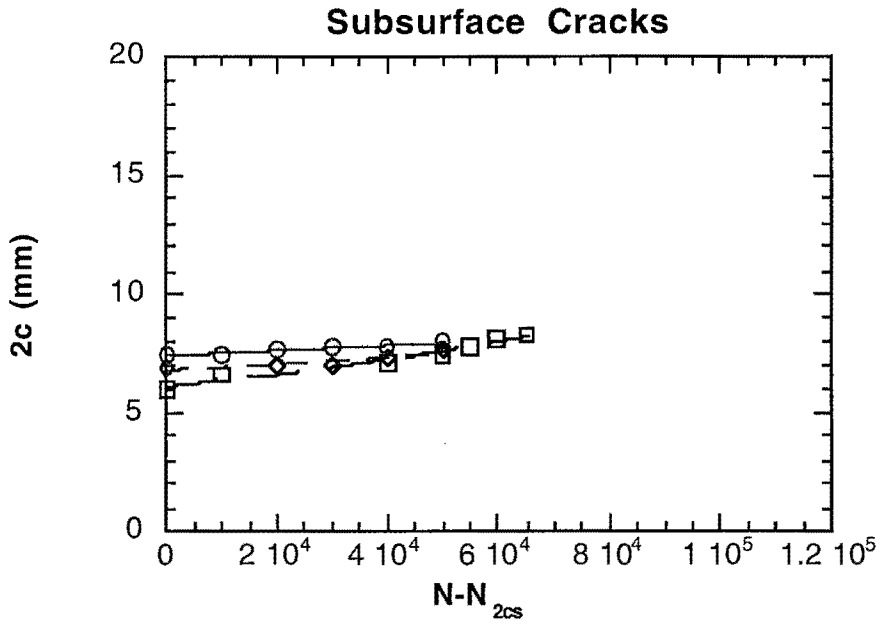

Fig. 5.7. Plot illustrating subsurface crack growth in three specimens different from those in Figure 5.6. Specimens were fatigued at a maximum nominal stress of 103 MPa.

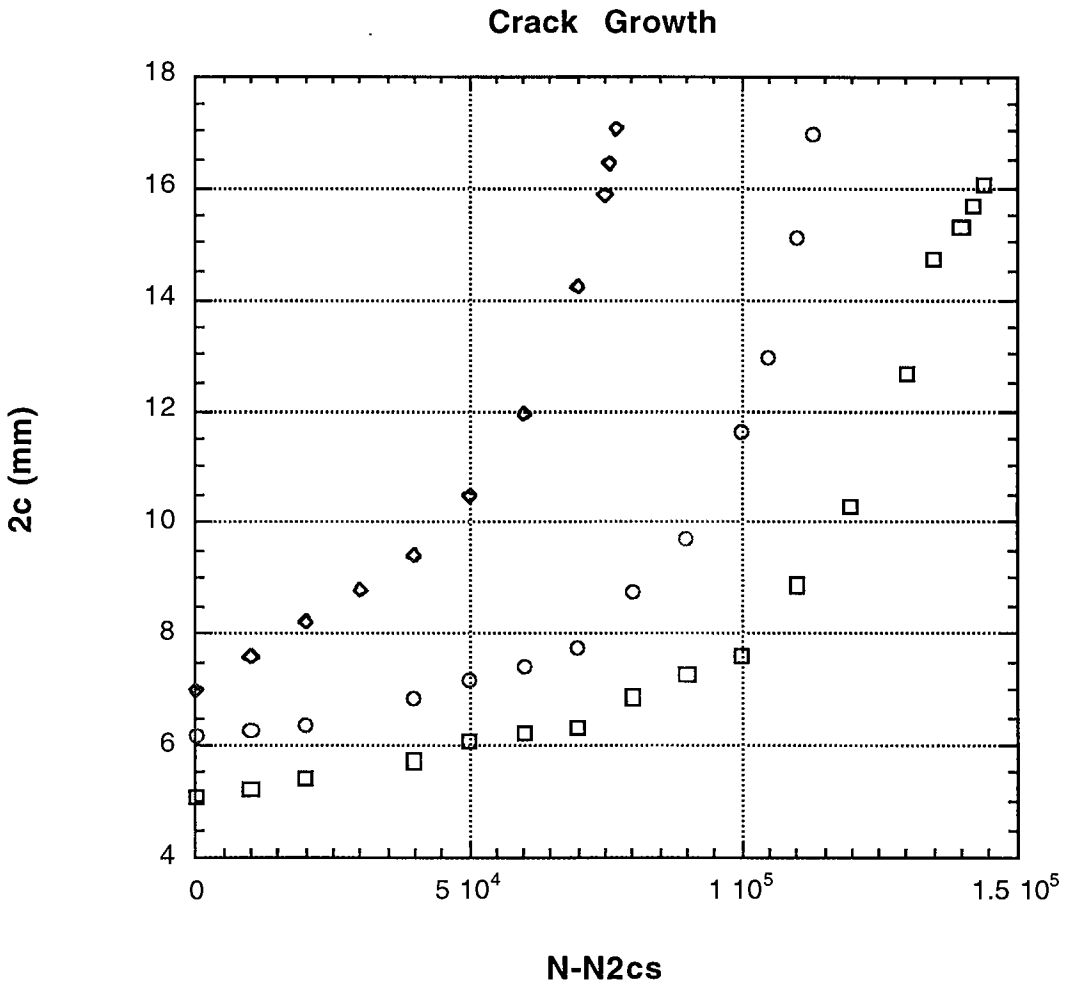

Fig. 5.8. Plot of crack growth for a maximum stress of 103 MPa as obtained with the SAM.

In Figures 5.9 and 5.10, dc/dN vs. $P(\pi c)^{1/2}$ were plotted, where P is the maximum load and c is defined in Figure 3.6 dc/dN was determined from the crack

growth curves, Figures 5.6 and 5.7. The data plotted in Figure 5.10 are for shorter cracks than the data plotted in Figure 5.9. The plot of dc/dN vs. $P(\pi c)^{1/2}$ for growth of the crack on the surface is given in Figure 5.9 and for crack growth measured subsurface in Figure 5.10. Considerable variation from specimen to specimen is noted in the subsurface crack growth rate, and there is evidence for crack arrest and crack growth retardation as commonly observed with microcracks. [Newman, 1994; Newman et al., 1997; Newman et al., 1994; Newman et al., 1988; Kaynak and Ankara, 1992; Wanhill and Schra, 1990] This could mean that the cracks hit some sort of barriers which they had to pass through (grain boundaries, precipitates, inclusions, etc.).

The main cause of the retardation in crack growth at low stress intensities when analyzing small crack data was found to be changing amounts of crack closure when analyzing small crack data. [Newman, Jr., 1995]

One reason for the growth of small cracks below the threshold for long cracks that has been advanced is smaller crack closure. Schijve (1982) has reasoned that a small crack has not had sufficient time to build up the plastic deformation equivalent to that of a long crack; and consequently, the crack closure effect is not so important in small cracks. Another factor is the change from a Stage I to a Stage II crack as it grows from a small to a large crack. [Schijve, 1982] Often, Stage II crack growth begins when

the crack reaches a grain boundary, inclusion or other obstacle. In a study performed by Pan et al. (1994), an acoustic microscope with a transducer frequency of 1 GHz was used to generated Rayleigh waves to image the near surface of an Al-Li 8090 alloy. Results of this study showed that the crack growth rate slowed when the crack tip neared a grain boundary and then increased after breaking through the grain boundary. It was determined by Wanhill and Schra (1990) that corrosion products can lead to crack blocking which in turn will lead to a slowing or arrest in fatigue crack growth in the near threshold regime. Wear particles in specimens in the research presented herein have been observed in the area of the fatigue cracks by EDS analysis as mentioned previously in Chapter 4.

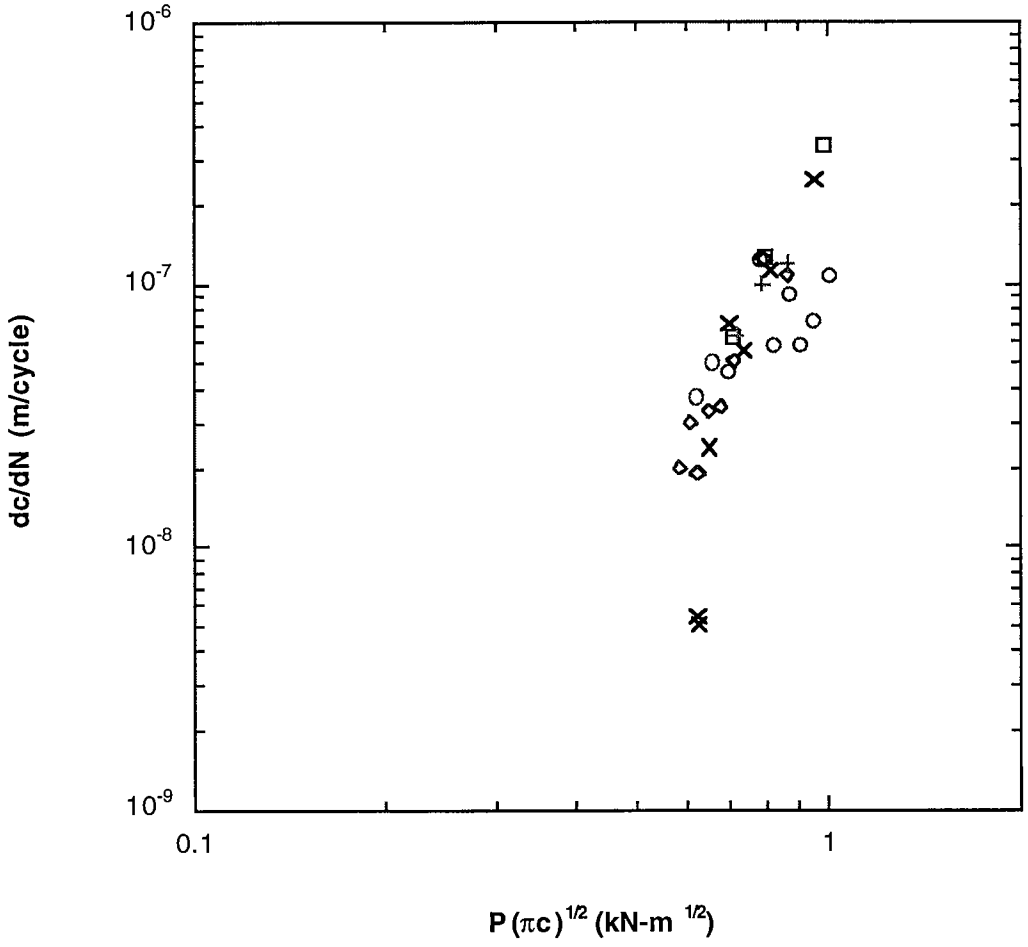

Fig. 5.9. Plot of dc/dN vs. $P(\pi c)^{1/2}$ for surface cracks that were measured using the optical microscope. Note these cracks are longer in the subsurface. Specimens fatigued at a maximum nominal stress of 103 MPa. dc/dN was determined from the crack growth curves, Figure 5.6.

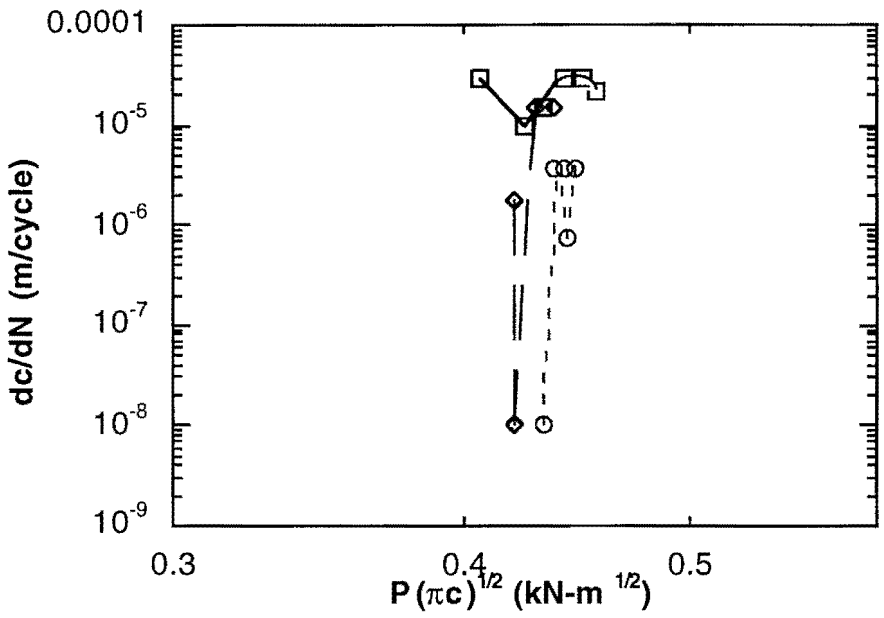

Fig. 5.10. Plot of dc/dN vs. $P(\pi c)^{1/2}$ for subsurface cracks that were measured using the scanning acoustic microscope. Note these cracks are longer in the subsurface. Specimens were fatigued at a maximum nominal stress of 103 MPa. dc/dN was determined from the crack growth curves, Figure 5.7

5.2.1. Comparison of Data Obtained at 103 MPa with SAM to FASTRAN-II

The computer code, FASTRAN-II, developed by Dr. J. C. Newman, Jr. (1992), was used to compare experimental results for specimens fatigued at a maximum nominal fatigue stress of 103 MPa to the predictions of the code. FASTRAN-II uses the crack closure concept, which says that the plastic deformation in the wake of the crack causes crack closure. From the crack opening stress equations developed by Newman

(1995), he then formed baseline ΔK_{eff}–rate relations used in FASTRAN II. The plot in Figure 5.11 gives the results of the FASTRAN-II analysis, which was run and then compared with results obtained with the use of the acoustic microscope. In FASTRAN, there are 17 defined crack configurations from which to choose. The surface crack configuration was used as the crack initiates a slight distance from the rivet on the fayed surface at a maximum stress of 103 MPa. When a lapjoint configuration was used that assumes a corner crack at the knife edge, the curve was much sharper than the observed behavior. Different types of cyclic loads may be applied. Constant amplitude was selected as the type of cyclic load to match the experiments. For the surface crack configuration, an initial, c_i, half-crack length and an initial flaw size, a_i, was specified. This is the nomenclature used in the FASTRAN program. Literally, a is the crack height and c is the half-crack length. Using the nomenclature in the FASTRAN program, an initial crack size of 2 mm was used as an approximation of the half-crack length at initiation. This is about half the distance between the initiation sites for the cracks on each side of the rivet hole. As the cracks at this nominal stress initiate away from the rivet hole and there are several initiation sites on each side of the rivet hole this is a very rough approximation. Also, it is not likely that the initial crack length would be as large as 2 mm. Initial flaw sizes of 15 μm and 30 μm were selected. Again this is not exactly representative of the types of

cracks that develop in the lap joint, because this assumes that there is only one initial flaw of height, a, when in actuality there are several initiation sites on each side of the rivet hole. The initial flaw size and initial crack size selected in conjunction with the type of load and crack configuration selected were made to give the best fit.

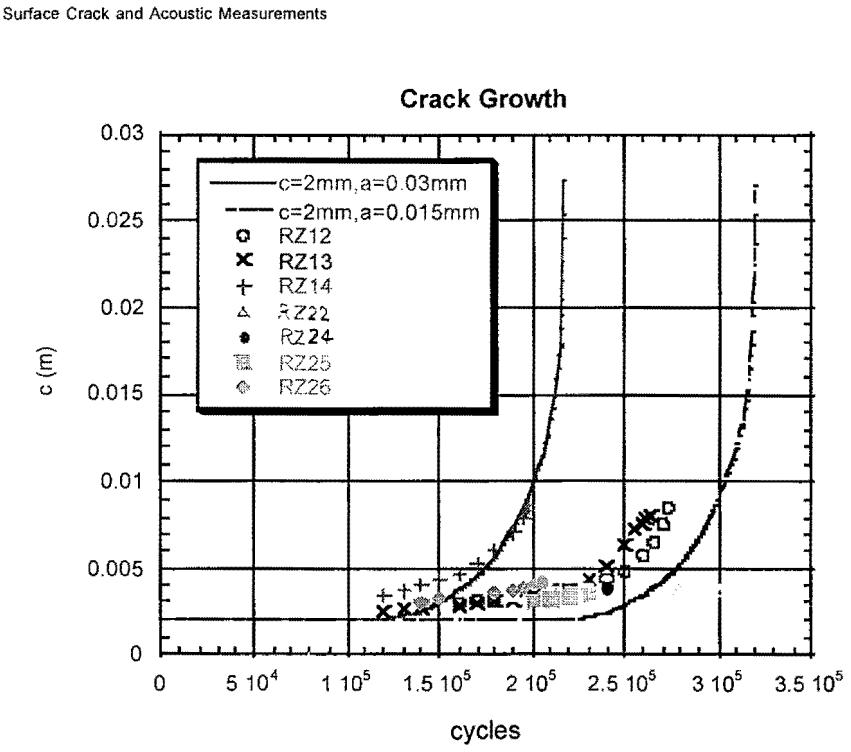

Fig. 5.11. Plot comparing crack length vs. number of cycles as obtained with the SAM and as acquired using FASTRAN-II analysis. Specimens were fatigued at a maximum nominal stress of 103 MPa. The solid and dashed lines are the FASTRAN-II predictions. As given in the language of the FASTRAN-II code, c is the half crack length and a_i is the initial flaw size.

5.3. Maximum Nominal Applied Stress of 154 MPa as Compared to Maximum Nominal Applied Stress of 103 MPa

The previous data taken with the optical microscope and with the acoustic microscope were on different specimens. Therefore, it was desirable to measure both on the same specimens. This was done for specimens fatigued at 154 MPa maximum nominal applied stress and for specimens fatigued at 103 MPa maximum nominal applied stress. Figure 5.12 is a plot of the crack growth of specimens fatigued at a maximum stress of 103 MPa and measured with the optical microscope and with the SAM. [Connor et al., 1998]. The first data points plotted are the numbers of cycles to when cracks were first observed with the SAM on both sides of the rivets. Recall the rivet head diameter is 6 mm. The chord length is included in 2c and this increases as the crack reorients to bec0me a normal crack. This plot shows slow, almost linear subsurface crack growth vs. time, but when the crack breaks through the outer surface, i.e. becoming a through crack, the crack growth rate increases rapidly. The surface crack lengths that were studied optically were consistently shorter than the measured values with the acoustic microscope (showing that the crack is longer on the inner surface of the specimens). Cracks were observed on average approximately 80,000 cycles earlier and at about a 2 mm shorter crack length, 2c, using the scanning acoustic microscope than by careful microscopic examination of the chamfered panel outside

surface. In Figure 5.13, dc/dN vs. $\sigma(c)^{1/2}$ was plotted, where σ is the maximum nominal applied stress and c is defined in Figure 3.6 dc/dN was determined from the crack growth curves, Figure 5.12. From the Paris region of this plot, the value for the exponent, m, is found to be approximately between 3.8 and 4.2. This approximation compares with an m value, 3, in 2024 Al-T4 as reported by Liaw et al. (1981).

As detailed in Chapter 4, the crack path is much different at 154 MPa than the crack path at 103 MPa maximum nominal stress, radial vs. eyebrow cracks. Figure 5.14 is a plot of the crack growth of specimens fatigued at a maximum stress of 154 MPa as measured with the optical microscope and with the SAM. As with the cracks formed at 103 MPa, the length of the crack on the back surface of the countersunk panel remains longer than the length of the crack on the front surface of the specimen even when 2c is 20+ mm. This may be due to the tensile bending moment on the back surface. Also, as was the case with the cracks formed at 103 MPa, the crack growth rate increases rapidly when the crack breaks through the outer surface so that it may be seen optically. Of course, the number of cycles is much smaller for the higher stress range as well as the number of cycles to reach a 15 mm crack length. The average number of cycles for a 15 mm crack to form at the lower stress is about 240,000 cycles while the average number of cycles at the higher stress is about 8,000 cycles.

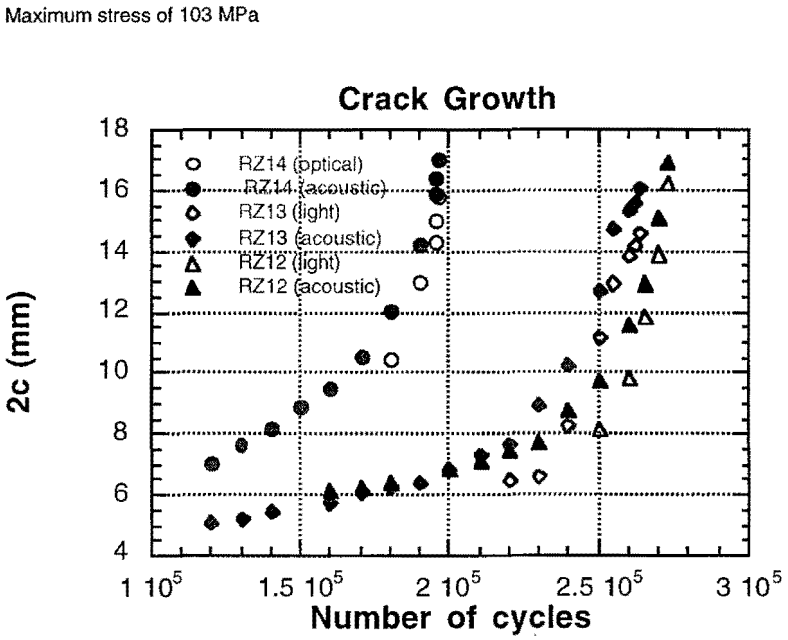

Fig. 5.12. Plot of the crack growth of specimens fatigued at a maximum stress of 103 MPa as measured with the optical microscope and with the SAM. The closed symbols are SAM measurements and the open symbols are optical measurements.

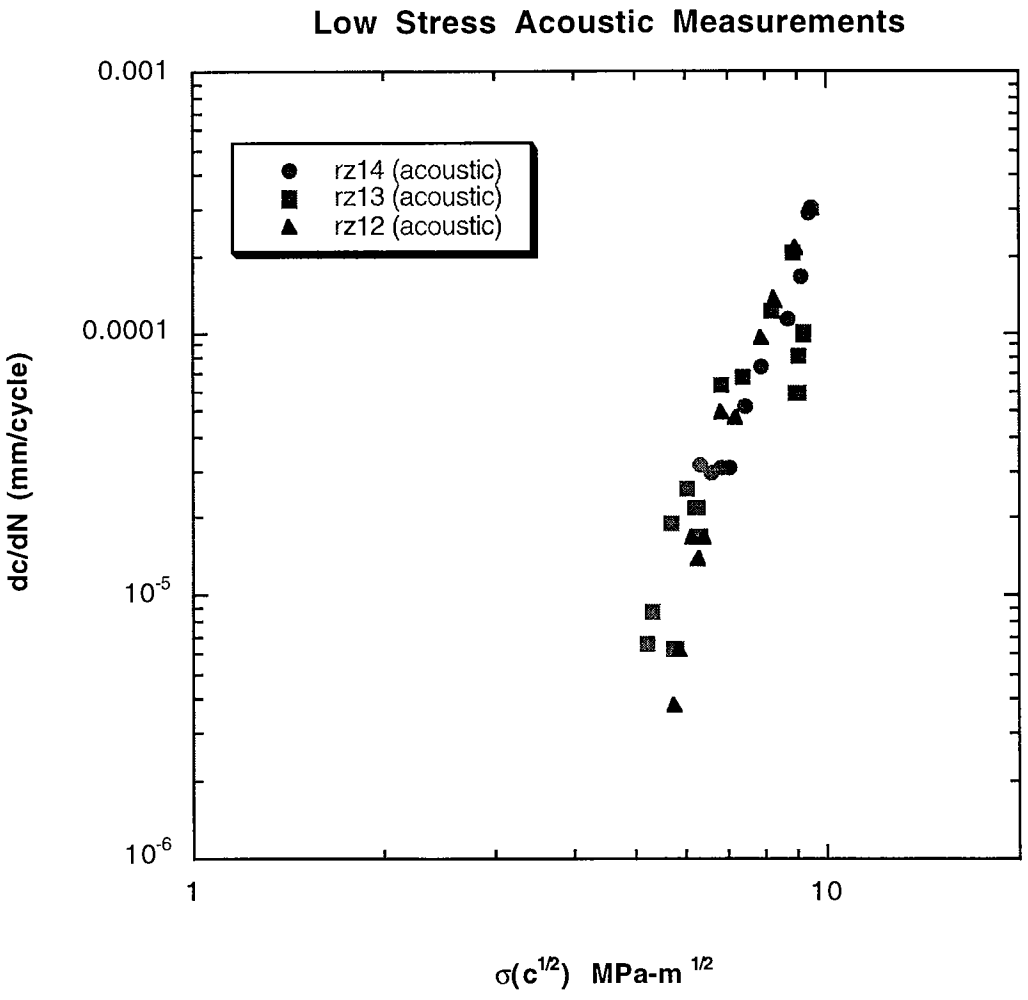

Fig. 5.13. Plot of dc/dN vs. $\sigma(c)^{1/2}$ at a maximum load of 4 kN as obtained with the acoustic microscope. Specimens were fatigued at a maximum nominal stress of 103 MPa. dc/dN was determined from the acoustic microscope crack growth curves, Figure 5.12

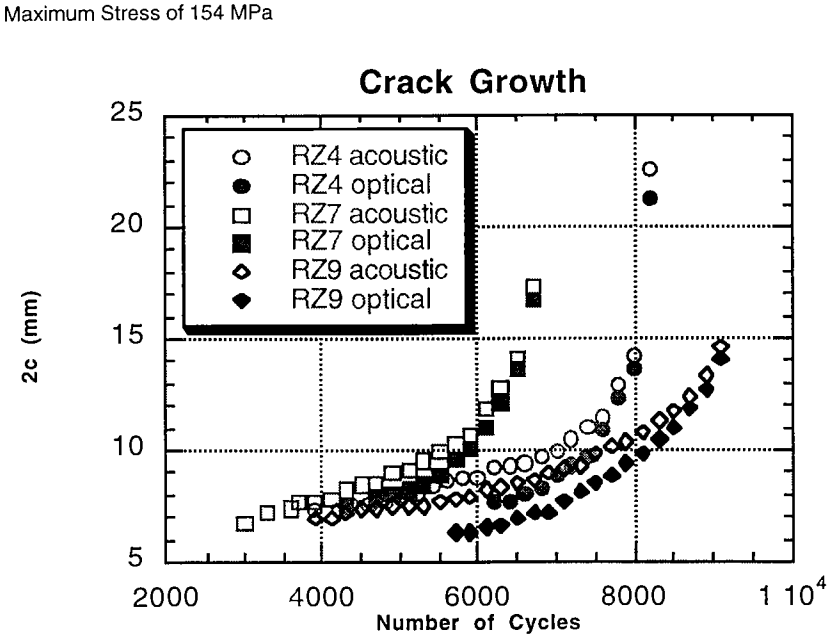

Fig. 5.14. Plot of the crack growth of specimens fatigued at a maximum stress of 154 MPa as measured with the optical microscope and with the SAM. The open symbols are SAM measurements.

The 2c crack lengths measured by SAM for 103 and 154 MPa nominal stress are compared on a normalized basis, N/N_{15}, in Figure 5.15. N_{15} is defined here as the number of cycles for a crack to reach a length of 15 mm. Cracks on both sides of the rivet were not detected by the SAM for both nominal stress ranges until about 45% of the N_{15}. The 2c lengths are about 5 and 7 mm for the first data points plotted. The "eyebrow" type cracks observed at lower stresses are detected at a shorter length, because they do not form at the diameter of the rivet but rather closer to the bottom

where the distance under the rivet head is shorter. As N/N_{15} approaches 1, the optical and acoustic measured data become coincidental when plotted on this reduced basis. The cracks have been normalized so they are coincidental when $N = N_{15\,mm}$.

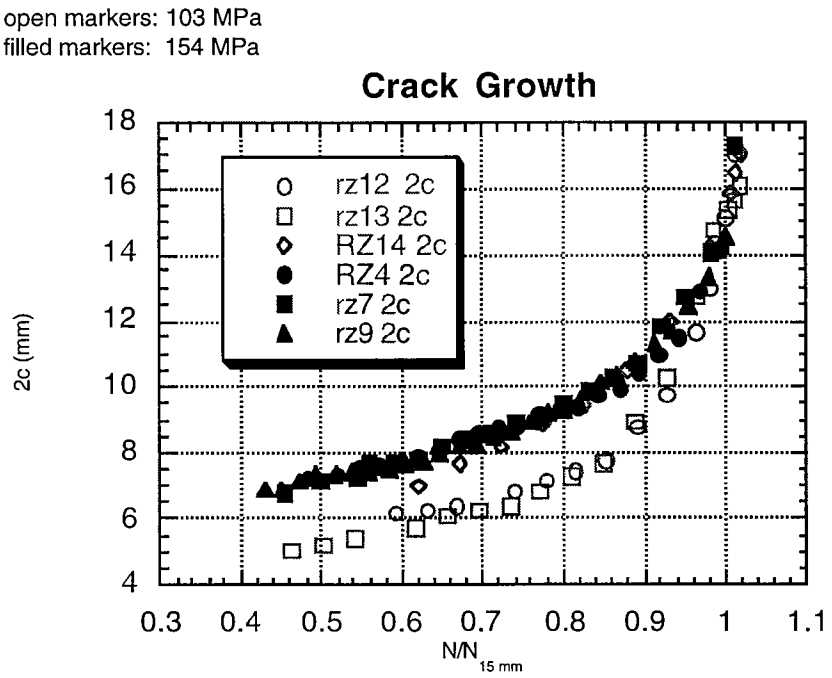

Fig. 5.15. Crack lengths compared on a normalized basis, N/N_{15}. The open markers and the x represent specimens fatigued at 103 MPa and the closed markers represent specimens fatigued at 154 MPa. Crack length measurements were taken with the scanning acoustic microscope.

When the cracks were observed on the outer (chamfered) surface, their lengths were measured optically. The optical and SAM measurements are compared in Figure 5.16 where $2c_{ac}/2c_{op}$ is plotted against $2c_{ac}$. The SAM measures the maximum crack length, which is always longer than the length of the same crack on the outside surface at least up to the lengths measured. This ratio decreases more rapidly at the higher stress to what appears to be a steady state value with crack length. A fingernail shaped through thickness crack front is normally observed with fatigue in panel specimens subjected to mode I loading. This is due to the different stress state at the surface than in the interior. At the lower load, the ratio is still decreasing when $2c_{ac}$ is 15 mm. The first data points plotted are at about 8 mm crack length; i.e. the crack is already 8 mm long subsurface before it is seen on the surface using an optical microscope. The ratio of $2c_{ac}/2c_{op}$ decreases from about 1.3 when cracks were first noted optically to about 1.05 when the cracks are 15 mm long. These findings are of considerable importance for assessing the extent of cracking at rivets by visual examination.

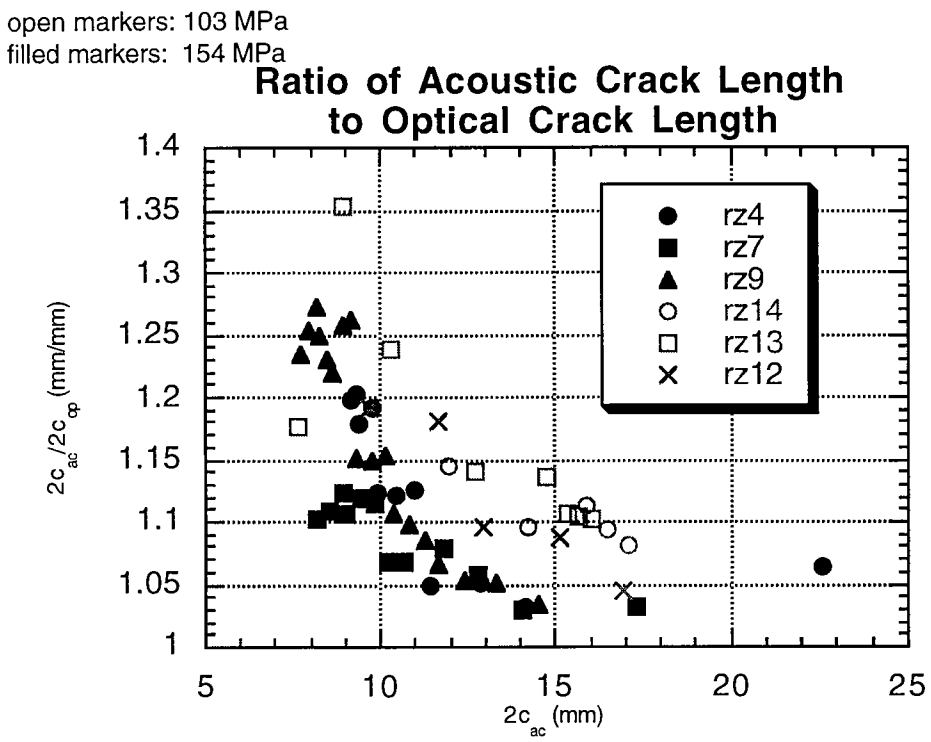

Fig. 5.16. Comparison of optical and acoustic measurements. The open markers represent specimens fatigued at 103 MPa and the closed markers represent specimens fatigued at 154 MPa.

5.4. Comparison of Alclad 2024-T3 and Alclad 2524-T3

To compare the new high purity alloy, 2524 aluminum, developed by Alcoa with the alloy 2024, specimens were made of each alloy and then fatigue at stresses of 103 MPa and 154 MPa. A total of twenty-one specimens of Alclad 2024-T3 and Alclad 2524-T3 were fatigue tested to failure at high and low loads as given in Table 5.1. The

thickness for the Alclad 2024-T3 and the Alclad 2524-T3 panels was 1.27 mm. The average life of the Alclad 2024-T3 specimens fatigued at 103 MPa was 248,694 cycles with a standard deviation of 38,095 while that for the Alclad 2524-T3 specimens was 353,981 cycles with a standard deviation of 68,636 so the Alclad 2524-T3 specimens had 42% longer fatigue life. The average life of the Alclad 2024-T3 specimens fatigued at 154 MPa was 22,379 cycles with a standard deviation of 9,137 while that for the Alclad 2524-T3 specimens was 17,347 cycles with a standard deviation of 4,172 so the Alclad 2024-T3 had 29% longer at the higher load. Fuselages of aircraft are not subjected to stresses as high as 154 MPa.

FATIGUE LIFE				
	103 MPa		154 MPa	
	2024-T3	2524-T3	2024-T3	2524-T3
	210,214	439,648	11,274	16,169
	274,783	380,686	35,776	13,230
	293,039	252,409	18,174	22,487
	214,394	363,012	20,923	13,900
	281,084	334,150	25,748	20,950
	218,649			
Average Life	248,694	353,981	22,379	17,347
Standard Deviation	38095	68636	9137	4172
% Longer Life		42%	29%	

Table 5.1. Comparison of 2024-T3 and 2524-T3

At both high and low stresses, there is not much difference in the crack propagation rates between the alloys after the cracks have reached the surface. This is shown in Figures 5.17 and 5.18, where N_I is the number of cycles until a crack was seen on the surface. However, at low stress, 103 MPa nominal stress, which is comparable to those experienced by aircraft skins, Alclad 2524-T3 undergoes many more cycles to surface crack appearance than Alclad 2024-T3. Thus the initiation and microcrack stages in the fatigue process are longer for the Alclad 2524-T3. As mentioned in Chapter 4, Section 4.3, this is expected since there are fewer inclusions in the 2524-T3 and so there are less fatigue crack initiation sites. At high stress, crack initiation (nucleation plus microcrack growth and coalescence) plays less of a role and the 2024-T3 has a longer life. Experiments performed by Filler (1981) on 7xxx series ultrahigh purity and commercial grade alloys displayed the long crack ΔK_o for the high purity alloys to be about 1.9 on average and for the commercial grade alloy to be 2.4. From this it was concluded that the deformation in the commercial grade alloy at low ΔK was more evenly distributed due to dislocation bypass of the constituent particles (inclusions). This may be the origin of the reversal in behavior between low and high stress.

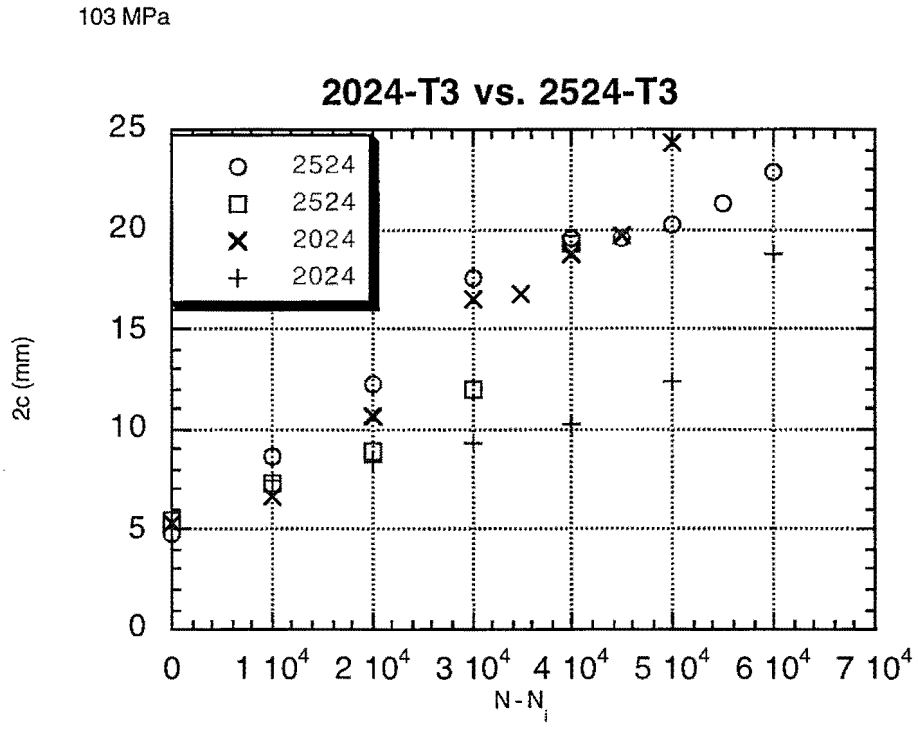

Fig. 5.17. Plot of crack growth as a function of 2c vs. $N-N_I$ where N_I is the number of cycles until a crack was seen on the surface for specimens fatigued at a maximum nominal stress of 103 MPa.

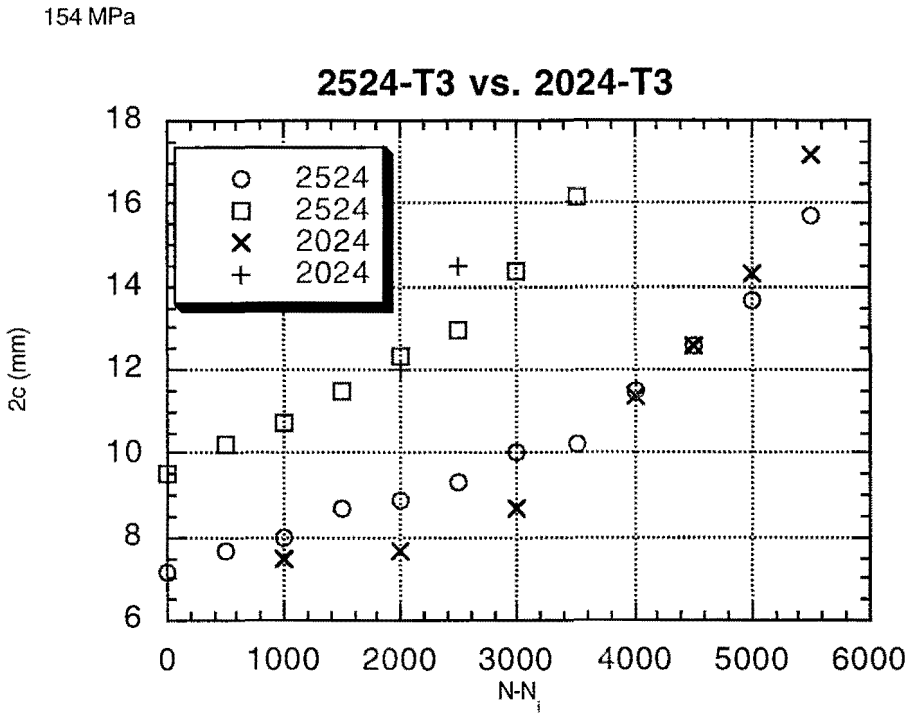

Fig. 5.18. Plot of crack growth as a function of 2c vs. $N-N_I$ where N_I is the number of cycles until a crack was seen on the surface for specimens fatigued at a maximum nominal stress of 154 MPa.

5.5. Summary

Crack growth curves and crack growth rate curves were generated on both surface and subsurface cracks at high and low stresses. Crack arrests were shown on the crack growth rate curve for crack measurements taken before the small cracks broke the surface. Quantitative crack growth data was taken using the SAM. The crack profiles are such that the crack is always longer in the interior of the riveted specimen

than on the outside surface. [Connor, 1997; Connor, 1998] It is suggested that this is due to the visible surface being in compression and the fayed surface being in tension due to the bending moment. Comparison of the crack growth for subsurface cracks in specimens is much slower than after they break the surface. This is most likely due to the crack no longer being constrained in that direction.

Using the FASTRAN-II computer code (Newman, 1992) and selecting a cyclic load of constant amplitude and a surface crack configuration with an initial crack size of 2 mm and initial flaw sizes of 15 μm and 30 μm, reasonable agreement was obtained between the crack growth curves generated by the computer code and the experimental data found with the use of the acoustic microscope and the optical microscope for specimens fatigued at a maximum nominal stress of 103 MPa.

The crack nucleation and microcrack stages were found to be longer for the more pure 2524 alloy than for the 2024 alloy at 103 MPa nominal stress, which is in the range of stresses normally experienced by aircraft.

6. Summary and Future Research

6.1. Summary

1. The fatigue crack initiation and propagation behavior varies with stress range. At high stress ranges a centerline crack develops and at lower stress ranges an eyebrow crack develops.
2. At low stress ranges, the fatigue cracks initiate a short distance from the rivet at or near the hidden surface of the chamfered panel. At higher stress amplitudes the cracks initiate at the blunt knife edge. Residual compressive stresses and fretting are suggested to play more important roles at lower stress ranges.
3. Both the centerline cracks and the eyebrow cracks initiate in a shear mode but transform to tensile, mode I, cracks as they grow. This transition occurs much more rapidly at the higher stress amplitude.
4. At both high and low stresses, the cracks are longer on the fayed surface of the panel than elsewhere and this difference could be due to one of three things or a combination of these. First, the bending moment results in the fayed surface being in tension and the opposite side being in compression. Secondly, it is easier for the crack to grow along the free surface in the x direction than it is for it to grow in the

constrained y direction as shown in the sketch in Figure 6.1. This would apply only until the crack broke the front surface. Thirdly, the preferred orientation of the grains enables the slip band cracks to extend across grains due to the adjacent grains having slip planes with nearly equivalent orientations. The x direction is the longitudinal (L) direction with respect to the orientation of the grains and the y direction is the short transverse (ST) direction with respect to the orientation of the grains.

5. The ratio of outer surface length to interior length decreases as the fatigue crack grows from about 1.3 when cracks were first seen optically on the outer surface to about 1.05 when the 2c crack length is 15 mm. The decrease occurs more rapidly with increase in crack length at the higher stress range.[Fine et al., 1999]
6. It is well known that inclusions and constituent particles are nucleation sites for fatigue cracks. As expected, the high purity aluminum alloy 2524 nucleates cracks at a greater number of cycles than the less pure aluminum alloy 2024.

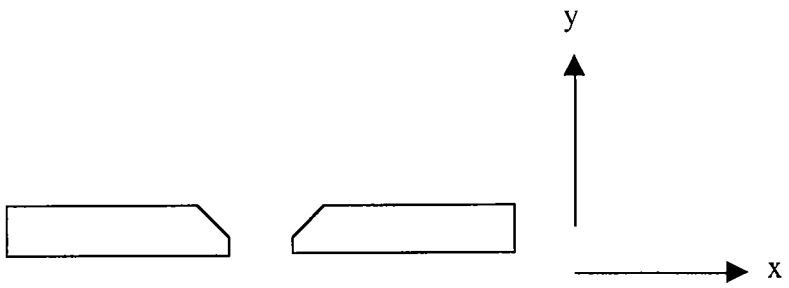

Fig. 6.1. Sketch showing x direction (growth along free surface) and y direction (growth in the constrained direction).

6.2. Future Research

Further tests need to be performed to determine the effects of such things as replacing the countersunk rivets with buttonhead type rivets, the difference in the number of cycles until crack initiation and fatigue life for clad and unclad material, and the testing of more complex specimens among other things. As always, it is important to understand the effects of changes before making them

6.2.1. Joints with Countersunk Rivets Replaced by Buttonhead Type Rivets

As mentioned in the introduction, service bulletins have been issued to replace the critical row of flat head rivets with button head type rivets. It has been found that when the flat heat rivets are replaced with the button head type rivets that cracks

develop at the rivet row opposite the critical rivet row and in the second layer. These second layer cracks would be even more difficult to detect. [Hsu, 1997] The study by Mayville and Sigelmann (1993) gave the surprising result that after this type of repair was made in laboratory specimens, cracks never initiated in the bottom row of rivets in the second layer even though the level of stress is higher here than in the middle row which did experience crack initiation. Further studies should be done to validate this surprising result as well as studies to characterize the initiation and growth of the cracks, which form after the repair. We need to be able to predict it and to detect these cracks. Therefore, fatigue tests need to be run on specimens that have had the counter sunk rivets replaced after a number of cycles with the buttonhead type rivets in the critical rivet (Rivet 3). Also, work should be performed on the adaptation of the acoustic microscope for use in the field.

6.2.2. Testing of New Materials

As previously mentioned, most tests have been performed on precracked or notched specimens, specimens containing a chamfered hole or riveted specimens that have been precracked or notched. Prior to a new material being used in the manufacture of the fuselages of an aircraft, it should be tested in riveted joints, because the fatigue life on simple notched specimens, a chamfered hole or a precracked or notched riveted specimen may not be the same as it is on riveted joints with naturally

occurring fatigue cracks. This is particularly true for the location of the crack initiation sites.

6.2.3. Testing of Material with Cladding on Outside only and not on the Mated Surfaces

The 1050 aluminum is used to clad the base metal and protect the base metal from corrosion; however, no studies have been performed to determine if the soft aluminum encourages adhesion during fretting fatigue thereby promoting crack initiation. Of course, it is necessary for corrosion resistance on the outside, but between the sheets, where fretting occurs, it would seem that this low strength material (see Table 3.2—Mechanical Properties of Materials) will allow nucleation to begin earlier. This soft pure aluminum cladding easily smears and easily oxidizes and may perhaps speed up the crack initiation process. Once the cladding is smeared, the base metal is exposed to the environment. Tests should be performed on riveted joints of 2024-T3 which have sheet material clad only on the outer surfaces and not on the mated surfaces to determine if this increases the lifetime of the joint. The most common cause of crack nucleation during fretting fatigue is adhesion. [Hurricks, 1970; Hoeppner et al., 1994] It is likely, therefore, that the soft Al cladding would be detrimental in that it would encourage adhesion and then crack nucleation. The particle in the micrograph in Figure 4.26 appears to be an adhesion and shows a crack

emanating from each side of the particle. EDS analysis shows this particle to be Al_2O_3. Schmidt et al. (1996) found that cracks nucleate earlier in clad material than in bare material. Figure 4.3 is a cross section taken through the center of the rivet in the riveted joint. A small lap in the soft aluminum cladding, probably as a result of the riveting process, is seen. Irregularities such as this or cracks in the cladding will act as stress raisers and will result in crack nucleation in the substrate. [Hoeppner, 1994; Beard, 1988]

6.2.4. Crack Location as a Function of Squeeze Force and Maximum Applied Load

As shown by Müller (1995), the squeeze force affects the location of the crack initiation. In this research, it is shown that the amount of maximum applied load affects the location of crack initiation. Because the stress is not the same close to the stringers as it is far away from the stringers and because not every rivet is installed with the same squeeze force, the interaction of these two variables would be of interest.

6.2.5. More Complicated Joints

Tests should be performed on more complex specimens containing nine or more rivets so that the effects of rivet interaction may be studied. When nine rivets are used, the first cracks will be at the outer rivets due to these rivets carrying a higher percentage of the load. [Müller, 1995] By placing only one rivet in the center row, the first crack to form was at the middle rivet in the critical row. Some preliminary tests were performed on a seven rivet specimen and the same eyebrow type cracks developed.

6.2.6. Modeling for Failure Prediction

Models have been developed for failure prediction and crack growth. [Bakuckas et al., 1996; Newman, 1992; NASGRO, 1994] In these models, some assumptions have been made such as initial flaw geometry, initial flaw size, initiation sites. Previously, experimental results were not available for modeling for failure prediction based on initiation microcrack stages. This research provides these experimental results; therefore, future models will more accurately represent fatigue crack growth and failure in riveted specimens.

6.2.7. Interaction of the Amount of Rivet Interference and Amount of Riveting Force

It has been shown that several factors, such as amount of interference fit, level of stress and riveting force, will affect the lifetime of the riveted lap joint. [Muller, 1995; Connor et al., 1998;] A 3-D diagram as shown in Figure 6.2 showing the effect of various amounts of interference and various amounts of riveting force on the lifetime of the joint should reveal an optimum condition for rivet force and interference fit.

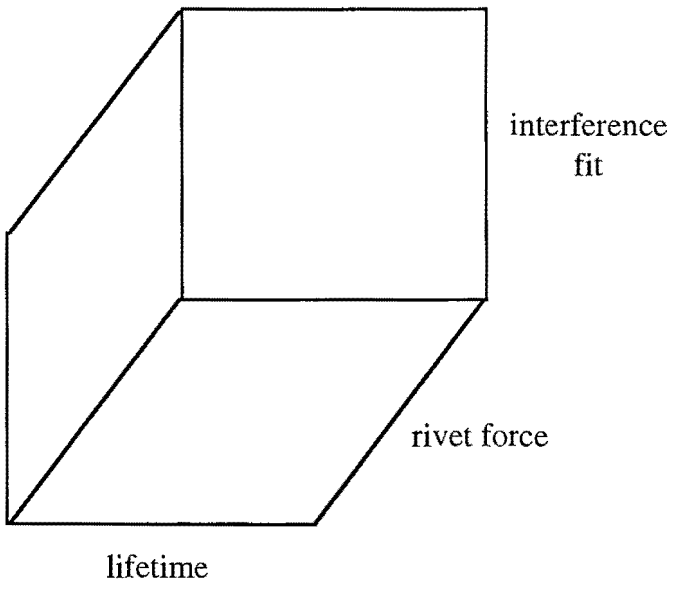

Fig. 6.2. 3-D Diagram showing the effects of various amounts of riveting force and various amounts of interference fit.

6.3. Concluding Remarks

Modeling of fatigue failure in riveted joints is generally based strictly on mechanics. [Newman, 1992; Müller, 1995; NASGRO, 1994] An initial crack is assumed to be present. Initiation of fatigue cracks and the microcrack stages of propagation are not included, yet these are the major part of the fatigue lifetime at low stresses.

A riveted laboratory specimen was developed, and the crack growth in these specimens appears to be qualitatively identical to the crack growth very close to single rivet cracks observed in full scale fuselage testing. Fatigue cracks do not become visible until at least 65% of the lifetime as seen in studies performed by Connor et al. (1997), Fawaz (1997), Müller (1995) and Piascik et al. (1994). Studies on early crack development in the subsurface have not previously been performed.

The scanning acoustic microscope is a useful tool in the study of subsurface cracks in the initiation and microcrack stage. With the help of this microscope, the formation and growth of subsurface cracks may be quantitatively characterized in detail revealing the fatigue crack initiation sites and determining the crack profile and growth kinetics. This characterization should be helpful in the development of NDE techniques for earlier detection of MSD and in modeling these cracks in lap joints. Knowing where fatigue cracks initiate and where they propagate vs. stress amplitude will aid in NDE inspection and in post crack analysis. Quantitative sub-surface fatigue

crack propagation rate data vs. stress amplitude will aid in selecting inspection intervals [Connor et al., 1997; Connor et al., 1998; Fine et al., 1999]

Also, subsurface cracks may be characterized in other alloys and with other types of rivets. This will benefit in the design of joints and in the selection of particular alloys.

References

Advances in acoustic microscopy. 1995. Ed. by A. Briggs and W. Arnold. Plenum Press, New York.

Albert, T. M. and D. A. Froom. 1993. High Throughput Technology for Aircraft NDE. In *Nondestructive Inspection of Aging Aircraft,* Proceedings of SPIE—the International Society of Optical Engineering. ed. by M. T. Valley, N. K. Del Grande, and A. S. Kobayashi, Bellingham, WA.: 20-36.

Almeida, A. and E. V. K. Hill. 1995. Neural Network Detection of Fatigue Crack Growth in Riveted Joints Using Acoustic Emission. *Materials Evaluation,* (January): 76-82.

Aluminum and Aluminum Alloys. 1993. The Materials Information Society, ASM International, Materials Park, OH, (December): 8-20, 35-40, 71, 603-615, 653-655.

Attal, J. and C. F. Quate. 1976. Investigation of some low ultrasonic absorption liquids. *Journal of the Acoustical Society of America,* 59(1) (January): 69-73.

Azevedo, S., H. E. Martz, and D. J. Schneberk. 1993. Potential of Computed Tomography for Inspection of Aircraft Components. In *Nondestructive Inspection of Aging Aircraft,* Proceedings of SPIE--the International Society of OpticalEngineering. ed. by M. T. Valley, N. K. Del Grande, and A. S. Kobayashi, Bellingham, WA.: 47-57.

Baird, J. P., R. B. Heslehurst, H. M. Williamson, B. Clark, and D. Hollamby. 1996. Life Determination of Riveted Aircraft Structure by Holographic NDE, *SPIE* 2945: 172-177.

Bakuckas, Jr., J. G., C. C. Chen, J. Yu, P. W. Tan, and C. A. Bigelow. 1996. Engineering Approach to Damage Tolerance Analysis of Fuselage Skin Repairs. Final Report No. DOT/FAA/AR-95/75, (November).

Bannantine, J. A., J. J. Comer and J. L. Hanrock. 1990. Fundamentals of Metal Fatigue Analysis. Prentice-Hall, Englewood Cliffs, NJ.

Beard, J. 1988. The Avoidance of Fretting. *Materials & Design,* 9(4): 220-227.

Bellinger, N. C., J. P. Komorowski and R. W. Gould. 1999. Corrosion Pillowing Cracks in Fuselage Joints. Proceedings of The Second Joint NASA/FAA/DoD Conference on Aging Aircraft, ed. by Charles E. Harris, NASA/CP-1999-208982/Part 1, January: 535-544.

Boeing Aging Airplane Service Bulletin Structural Modification Program, Model 727, No. D6-54860. 1989. Structures Engineering, Renton Division, (March): 3.2.3.

Boeing Aging Airplane Service Bulletin Structural Modification Program, Model 737 - 100 / - 200 / -200C, No. D6-38505. 1989. Structures Engineering, Renton Division, (March): 3.2.1.

Boeing Aging Airplane Service Bulletin Structural Modification Program, Model 747, No. D6-35999.1989. Structures Engineering, Everett Division, (March): 3.2.3.

Boeing Part Standard, BACR15CE RIVET, 100° Shear Head, Boeing Co., 22 JUL 87.

Boeing Company 737 Structural Repair Standard (1970).

Bray, G. H., R. J. Bucci, M. Kulak, C. J. Warren, A. F. Grandt, Jr., P. J. Golden, D. G. Sexton. 1999. Benefits of Improved Fuselage Skin Sheet Alloy 2524-T3 in Multi-Site Damage Scenarios. Proceedings of The Second Joint NASA/FAA/DoD Conference on Aging Aircraft, ed. by Charles E. Harris, NASA/CP-1999-208982/Part 2, January: 503-512.

Bray, R. C., C. F. Quate, J. Calhoun, and R. Koch. 1980. Film Adhesion Studies with the Acoustic Microscope. *Thin Solid Films,* 74: 295-302.

Briggs, Andrew. 1992. Acoustic Microscopy, ed. by R. Brook, P. B. Hirsch, C. J. Humphreys, and N. F . Mott. Clarendon Press. Oxford: . 17, 29-31, 49-58, 62-63, 105-107, 114.

Briggs, G. A. D. and M. Hoppe. 1991. Acoustic Microscopy. Images of Materials, ed. by D. B. Williams et al., New York, Oxford University Press, Inc.: 114.

Briggs, G. A. D., C. M. W. Daft, A. F. Fagan, T. A. Field, C.W. Lawrence, M. Montoto, S. D. Peck, A. Rodriguez, and C. B. Scruby, C. B. 1989. Acoustic Microscopy of Old and New Materials. *Acoustical Imaging,* 17: 1-16.

Burnside, H. 1993. Flying Longer with Confidence. *Technology Today,* (Sept.).

Carlyle, J. M. 1993. Experiences in testing a fleet of aging aircraft using an acoustic nondestructive testing technique. In *Nondestructive Inspection of Aging Aircraft:* Proceedings of SPIE--the International Society for Optical Engineering, chaired and edited by Michael T. Valley, Nancy K. Del Grande, Albert S. Kobayashi; SPIE--the International Society for Optical Engineering; SEM--Society of Experimental Mechanics, Bellingham, Washington: 14-19.

Chase, S. B. 1994. NDE for the steel bridges FHWA research past present and future. *Structures Congress XII Proc Struct Congr 94,* Proceedings of the Structures Congress '94, ASCE, New York, NY, USA: 1060-1064.

Connor, Z. M., M. E. Fine and J. D. Achenbach. 1998. Quantitative Investigation of Surface and Subsurface Cracks Near Rivets in Riveted Joints Using Acoustic, Electron and Optical Microscopy. Proceedings of The Second Joint NASA/FAA/DoD Conference on Aging Aircraft, (August 31-September 3), ed. by C. E. Harris, Williamsburg, Virginia: ERRATA, NASA/CP-1999-208982/PART1, 240-243-H.

Connor, Z. M., M. E. Fine and J. D. Achenbach. 1997. Fatigue Crack Initiation and Propagation on Hidden Surfaces: Riveted Joints of Alclad 2024. Proceedings of The First Joint DoD/FAA/NASA Conference on Aging Aircraft, Vol I, (July 8-10), Ogden, Utah: 665-685.

Connor, Z, M., M. E. Fine, and J. D. Achenbach. 1997. Acoustic, Electron and Optical Microscopy Visualization of Surface and Sub-surface Cracks. *Review in Progress in Quantitative Nondestructive Evaluation*, 17B: 1581-1588.

Connor, Z.M., W. Li, M. E. Fine and J. D. Achenbach. 1997. Fatigue Crack Initiation and Growth in Riveted Specimens. *International Journal of Fatigue*, pp. S331-S338.

Connor, Z.M., M. E. Fine, and B. Moran. 1996, A Study of Fatigue Crack Generation and Growth in Riveted Alclad 2024T3 Specimens. Proceedings of FAA-NASA Symposium on Continued Airworthiness of Aircraft Structures, Atlanta, GA, pp. 631-642.

Cordell, T. M. 1995. Life management of aging air force aircraft: NDE perspective. In *Nondestructive Evaluation of Aging Aircraft, Airports, Aerospace Hardware, and Materials:* Proceedings of SPIE--the International Society for Optical Engineering, chaired and edited by Tobey M. Cordell and Raymond D. Rempt, Bellingham, Washington: 34-44.

Courtney, T. Hill. 1990. Mechanical Behavior of Materials. McGraw Hill, Inc., United States: 209, 426, 567, 573, 576.

CRC, Handbook of Chemistry and Physics. 1978. ed. by R. C. Weast and M. J. Astle, Florida, CRC Press, Inc., p. E-47.

Cunningham, J. A. and C. F. Quate. 1973. High-resolution Acoustic Imaging by Contact Printing. *Acoustical Holography,* Vol. 5, Proceedings of the Fifth International Symposium on Acoustical Holography, ed. by P. S. Green, Plenum Press, New York, (July): 83-102.

DeMeis, R. 1989. Aging aircraft. *Aerospace America*, (July): 38-42.

Ekvall, J. C. 1986. Fatigue of Riveted Metallic Joints. In *Fatigue in Mechanically Fastened Composite and Metallic Joints, ASTM STP 927.* ed. by J. M. Potter, American Society for Testing and Materials, Philadelphia, PA: 172-189.

Endo, K. 1981. Practical Observations of Initiation and Propagation of Fretting Fatigue Cracks. *Fretting Fatigue,* Applied Science Publishers Limited, ed. by R. B. Waterhouse, London, England: 127-141.

Fadragas, M. I. 1993. *Tensile Fatigue Crack Initiation and Growth Database for Chamfered Rivet Holes in Alclad 2024-T3 Aluminum Alloy.* Masters of Science Thesis, Northwestern University, Evanston, IL.

Favro, L. D., P. K. Kuo, R. L. Thomas, T. T. Ahmed, Y. X. Wang. 1993. Thermal-wave Imaging of Corrosion and Disbonds in Aircraft Structures. *Nondestructive Inspection of Aging Aircraft,* Proceedings of SPIE--the International Society of Optical Engineering, ed. by M. T. Valley, N. K. Del Grande, and A. S. Kobayashi, Bellingham, WA: 88-91.

Fawaz, S. C. 1997. *Fatigue Crack Growth in Riveted Joints.* Masters of Science Thesis, Technische Universiteit Delft, Holland.

Filler, L. C. 1981. *Effects of Disperoid, Purity and Overaging on Threshold for Macrofatigue Crack Propagation in Al-Zn-Mg-Cu Alloys.* Masters of Science Thesis, Northwestern University, Evanston, IL.

Fine, M. E. 1980. Fatigue Resistance of Metals, The 1979 Campbell Memorial Lecture. *Metallurgical Transactions A.* Vol. 11A, No. 3, (March): 365-379.

Fine, M. E., C. Y. Kung, M. I. Fadragas, and J. D. Achenbach. 1992. Fatigue Crack Initiation and Microcrack Propagation Data Base in Precipitation Hardened Aluminum Alloys. *Durability of Metal Aircraft Structures*, Proceedings of the International Workshop on Structural Integrity of Aging Airplanes, Atlanta Technology Publications, edited by S. N. Atluri, C. E. Harris, A. Hoggard, N. Miller, and S. G. Sampath, Georgia: 297-310.

Fine, M. E., Z. M. Connor and J. D. Achenbach. 1999. Early Stages of Fatigue Damage in Riveted Alclad 2024-T3 Aluminum Alloy Lap Joint Specimens. *Nondestructive Evaluation (NDE) and Material Properties IV,* edited by P. K. Liaw, R. J. Arsenault, R. E. Green, Jr., K. L. Murty and R. B. Thompson, The Minerals, Metals & Materials Society, pp. 1-9.

Fisher, J. L., G. L. Burkhardt, J. S. Stolte, J. P. Buckingham, P. C. McKeighan, J. Fitzgerald, G. Burkhardt. 1999. Reliability Study of Magneto-Optic (MOI) Imaging Inspection of C-5 Aircraft Fuselage. Proceedings of The Second Joint NASA/FAA/DoD Conference on Aging Aircraft, ed. by C. E. Harris, Williamsburg, VA, (January): 230-239.

Fitzgerald, T. J. and J. B. Cohen. 1994. Residual Stresses in and Around Rivets in Clad Aluminum Alloy Plates. *Materials Science and Engineering*, A188: 51-58.

Fitzpatrick, G. L., D. K. Thome, R. L. Skaugset, E. Y. C. Shih, W. C. L. Shih. 1993. Magneto-Optic/Eddy Current Imaging of Aging Aircraft, A New NDI Technique. *Materials Evaluation*, (December): 1402-1407.

Forsyth, P. J. E. 1981. Occurrence of Fretting Fatigue Failures in Practice. *Fretting Fatigue,* Applied Science Publishers Limited, ed. by R. B. Waterhouse, London, England: 99-125.

For want of rivets, Titanic was lost, scholars speculate. 1998. Associated Press, (January 28).

Fossheim, K., T. Bye, S. Sathish, G. and Heggum. 1988. Acoustic scanning microscopy of grain structure in isotropic solids: pure aluminium and Al-2.5% Mg alloy. *Journal of Materials Science,* (23): 1748-1751.

Frost, N. E., K. J. Marsh and L. P. Pook. 1974. Metal Fatigue. Clarendon Press, Oxford [Eng.], 499 p.

Ghorbanpoor, A. and A. T. Rentmeester. 1993. NDE of steel bridges by acoustic emission. *Structural Engineering in Natural Hazards Mitigation Proc Symp Struct Eng Nat Hazard Mitigation,* Proceedings of the Symposium on Structural Engineering in Natural Hazards Mitigation, ASCE, New York, NY, USA: 1008-1013.

Gilmore, R. S., K. C. Tam, J. D. Young, and D. R. Howard. 1986. Acoustic microscopy from 10 to 100 MHz for industrial applications. *Philosophical Transactions of the Royal Society of London A,* 320: 215-235.

Gruber, M. L., C. J. Mazur, K. E. Wilkins, and R. E. Worden. 1996. Investigation of Fuselage Structure Subject to Widespread Fatigue Damage. DOT/FAA/AR-95/47, Final Report, February.

Gruber, M. L., K. E. Wilkins and R. E. Worden. 1997. Investigation of Fuselage Structure Subject to Widespread Fatigue Damage. Proceedings of the FAA-NASA Symposium on the Continued Airworthiness of Aircraft Structures. DOT/FAA/AR-97/2,I: July: 439-460.

Hageniers, O. L. 1993. D Sight for Large Area Aircraft Inspection. *Nondestructive Inspection of Aging Aircraft,* Proceedings of SPIE--the International Society of Optical Engineering, ed. by M. T. Valley, N. K. Del Grande, and A. S. Kobayashi, Bellingham, WA: 245-256.

Hageniers, O., F. Harpala, D. J. Willie. 1995. D Sight for NDE of Aging Aircraft. *Nondestructive Evaluation of Aging Aircraft, Airports, Aerospace Hardware, and Materials,* Proceedings of SPIE--the International Society of Optical Engineering, ed. by T. M. Cordell and R. D. Rempt, Bellingham, WA: 182-189.

Hagemaier, D. and G. Kark. 1997. Eddy Current Detection of Short Cracks Under Installed Fasteners. *Materials Evaluation,* 55(1): 25-30.

Hagemaier, C. and D. Wilson. 1997. Improved Nondestructive Inspection Techniques for Aircraft Inspection. Proceedings of the FAA-NASA Symposium on the Continued Airworthiness of Aircraft Structures, ed. by C. A. Bigelow, Atlanta, GA: 403-415.

Harlow, D. G. and R. P. Wei. 1999. Aging of Airframe Materials: Probability of Occurrence versus Probability of Detection. Proceedings of The Second Joint NASA/FAA/DoD Conference on Aging Aircraft, ed. by C. E. Harris, Williamsburg, VA, (January): 275-283.

Hartman, A. 1968. The influence of manufacturing procedures on the fatigue life of 2024-T3 alclad riveted single lap joints. *National Aerospace Laboratory* NLR TR 68072 U, Amsterdam, The Netherlands.

Hartman, A. 1971. The Effect of Secondary Bending on the Fatigue Strength of (Clad 2024-T3 and 7075-T6) Aluminium Alloy Riveted Joints. NLR TR 72007 U, (December).

Heat Treating. 1981. Metals Handbook Ninth Edition, American Society for Metals, New York, 4, (November): 677-678.

Hills, D. A., D. Nowell, and J. J. O'Connor. 1988. On the Mechanics of Fretting Fatigue.*Wear,* 125: 129-146.

Hocson, A. R. and T. N. White. 1999. An Application on Fracture Mechanics Principles in Determining a Service Life Enhancement Interval for the US Navy's C-2 Outer Wing. Proceedings of The Second Joint NASA/FAA/DoD Conference on Aging Aircraft, ed. by Charles E. Harris, NASA/CP-1999-208982/Part 1, January: 63-69.

Hoeppner, D. W., C. B. Elliot III, and M. W. Moesser. 1996. The Role of Fretting Fatigue on Aircraft Rivet Hole Cracking. Final Report, DOT/FAA/AR-96-10, (October).

Hoeppner, D., S. Adibnazari, and M. W. Moesser. 1994. Literature Review and Preliminary Studies of Fretting and Fretting Fatigue Including Special Applications to Aircraft Joints. Final Report, DOT/FAA/CT-93/2, (April).

Hoggard, A. W. 1991. Maintaining the Safety of an Aging Fleet of Aircraft. 1991 International Conference on Aging Aircraft and Structural Airworthiness, ed. by Charles E. Harris, Washington, D. C.: 49-65.

Hoppe, M. and A. Thaer. 1986. Scanning Acoustic Microscopy. Topics in Current Physics:Microscopic Methods in Metals, ed. by U. Gonser, Vol 40, Springer-Verlag Berlin Heidelberg, Germany: 7-28.

Hoppe, M. and J. Bereiter-Hahn. 1985. Applications of Scanning Acoustic Microscopy—Survey and New Aspects. *IEEE Transactions on Sonics and Ultrasonics.* Vol. SU-32(2): March, pp. 289-301.

Hsu, D. 1997. Private conversation with Dr. David Hsu.

Hurricks, P. L. 1970. The Mechanism of Fretting--A Review. *Wear,* 15: 389-409.

Inman, M. E., R. G. Kelly, S. A. Willard and R. S. Piascik. 1997. Coordinated Metallographic, Chemical, and Electrochemical Analyses of Fuselage Lap Splice Corrosion. Proceedings of the FAA-NASA Symposium on the Continued Airworthiness of Aircraft Structures. DOT/FAA/AR-97/2,I: July, 129-146.

Installation, Inspection and Removal Methods for Aerolock 905,906,907 and 908 Rivets, H. D. Little Co., September 10, 1990.

Jappe, W., N. Wood and M. Johnson. 1995. The Transition Process from Emerging NDT Technology to Production Inspection Applications. Nondestructive Evaluation of Aging Aircraft, Airports, Aerospace Hardware, and Materials: Proceedings of SPIE--the International Society for Optical Engineering, chaired and edited by Tobey M. Cordell and Raymond D. Rempt; Bellingham, Washington: 94-101.

Jones, D. R. H. 1993. Engineering Materials 3: Materials Failure Analysis--Case Studies and Design Implications. Pergamon Press, Oxford, NY: 131-142.

Jones, R., D. Rees, and R. Kaye. 1992. Stress Analysis of Fuselage Lap Joints. *Durability of Metal Aircraft Structures,* Proceedings of the International Workshop on Structural Integrity of Aging Airplanes, ed. by S. N. Atluri, C. E. Harris, A. Hoggard, N. Miller, and S. G. Sampath, Atlanta Technology Publications, Georgia: 118-131.

Kaynak, C. and A. Ankara. 1992. Short Fatigue Crack Growth in Al 2024-T3 and Al 7075-T6. *Engineering Fracture Mechanics,* 43(5): 769-778.

Kessler, L. W., P. R. Palermo, and A. Korpel. 1972. Practical High Resolution Acoustic Microscopy. *Acoustical Holography,* Vol. 4, Proceedings of the Fourth International Symposium on Acoustical Holography, ed. by G. Wade, Plenum Press, New York, (April): 51-71.

Kung, C. Y. and M. E. Fine. 1979. Fatigue Crack Initiation and Microcrack Growth in 2024-T4 and 2124-T4 Aluminum Alloys. *Metallurgical Transactions A,* 10A, (May): 603-610.

Laser Heating Reveals Aircraft Cracks. 1999. Industry News website http://perl.spie.org/cgi-bin/news.pl?id=1482, November 26.

Lemons, R. A. and C. F. Quate. 1974. Acoustic microscope--scanning version. *Applied Physics Letters,* 24(4), (February 15): 163-165.

Leon, A. 1997. The Adaptable Split Mandrel Coldworking Processin Various Military and Commercial Life Extension Applications. Proceedings of The First Joint DoD/FAA/NASA Conference on Aging Aircraft, Vol. II, Ogden, Utah, July 8-10: 1669-1681.

Lesniak, J. R. and B. R. Boyce. 1993. Forced-diffusion thermography. *Nondestructive Inspection of Aging Aircraft,* Proceedings of SPIE--the International Society of Optical Engineering, ed. by M. T. Valley, N. K. Del Grande, and A. S. Kobayashi, Bellingham, WA: 92-102.

Liaw, P. K., S. I. Kwun and M. E. Fine. 1981. Plastic Work of Fatigue Crack Propagation in Steels and Aluminum Alloys. *Metallurgical Transactions A.* 12A(1): 49-55.

Lincoln, J. W. 1997. Aging Aircraft-USAF Experience and Actions. Presented at the International Committe on Aeronautical Fatigue, Edinurgh, Scotland, June 16-20.

Ma, Y. P., and J. P. Wikswo, Jr. 1993. Detection of Subsurface Flaws Using SQUID Eddy Current Technique. *Nondestructive Inspection of Aging Aircraft,* Proceedings of SPIE--the International Society of Optical Engineering, ed. by M. T. Valley, N. K. Del Grande, and A. S. Kobayashi, Bellingham, WA: 191-199.

Mayville, R. and M. Sigelmann. 1993. Laboratory Study of Multiple Site Damage in Fuselage Lap Splices, Final Report, DOT/FAA/CT-93/74, (December).

McBride, S. L., J. P. Scott and G. F. Eastough. 1999. Use of Acoustic Emission Monitoring to Detect, Locate and Measure Multiple Site Damage (MSD) Fatigue Crack Growth Underneath Rivet Heads. Proceedings of The Second Joint NASA/FAA/DoD Conference on Aging Aircraft, ed. by Charles E. Harris, NASA/CP-1999-208982/Part 1, January: 303-312.

McGraw-Hill Dictionary of Science and Engineering. 1984. Ed. by S. P. Parker, M. Weil and B. Richman, McGraw-Hill Book Company: 216, 385.

McMillan, J. C. and R. M. N. Pelloux, 1967. Fatigue Crack Propagation Under Program and Random Loads. *Fatigue Crack Propagation, ASTM STP 415,* Am. Soc. Testing Mats.: 505-535.

Moore, J. J. 1990. Chemical Metallurgy. ed. by J. J. Moore: co-authors, E. A. Boyce, M. J. Brooks, B. Perry and P. J. Sheridan, Butterworth & Co. Ltd, London, England: 343-346.

Müller, R. P. G. 1995. *An Experimental and Analytical Investigation on the Fatigue Behaviour of Fuselage Riveted Lap Joints.* Ph.D. Thesis, Delft University of Technology, The Netherlands.

NASGRO Fatigue Crack Computer Program, Version 2.01, NASA JSC-22267A, 1994.

Newman, J. C., Jr., C. E. Harris and M. A. James. 1997. Fatigue-Life Prediction of Riveted Lap-Splice Joints Using Small-Crack Theory. Presented at the International Committee on Aeronautical Fatigue, Edinburgh, Scotland, June 16-20.

Newman, J. C., Jr., K. N. Shivakumar, and M. A. James. 1997. Fatigue-Life Prediction of Riveted Lap-Splice Joints Using Small-Crack Theory. Proceedings of The First Joint DoD/FAA/NASA Conference on Aging Aircraft, Vol. I, Ogden, Utah, July 8-10: 163-192.

Newman, J. C., Jr. 1996. Private conversation with Dr. James C. Newman.

Newman, J. C., Jr. 1995. Fatigue-Life Prediction Methodology Using a Crack-Closure Model. *Journal of Engineering Materials and Technology.* Vol. 117, (October): 433-439.

Newman, J. C., Jr. 1995. Fracture Analysis of Stiffened Panels Under Biaxial Loading with Widespread Cracking. NASA Technical Memorandum 110197, (October).

Newman, J. C., Jr., X. R. Wu, S. L. Venneri and C. G. Li. 1994. Small-Crack Effects in High-Strength Aluminum Alloys--A NASA/CAE Cooperative Program. NASA Reference Publication 1309, (May).

Newman, J. C., Jr. 1994. A Review of Modelling Small-Crack Behavior and Fatigue-Life Predictions for Aluminum Alloys. *Fatigue Fract. Engng. Mater. Struct.,* 17(4): 429-439.

Newman, J. C., Jr. 1992. Fracture Mechanics Parameters for Small Fatigue Cracks. *Small -Crack Test Methods, ASTM STP 1149,* ed. by J. Larsen and J. E. Allison, American Society for Testing and Materials, Philadelphia: 6-33.

Newman, J. C., Jr., M. H. Swain, E. P. Phillips, X. R. Wu, W..Zhao, and C. F. Ding. 1992. Small-Crack Growth Behavior in High-Strength Aluminum Alloys--A NASA/CAE Cooperative Program. 18th Congress of the International Council of the Aeronautical Sciences, Beijing, China, (September 20-25): 799-820.

Newman, Jr., J. C. 1992. "FASTRAN II - A Fatigue Crack Growth Structural Analysis Program", NASA Technical Memorandum 104159, February.

Newman, J. C., Jr. and Edwards, P. R. 1988. Short-Crack Growth Behaviour in an Aluminum Alloy-an AGARD Cooperative Test Programme. AGARD Report No. 732. Paris, France.

Nishioka, K. and K. Hirakawa. 1969. Fundamental Investigations of Fretting Fatigue (Part 3, Some Phenomena and Mechanisms of Surface Cracks). *Bull. JSME,* 12(51): 397-497.

Nishioka, K. and K. Hirakawa,. 1972. Fundamental Investigations of Fretting Fatigue, (Part 6, Effects of Contact Pressure and Hardness of Materials). *Bull. JSME,* 15(80) (February): 135-144.

Oster, C. V., J. S. Strong, and C. K. Zorn. 1992. Why Airplanes Crash: Aviation Safety in a Changing World, Oxford University Press, Inc., New York: 127-142.

Pan, J. Z., U. S. Fernando, K. J. Miller and E. R. de los Rios. 1994. Combined optical-acoustic microscopy for investigating short fatigue crack propagation. *Materials Science and Technology,* 10 (April): 265-271.

Piascik, R. S., S. A. Willard, and M. Miller. 1994. The Characterization of Widespread Fatigue Damage in Fuselage Structure. FAA/NASA Symposium, ed. by C. E. Harris, NASA CP 3274, (May): 563-580.

Piascik, R. S. and S. A. Willard. 1997. The Characteristics of Fatigue Damage in the Fuselage Riveted Lap Splice Joint. NASA/TP-97-206257, (Nov.).

Quate, C. F. 1985. Acoustic microscopy. *Physics Today,* 38 (August): 34-42.

Quate, C. F., A. Atalar, and H. K. Wickramasinghe. 1979. Acoustic Microscopy with Mechanical Scanning--A Review. Proceedings of the IEEE, 67(8): 1092-1114.

Reed-Hill, R. E and R. Abbaschian. 1992. Physical Metallurgy Principles. PWS Kent Publishing Company, Boston MA, 926 p.

Reeves, R. K. and D. W. Hoeppner. 1976. The effect fretting on fatigue. *Wear,* 40: 395-397.

Reid, L. and J. Restis. 1997. Life Enhancement of Repairs Subject to the Repair Assessment Program. Proceedings of The First Joint DoD/FAA/NASA Conference on Aging Aircraft, Vol. II, Ogden, Utah, July 8-10: 1651-1667.

Safety of Aging Aircraft Undergoes Reassessment. 1988. Aviation Week and Space Technology, May 16: 16-18.

Samavedam, G. and D. Hoadley. 1994. Fracture and Fatigue Strength Evaluation of Multiple Site Damaged Aircraft Fuselages - Curved Panel Testing and Analysis. Final Report, DOT/FAA/CT-94/10, FAA Technical Center, Atlantic City International Airport, NJ, January.

Samsonov, P. 1995. Nondestructive Visual Inspection of Aging Aircraft. *Nondestructive Evaluation of Aging Aircraft, Airports, Aerospace Hardware, and Materials*: Proceedings of SPIE--the International Society for Optical Engineering, chaired and edited by Tobey M. Cordell and Raymond D. Rempt; Bellingham, Washington: 190-196.

Schijve, J. 1994. Fatigue Predictions and Scatter. *Fatigue Fract. Engng Mater. Struct.,* 17(4): 381-396.

Schijve, J. 1992. Multi-Site-Damage Fatigue of Riveted Joints. *Durability of Metal Aircraft Structures*, Proceedings of the International Workshop on Structural Integrity of Aging Airplanes, ed. by S. N. Atluri, C. E. Harris, A. Hoggard, N. Miller, and S. G. Sampath, Atlanta Technology Publications, Georgia: 2-27.

Schijve, J. 1982. Difference between the Growth of Small and Large Fatigue Cracks in Relation to Threshold K Values. *Fatigue Thresholds: Fundamentals and Engineering Applications,* Engineering Materials Advisory Services Ltd. Stockholm: 881-908.

Schmidt, C. G., J. E. Crocker, J. H. Giovanola, C. H. Kanazawa and D. A. Shockey. 1996. Characterization of Early Stages of Corrosion Fatigue in Aircraft Skin. Final Report, DOT/FAA/CT-95/108, Department of Transportation, FAA, Office of Aviation Research, Washington, D.C., February.

Scott, J. P. 1997. *Corrosion and Multiple Site Damage in Riveted Fuselage Lap Joints*. Master of Engineering Thesis, Carleton University, Ottawa, Ontario.

Sheppard, W. R. and O. V. Manning. 1995. Low Frequency Eddy Current Array Assessment at the FAA NDI Validation Center. *Materials Evaluation,* (July): 844-847.

Singh, R., J.H. Park and S. N. Atluri. 1994. Growth of Multiple Cracks and Their Linkup in a Fuselage Lap Joint. *AIAA Journal,* 32(11): 2260-2268.

Sproat, W. H. 1999. Airframe Life Extension Through Quantitative Rework Inspections. Proceedings of the FAA-NASA Symposium on the Continued Airworthiness of Aircraft Structures. DOT/FAA/AR-97/2,I: July: 1-16.

Swain, M. H. and J. C. Newman, Jr. 1984. On the Use of Marker Loads and Replicas for Measuring Growth Rates for Small Cracks. AGARD CP-376, Paris, France.

Tsai, Chen S. and Chin C. Lee. 1987. Nondestructive imaging and characterizations of electronic materials and devices using scanning acoustic microscopy. *Pattern Recognition and Acoustical Imaging,* Proceedings of SPIE, Vol. 768, (February): 260-266.

Wanhill, R. J. H. and L. Shra. 1990. Corrosion Fatigue Crack Arrest in Aluminum Alloys. *Quantitative Methods in Fractography, ASTM STP 1085,* ed. by B. M. Strauss and S. K. Putatunda, American Society for Testing and Materials: 144-165.

Waterhouse, R. B. 1981. Avoidance of Fretting Fatigue Failures. *Fretting Fatigue,* Applied Science Publishers Limited, ed. by R. B. Waterhouse, London, England: 221-240.

Waterhouse, R. B. 1981. Introduction to Fatigue. *Fretting Fatigue,* Applied Science Publishers Limited, ed, by R. B. Waterhouse, London, England: 1-21.